University of Strathclyde

Department of Pure and Applied Chemistry

Detection of Pentaerythritol Tetranitrate (PETN) by Resonance Raman and Surface Enhanced Raman Scattering (SERS)

By Bethany Ross

A thesis submitted to the Department of Pure and Applied Chemistry, University of Strathclyde, in fulfilment of the requirements for the degree of Doctor of Philosophy

October 2020

This thesis is the result of the author's original research. It had been composed by the author and has not been previously submitted for examination which has led to the away of a degree

The copyright of this thesis belongs to the author under the terms of the United Kingdom Copyright Acts as qualified by University of Strathclyde Regulation 3.50. Due acknowledgement must always be made use of any material contained in, or derived from, this thesis

Signed: Date:

Acknowledgements

I would like to start by thanking my supervisors Distinguished Professor Duncan Graham, Professor Karen Faulds and Professor Neil Shand for allowing me this opportunity to carry out research in this area and in this department. I would also like to thank Professor Ewan Smith, who was always available to cast an eye over my research and give me pep talks! Thank you for all of your input and guidance throughout my PhD, I am truly grateful for all I have learned. I also extend my thanks to DSTL for funding this PhD.

I would also like to thank Clare Nixon at DSTL for the explosive samples you have sent me over the past 4 years, and all of the silly questions you have answered. Best of luck to you for the rest of your PhD!

To the members of the Centre for Nanometrology – what a whirlwind these past 4 years have been, but it was great knowing that there has always been someone available to chat and give advice. Thank you for the memories and thank you for putting up with my introverted behaviour!

I would like to thank Drs Sam Mabbott, Stacey Laing, Hayleigh Kearns, Sian Sloan-Dennison, Will Tipping, Waleed Hassanain for being fabulous post docs who are always there to have a chat with you, whether it's about your results or life! Sam, you were the one to introduce me to this field of research and spark my interest in the topic when you advised me on my masters project, thank you so much! Corinna and Gillian, thank you for always being there to answer any questions I had on anything paperwork related! Even if you didn't know the answer when I asked, you always go back to me on the topic super fast!

To Drs Kirsty Milligan, Jenny Gracie, Danny MacDonald and Craig Ward, thank you for always having time to help me out and listen to my moans, and for being endless fountains of advice!

Special thanks to all the folk sitting in Yosemite (Sam, Marie, Matthew, Andrew) its been a blast! Thank you for being caring and funny people, who work as hard as they gossip. To Maria Plunkett – thank you so much for all of your organic chemistry help, SEM fun times and random walks to get cake over the past few years.

To Fatima, thank you for always being there in the past four years, I honestly don't know if I would have made it without you being by my side every step of the way. Thank you for your friendship, the holiday adventures we went on (three words – Stranded in Budapest), all the trips we made to Desseerts where we chatted for hours and all of the late evenings we spent working in the office! It's going to be a struggle working in different jobs!

And last but not least, huge thanks much go to my family and friends, both extended and close. Thank you for listening to my complaints and not getting too annoyed at me! Mum, Dad, Iona and Angus, thank you for believing in me and supporting me - especially the past 6 months during quarantine while I've been writing up, thank you for all of the food and company and generally keeping me sane!

Abstract

Military grade explosives such as pentaerythritol tetranitrate (PETN) remain both security and environmental threats. One common method of detecting explosives involves colourimetric testing which is rapid and portable, however, this method lacks specificity as it reacts to specific functional groups in a molecule, therefore resulting in false positives for non-explosive molecules containing the same functional group. Bulk samples of explosives can also be detected using X-ray diffraction and ion-mobility spectroscopy, however, these techniques require large, expensive instrumentation and highly trained staff to operate them. The techniques commonly used today for explosive detection work best on nitro-aromatic explosives.

The aim of this research was to develop a method of detecting PETN in a quick and sensitive assay format, which could be used for in field analysis.

Initially, this research focused on the detection of PETN using a previously commercially available substrate called Klarite^{TM}. The enhancement observed was investigated to find out if the PETN molecule concentrated into the structural pits of the substrate, or the roughened gold top layer was responsible for the enhancement. However, evidence was found to support both theories and no conclusions could be drawn.

As it was difficult to detect low levels of PETN using surface enhanced Raman scattering (SERS), it was decided to fragment the analyte and use the product in an azo reaction. This resulted in the development of four assays which could detect PETN using absorption and/or resonance Raman spectroscopy. However, the assays required a lengthy reaction process (75 minutes), making the assays unlikely to be useful for in field detection.

Finally, the resonance Raman assays were further developed into a single SERS assay, which resulted in more sensitive detection of PETN. The timings of the reaction were

optimised and reduced so completion was reached within 10 minutes. The assay was found to be translatable for use in field detection as the Raman instrumentation used was portable, and the reaction was fast.

Overall, SERS substrates and Raman spectroscopic techniques (resonance Raman and SERS) can be applied to detect PETN to 1 mg L^{-1} (3.2 μM), leading to comparable limits of detection and quicker reaction times than those found in recent literature regarding the detection of PETN with similar methods.

Abbreviations

λ_{max}	Absorbance maxima wavelength (lambda max)
Abs	Absorbance
ACN	Acetonitrile
AgNP	Silver nanoparticles
a.u.	Arbitrary units
AuNP	Gold nanoparticles
Conc.	Concentration
Cu^{2+}	Copper sulfate
DLS	Dynamic light scattering
DMA	3,5-dimethoxyaniline
DNT	2,4-dinitrotoluene
ELISA	Enzyme-linked immunosorbent assays
ETK	Explosive testing kit
HMX	High velocity military explosive (octahydro- 1,3,5,7-tetranitro-1,3,5,7-tetrazocine)
IPA	Isopropyl alcohol
IR	Infra-red spectroscopy
LSPR	localised surface plasmon resonance
Max.	Maximum
MGITC	Malachite green isothiocyanate
Na_2CO_3	Sodium carbonate
NaOH	Sodium hydroxide
$NaNO_2$	Sodium nitrite
NED	N-(1-naphthyl)ethylenediamine
ng	Nanogram
nm	Nanometres

NNA	Nanosecond neutron analysis
NO_2^-	Nitrite ion
NO_3^-	Nitrate ion
NP	Nanoparticles
PETN	Pentaerythritol tetranitrate
pg	Picogram
pM	Picomolar
ppb	Parts per billion
ppq	parts per quadrillion
RDX	Royal Demolition eXplosive (1,3,5-trinitroperhydro-1,3,5-triazine)
RGB	red-green-blue
RR	resonance Raman spectroscopy
SEM	Scanning electron microscopy
SERS	Surface enhanced Raman scattering
SERRS	Surface enhanced resonance Raman scattering
t	time (minutes)
TATP	triacetone triperoxide
TEM	transmission electron microscopy
TMB	3,3',5,5'-tetramethylbenzidine
TNT	2,4,6-trinitrotoluene
UV-Vis	Ultraviolet-visible
X-ray CT	X-ray diffracted computed tomography
4-ATP	4-aminothiophenol
4-ATP-NP	4-aminothiophenol conjugated nanoparticles
µL	Micro litre
µM	Micromolar

Table of Contents

Chapter 1 : Introduction

1.1 Nanotechnology

Nanotechnology is the term used to refer to the study of objects with one dimension or more within the range of 1-100 nm, which can also be classed as the nanoscale range. For example, graphene sheets have one dimension in the nanoscale range as they are formed of a single layer of carbon atoms arranged in a hexagonal lattice. Carbon nanotubes have two dimensions in this region, and spherical nanoparticles and quantum dots are nanomaterials with three dimensions in the nanoscale.[1] When objects are on this scale, they show new chemical, physical and biological properties which are often an enhancement compared to those present in their bulk materials.[2]

A large increase of interest in nanotechnology has been observed in recent years, with research being performed in a large variety of areas, including the cosmetic industry,[3] food industry,[4] textile industry[5] and in the medical field where research is being performed for diagnostics and drug-loading.[6]

1.1.1 History of Nanoparticles

Richard P. Feynman first suggested that the capability to manipulate singular atoms and molecules existed, in his lecture entitled "There's Plenty of Room at the Bottom" in 1959.[7] This lecture is often accredited to have sparked the interest in nanotechnology and nanoparticles.

Many metals can be found as a colloidal suspension of nanoparticles, the most common of which are gold, silver, copper, and iron.[8] The most famous example of the use of nanoparticles can be seen in the Lycurgus cup (Figure 1.1),[9] a Roman goblet dating back to the 4th century. The goblet was made from dichroic glass, where gold and silver nanocrystals were unknowingly incorporated into the glass. These

nanoparticles provided the cup with unique optical properties, where the glass appears red in transmitted light and green in scattered light.[10]

Figure 1.1: The Lycurgus cup appears red in transmitted light (right) and green in reflected light (left).[9]

In 1859, Michael Faraday produced a ruby red solution when reducing aqueous chloroaurate ($AuCl_4^-$). He noted that the colour of the solution changed to blue with the addition of a salt solution. This was the first recorded synthesis of gold colloidal nanoparticles.[11]

1.1.2 Nanoparticle Synthesis

Colloidal gold and silver nanoparticles are routinely used for experimental investigations due to their ease of synthesis and functionalisation, chemical stability, and the resulting nanoparticle size and charge being reproducible.[12] Gold nanoparticles are relatively non-toxic compared to silver nanoparticles and are therefore important in the biological field. The size of nanoparticles are also very important when synthesising for biological applications. For example, passive cellular uptake of nanoparticles is much greater for smaller ones.[13] However, the Raman surface enhancement experienced by smaller nanoparticles is typically much less than the larger ones,[14] therefore, there are pros and cons associated with each and careful consideration when choosing what nanoparticle size to synthesise must be

made to achieve the best results for their given application. Silver nanoparticles are optically brighter than gold nanoparticles as they have a higher scattering to absorption ratio and the surface plasmons are more polarisable.[15] However, silver nanoparticles are more difficult to work with as they are easily photo-oxidised.[16] Despite the disadvantages listed, both metallic nanoparticles are particularly attractive for research.

Many different nanoparticle synthesis methods are now available, the most common being the Turkevich method, which produces citrate reduced gold nanoparticles. This method was first reported by J. Turkevich *et al*.[17] and produces gold nanoparticles with an average diameter between 10-20 nm. 20 nm spherical gold nanoparticles typically result in an extinction profile with a maximum absorbance of ~520 nm.

P. C. Lee and D. Meisel altered the Turkevich method to allow for the synthesis of silver nanoparticles.[18] This method results in the citrate reduction of $AgNO_3$, producing silver nanoparticles with an average diameter of ~40 nm, an extinction maximum of ~400 nm and a yellow/green colour.

N. Leopold and B. Lendl reported another method in which hydroxylamine hydrochloride could be used as a capping agent for silver nanoparticles.[19] This produces nanoparticles with an average diameter of ~25 nm, an extinction maximum of 408 nm and a green/brown colour.

The resulting size of the spherical nanoparticles can be increased by altering the existing synthesis methods, such as varying the citrate to gold ratio. The increase in size results in an increase in wavelength, which changes the colour of the solution (gold nanoparticles go from ruby red to blue, silver nanoparticles go from green/yellow to brown) and the extinction maxima, recorded using UV-Vis spectroscopy, will experience a red-shift. Altering the synthesis of nanoparticles can also result in a variety of differently shaped nanoparticles including rods, stars, cubes

and spheres.[20] These changes result in different optical properties and ultimately widens their potential applications.

1.1.3 Optical Properties of Nanoparticles

Gold and silver nanoparticles absorb in the visible spectrum of light. Specific colours for each are observed by eye, [21] and are dependent on the diameter and shape of the particle. The colours result from the excitation of the conductance band electrons when coupled with light of a specific wavelength. To characterise the 'colour' nanoparticles can be investigated by extinction spectroscopy. Other important characterisation techniques including dynamic light scattering (DLS) and zeta potential which determine the diameter, shape and stability of the nanoparticle. DLS works by measuring the Brownian motion (random motion of particles suspended in a liquid or gas) and relating this value to the size of the nanoparticle. For example, the Brownian motion will be smaller for larger particles, as they will experience slower movement.[22]

The zeta potential of nanoparticles is either positive or negative depending on the molecules or capping agents present on the surface of the nanoparticle. In general, the larger the zeta potential value, the more stable the nanoparticle is due to repulsion. Citrate reduced silver nanoparticles have electrons surrounding their surface which provide the nanoparticles with a negative zeta potential. These electrons come from the citrate groups used to stabilise the nanoparticle.

Scanning electron microscopy (SEM) and transmission electron microscopy (TEM) can also be used to characterise the nanoparticles as the electrons in the beam will interact with the atoms in the particles, thus resulting in information about particle size and even composition. The main difference between these two techniques is that SEM detects reflected or secondary electrons which are emitted by atoms excited by the electron beam, and TEM uses electrons passing through the sample to create an image.[23]

1.1.3.1 Localised Surface Plasmon Resonance

Metal nanoparticles are surrounded by a cloud of oscillating electrons, which can be referred to as the nanoparticle surface plasmon. The oscillation frequency of a surface plasmon depends on the shape, metal type, size, interparticle distance and the composition of the nanoparticle solution's environment. If an electromagnetic wave (or radiation) contains photons with a similar frequency that matches the natural oscillation frequency in the metallic nanoparticles, then the conductive band electrons of the nanoparticle will collectively oscillate with the electromagnetic wave. This optical spectacle is known as localised surface plasmon resonance (LSPR). (Figure 1.2).

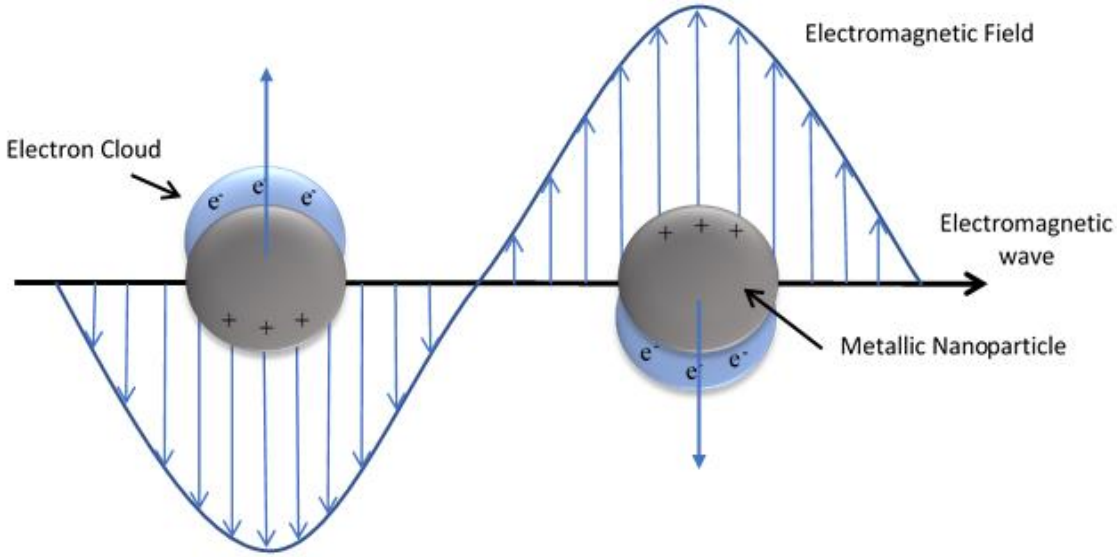

Figure 1.2: A schematic representation of surface plasmon resonance. The interaction between the electromagnetic field and the metallic nanoparticles causes a displacement of electrons in the opposite direction to the field. This results in a charge difference across the sphere.

Gustav Mie pioneered a theory in 1908 which explained the LSPR phenomenon that spherical particles under 100 nm experience.[24] Mie proposed that as the spherical nanoparticle diameter increases, the LSPR wavelength will increase. This results in a larger frequency due to the larger surface plasmon present in each nanoparticle. This theory can be observed when comparing gold nanoparticles of different sizes. 10-20 nm gold nanoparticles are deep ruby red in colour and have an LSPR around 500 nm

whereas larger diameter gold nanoparticles (80-100 nm) are purple and the LSPR red shifts to 550-600 nm. The LSPR can also be influenced by the shape of the nanoparticle, the interparticle distance, by the nanoparticles surrounding environment and by the nanoparticle material. For example, the LSPR shape influence can be observed in nanostars, where the plasmon will change depending on the length of the nanostar arms, large particles being more effective at scattering at longer wavelengths when compared to smaller particles. Nanoparticle aggregation also affects the interparticle distance, causing an LSPR red shift to be experienced. Nanoparticle metal type also results in different LSPR maximums, with silver nanoparticles generally having an LSPR of around 400 nm, and gold at around 500 nm.

Conjugation of a molecule (affected by the nanoparticle surrounding environment) to the surface of a nanoparticle also affects the LSPR as the dielectric constant surrounding the nanoparticle changes. These LSPR changes can be monitored and therefore used in detections schemes, such as the glucose detection device in serum by Laura et al.[25]

1.2 Raman Scattering Spectroscopy

There are three main ways in which light can interact with a molecule; the light is either scattered, absorbed or transmitted by the molecules. Vibrational spectroscopy can be broadly divided into two approaches which exploit scattered (Raman) or absorbed (Infra-red) light. IR and Raman spectroscopy are techniques which can observe the rotational, vibrational and other low-frequency modes of a system.[26] IR and Raman tend to be complementary when measuring bond vibrations, as any given bond vibration in a molecule with a centre of symmetry contains vibrations can be either Raman active or IR active, but not both. This is known as the principle of mutual exclusion.[27] Any given bond vibration in a complex molecule, which has no centre of symmetry, can potentially be both Raman and IR active, however, rarely are both observed simultaneously. A schematic representation of Raman (A) and IR (B + C) active stretches can be found in Figure 1.3.

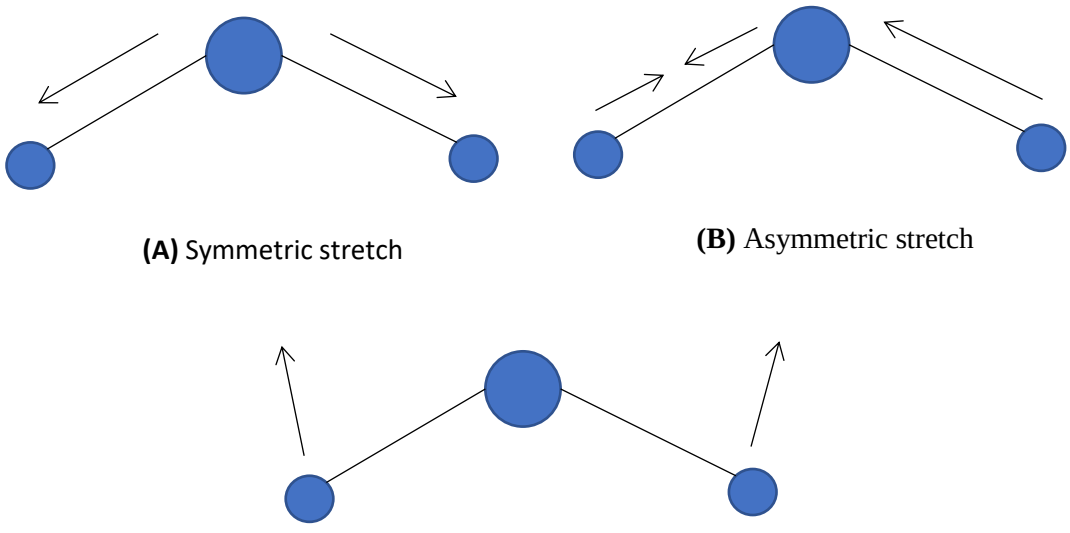

Figure 1.3: A schematic representation of the different modes of bond vibration in a triatomic molecule. ***(A)*** *Symmetric stretching, where there is no change in dipole moment observed but there is a change in polarizability, therefore this is a Raman active stretch.* ***(B)*** *Asymmetric stretching, where there is a resulting dipole change in the molecule and* ***(C)*** *Bending, which can be wagging, twisting, scissoring or rocking. Depending on the type of bending, a change in dipole moment can be observed. Both* ***(B)*** *and* ***(C)*** *represent IR active stretching modes.*

In general, for a molecule to be Raman active, it must be able to undergo a change in polarisability of the electron cloud surrounding a molecule during the particular vibration (Figure 1.3 (A)). During light scattering, the light interacts with the electron cloud surrounding a molecule and creates a polarised state that is short-lived and unstable, and therefore when the electron cloud relaxes, scattering occurs.[28] The scattering of light by molecules can be broken down into two events; elastic and inelastic scattering. Figure 1.4 illustrates the different types of scattering associated with monochromatic light.

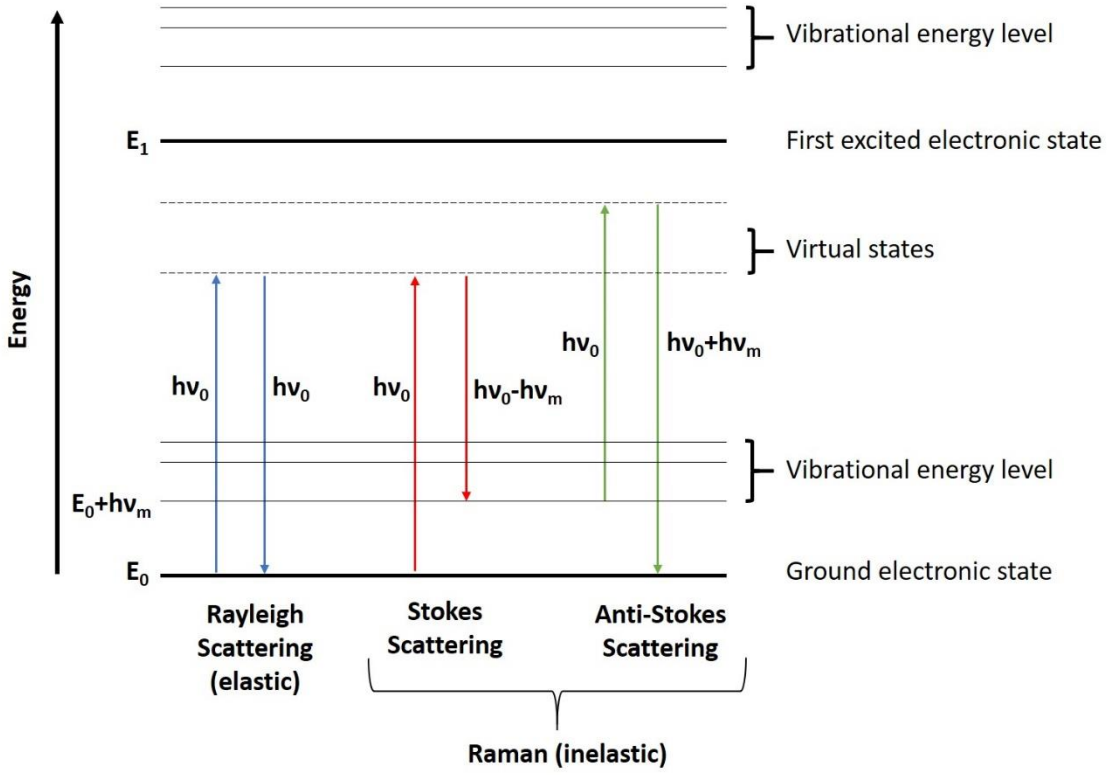

Figure 1.4: Jablonski diagram depicting the energy transitions that occur for Rayleigh (blue), Stokes (red) and anti-Stokes scattering (green).$h\nu_0$ is the energy of the incident light, $h\nu_0$- $h\nu_m$ and $h\nu_0$+ $h\nu_m$ is the energy of the emitted Raman scattering respectively after Stokes and anti-Stokes

Elastic, or Rayleigh scattering (blue), is where an electron in the molecule is excited from the ground electronic state to a virtual state. The incident photon exciting the molecule will have the same energy as the scattered photon emitted when the electron returns to the ground electronic state.[28]

Occasionally the scattered photon has a different amount of energy than the incident photon. This leaves the molecule in a changed quantum state and is called inelastic scattering, or Raman scattering. Inelastic scattering can be separated into a further two events. Stokes Raman scattering (red) occurs when the molecule is promoted to a virtual state, and then relaxes into a higher energy state than the original state. This means that energy is gained by the molecule and the scattered light is of lower energy. Anti-Stokes Raman scattering (green) occurs when the molecule is promoted to a virtual state from a state of higher energy than the ground state. The molecule then relaxes to a state of lower energy than the initial state. This means that energy is lost from the molecule and the scattered light is of higher energy.[29]

The Boltzmann distribution equation (Equation 1) can be used to determine the ratio between Stokes and anti-Stokes scattering at different temperatures, where N_1 is the number of molecules in a high vibrational state, N_0 is the number of molecules in a low vibrational state, g is the degeneracy of the electron levels, ΔE is the energy difference between different energy states, k is the Boltzmann's constant (1.3807 $x10^{-23}$ J K^{-1}) and T is the temperature (K).

Equation 1: Boltzmann distribution equation

$$\frac{N_1}{N_0} = \frac{g_1}{g_0} \exp\left[\frac{-(\Delta E)}{kT}\right]$$

It is found at low temperatures, that more molecules will be in the lower vibrational state, and therefore the Boltzmann distribution equation shows that Stokes scattering will be more intense than anti-Stokes at this temperature. At higher temperatures, this ratio switches.[30]

Spontaneous Raman scattering is very weak in comparison to Rayleigh scattering, as only 1 in 10 million photons incident to a sample are inelastically scattered.[31] The intensity of it can be calculated using equation 2 where I is the Raman intensity, K is a constant, I_L is the power of the laser, α is the polarizability and ν is the frequency.

Equation 2: The intensity of Raman scattering

$$I = KI_L\alpha^2\nu^4$$

This equation explains that the intensity of Raman scattering of a molecule can be affected by two factors controlled by the analyst, the power and the frequency of the laser. The intensity of this signal can be maximised by either increasing the laser power, which has a directly proportional relationship to the intensity, or by increasing the frequency which is proportionate to the 4th power. However, when choosing the laser frequency, the molecular properties need to be considered, as they might absorb light in specific regions of the UV spectrum, causing either sample degradation or fluorescence.

Elastically scattered radiation can be filtered from the collected light when it contains a similar wavelength to the incident laser, thus making Raman scattering spectra simpler to interpret than spectra containing both elastic and inelastically scattered radiation. While Raman scattering can be used to detect strong vibrational bonds, for example the tracking of alkynes in cells,[32] methods must be used to increase the resulting signal for molecules with weaker Raman cross-sections.

1.2.1 Resonance Raman Scattering

One method of increasing Raman scattering intensity is to use a laser frequency that is close in energy to the absorbance maximum or electronic transition of the molecule of interest. Instead of the molecule being promoted to a virtual state within the ground electronic state, as seen in Raman scattering, the molecule is excited to a virtual state existing in the first excited electronic state. The change in state will result in enhanced molecular vibrations and increased polarisability of the molecules, therefore enhancing the Raman signal. This type of scattering is known as resonance Raman scattering and can result in an increased Raman intensity of factors up to 10^4.[33]

Resonance Raman works well with chromophores that have an absorbance maximum which lies within the visible region, rather than the ultra-violet or infra-red region, thus allowing for the use of a laser closer in energy to the molecules absorbance maximum. By using a less energetic laser, sample bleaching and burning can be avoided. Laing et al[34] proposed a method of using resonance Raman scattering to detect 3,3',5,5'-tetramethylbenzidine (TMB) which is conventionally used in enzyme-linked immunosorbent assays (ELISA). This resulted in improved quantification of TMB in solution when using a resonant laser wavelength. Molecules with chromophore regions are usually fluorescently active which causes problems as fluorescent signals have longer excitation state lifetimes and generally result in stronger signals than the weak Raman signal, therefore overwhelming the signal.[35] Consequently, another method must be used to increase the Raman signal further, and combat the fluorescence signal.

1.2.2 Surface-Enhanced Raman Scattering Spectroscopy (SERS)

Nanoscale surface roughened metallic surfaces can be used to increase the Raman scattering in a technique called surface-enhanced Raman scattering (SERS) which is capable of increasing the Raman scattering up to 10^7 - 10^{10}.[36]

There are two proposed mechanisms which are associated with the enhancement observed in SERS – electromagnetic and chemical enhancement. While there is much debate on which enhancement is the strongest, it is believed that electromagnetic is the greater of the two.[37]

Electromagnetic enhancement originates from the interaction between an incident electromagnetic wave of the adsorbed molecule and the electrons on a roughened metal surface. The electrons in the molecule adsorbed on the surface interact with the electron cloud of the surface plasmon, causing greater polarisation around the molecule as electron transfer occurs. This transfer will form new electronic states and contribute to the Raman signal enhancement. This increase in polarisation

directly affects the Raman intensity observed as field intensity and polarisability are directly proportional to intensity strength. The greatest enhancement occurs when the plasmon oscillations are perpendicular to the surface, as in-plane oscillation will only absorb rather than scatter the light, and when the laser excitation radiation is in resonance with the plasmon of the roughened metal surface. Perpendicular oscillation of the surface plasmons are achieved only when the surface is roughened, as the plasmon is located in the valleys of the roughened surface and light will be scattered as the plasmon traverses up to the peaks.[38]

Chemical enhancement describes the charge transfer between the metal surface and a molecule bound to the metal surface. This charge transfer or bond creates a new state which is in resonance with the laser excitation wavelength and largely increases the polarisability of the adsorbed molecule.[37]

SERS signals are strongest in the presence of electromagnetic 'hot spots'. One method of creating a hotspot is observed in the creation of nanoparticle dimers and trimers,[39] where a colloidal solution of nanoparticles is aggregated resulting in an enhanced SERS signal. Aggregation causes nanoparticles to form clusters, when the particle gap is less than 1 nm this creates highly confined areas containing enhanced local electromagnetic fields. This allows the interparticle plasmons to interact, concentrating the incident electromagnetic field and amplifying any molecular vibrations of the analyte. This 'hot-spot' creates an intense SERS signal for any molecules within proximity to the particle.[40] Braun et al[41] used a Raman active molecular linker to create nanoparticle dimers and small clusters which enhanced the resulting SERS signal.

Another method of creating a hot spot is to fabricate them onto surfaces. Kamińska et al[42] used this method by fabricating gold-coated nanopillars which obtained SERS enhancements of the order of 2.8 $x10^6$. These nanopillars can also be made fabricated to lean against each other after the addition of a sample, thus creating hot spots.[43]

1.2.3 Surface-Enhanced Resonance Raman Scattering Spectroscopy (SERRS)

Surface-enhanced resonance Raman spectroscopy (SERRS) is the name given to the combination of resonance Raman with SERS, resulting in combined signal enhancement. This occurs when an analyte has a chromophore containing an absorption maximum which is close in energy to the laser wavelength used to excite the plasmon of the roughened surface. The fluorescence of these chromophores is quenched by using a roughened surface resulting in improved spectra, and enhancement from the metal surface is observed as SERS occurs. The combination of these effects results in a large increase in SERS intensity up to 10^{14}.[37, 44] Many commercially available Raman reporters such as malachite green isothiocyanate (MGITC)[42] and 4-mercaptobenzoic acid (4-MBA) are often used in SERRS spectroscopy. Another example of SERRS can be found in Keir et al's work, where a microflow cell designed to detect an azo dye derived from an explosive was used to detect limits down to 10 femtomolar.[45]

Most of the methods above have described labelled detection, which uses Raman active linkers and dyes. Label-free assays can also be used to detect molecules, however, the molecules are required to be Raman active to obtain a signal. One of the reasons explosives are so difficult to detect using SERS spectroscopy is that the explosive molecules usually don't contain thiols to assist binding to the nanoparticle surface, or chromophores which can be easily detected using resonance Raman or SERRS.

1.3 An Introduction to Explosives

> Terrorism is defined as "The unlawful use of violence and intimidation, especially against civilians, in the pursuit of political aims." – *Oxford English Dictionary*[46]

Violent acts of terror have risen across the world, occurring countless times a year, often with serious repercussions such as the loss of innocent lives. With the

advancements in technology over the past 100 years and information being readily available online, national security threats are even more of a problem than before. Explosives, in the form of bombs, are one method in which these attacks can occur.

In recent years, there have been many bomb threats that have either been successful and have taken many lives, or that have been detected and stopped before they occurred.

In 2009, Umar Farouk Abdulmutallab, nicknamed as the "underwear bomber" was arrested for a terrorist attempt on a flight from Amsterdam to Detroit. He concealed a packet of explosives, containing pentaerythritol tetranitrate (PETN) and triacetone triperoxide (TATP), by sewing them into his underwear.[47] These were not detected during the usual screening process found in airports and were only discovered during the flight. While in the air, Abdulmutallab attempted to set his trousers alight under a blanket to ignite the explosives, however, the explosives failed to properly ignite as they had been stored in Abdulmutallab's underwear for some time. It is reported that a fellow passenger, Jasper Schuringa, noticed the fire and subdued Abdulmutallab before the explosion could properly occur.[48]

However, luck is not always on our side. In 2017 Salman Ramadan Abedi was a suicide bomber who attacked the Manchester Arena during a concert. The device he used was carried in a backpack and filled with TATP.[49] It was also packed with nuts and bolts which acted as shrapnel, killing 23 people including the attacker and injuring over 500 others.[50, 51]

Obviously, terrorist attacks can have dreadful consequences if not prevented through intel or detection of explosives. However, the detection, especially of high-grade explosives, is incredibly difficult as they produce very small amounts of vapour pressure. Methods of detection which involve vapour pressure need to be very sensitive and have low detection limits for terrorist attacks to be prevented.[52]

Therefore, research into the sensitive detection of explosive molecules is very important.

1.3.1 Classification of Explosives

Black power, also known as gunpowder, was the first recorded chemical explosive to be synthesised in 9th century China.[53] It was used almost exclusively for signals, firecrackers and fireworks before it was weaponised into fire arrows during the 10th century.[54] By the 13th century, bombs and guns had been developed, thrusting warfare into a whole new era.[55]

Black powder consists of a mixture of sulfur, carbon and potassium nitrate. These ingredients can be split into two categories, the fuel (carbon and sulfur) and the oxidiser (potassium nitrate). The oxidation or decomposition of the oxidiser releases a large amount of energy. This energy can be expressed as both thermal and kinetic energy, rapidly expanding and heating the surrounding gas in a short period of time. The energy expands in all directions from the origin centre with respect to time (t), travelling faster than the speed of sound. Energy is expended in heating the surrounding medium, thus dissipating as it travels further from the centre. This

phenomenon is known as a shock wave (Figure 1.5), which can be very destructive to surroundings. [56]

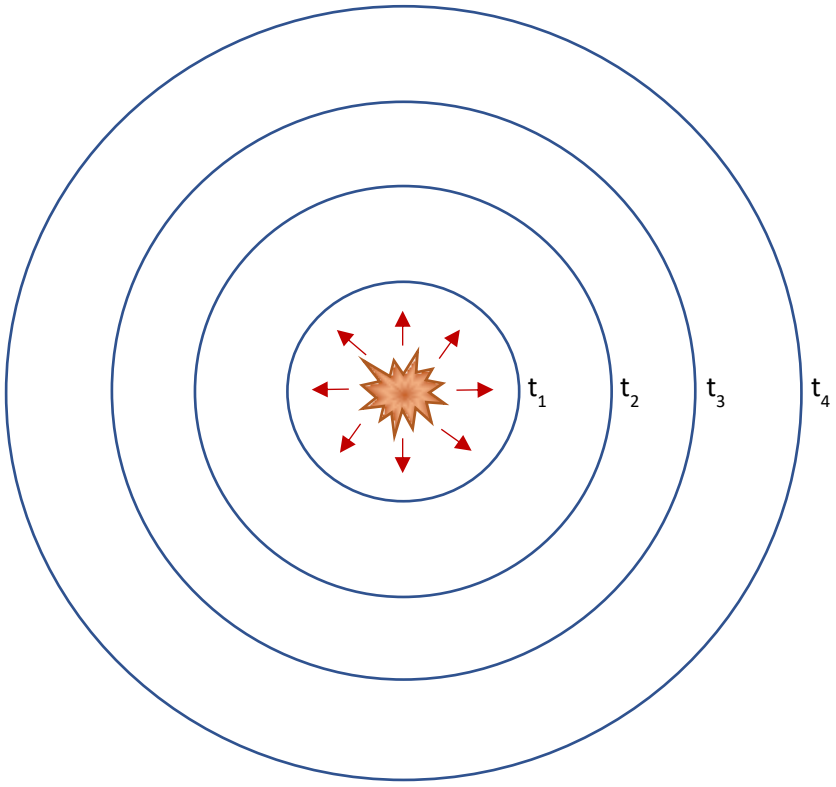

Figure 1.5: Diagram of a shock wave. The wave originates from the centre of the explosion, and propagates out equally, in all directions. As time (t) proceeds, the wave will expand, and the energy will decrease with distance from the detonation centre.

Explosions can be divided into three categories: physical, atomic and chemical.[57] Physical explosions occur when a gas or liquid undergoes a rapid physical transformation while under compression. The potential energy of the gas or liquid is converted to kinetic energy, that results in a shockwave. An example of a physical explosion would be the eruption of a volcano, where the crust of the earth ruptures, allowing lava and gases to escape confinement. Atomic explosions, also known as nuclear explosions, produce significantly larger quantities of energy than physical or chemical explosions (10^6 - 10^9 times larger).[57] The shockwaves produced last longer than chemical explosions, and the products of the explosion include several radiation species (gamma, infra-red and ultra-violet radiation) that can be harmful to the body resulting in a large, fatal exposure to neutrons for those in close vicinity to the

explosion. A chemical explosion results from a change of state of a substance, from solid to gas, or from a chemical reaction that happens in a very short timeframe and results in the rapid exothermic production of gases and vapours. Due to the speed of the reaction, the new gases and vapours fill the area in the container previously occupied by the explosive material for a fraction of a second. The change in state and the subsequent high temperature of the gases results in a rapid increase in pressure in the holding container, causing the gases to expand and escape in a "blast wave", or a shockwave as seen in Figure 5.[57]

Technology involving explosives had come a long way since the 9th century. However, one thing that has not changed, which is that for any substance to be classified as a chemical explosive, it must contain a fuel and an oxidiser.[58] Many organic compounds can be considered explosive if they contain the elements oxygen, nitrogen, carbon and hydrogen, as these elements are oxidizable, and can therefore be labelled as fuels.[59] In many explosives materials, oxygen and nitrogen are often found coupled in nitro groups like NO, NO_2 and NO_3. Explosive azides, like lead azide (PbN_6) and azoimide (HN_3) are the exceptions to this, as they are nitrogen compounds containing no oxygen. Lead azides are quite unusual as the energy in a chemical explosion usually comes from the separation of the nitrogen and oxygen atoms. This releases a large amount of energy and results in the formation of hot (energetic) gases.

Chemical explosions are the most common type and the focus of this thesis. Chemical explosions can be separated into three categories; propellants, and primary and secondary explosions, which are classified depending on the rate of detonation.[60] The rate of detonation is the measure of the velocity of the expanding gases after the explosion (detonation velocity). In general, the larger the detonation velocity is, the more destructive the explosion.[61]

Propellants are materials containing all of the oxygen needed for combustion. Ignition only requires a flame or a spark, and the material burns slowly rather than exploding. Burning proceeds rather violently, but the propellant will change from a

solid to a gas relatively slowly in comparison to primary and secondary explosives.[62] One major difference between propellants and primary and secondary explosives can be found from listening and viewing the compound during burning or detonation. Propellant burning is accompanied by the visuals of flames and sparks, and hissing or crackling will be heard, whereas a loud and sharp bang will be heard during a detonation.

Primary explosives are very sensitive to external forces such as impact, heat, electric spark and friction.[63] This sensitivity causes the molecules to dissociate and results in a vast amount of heat and energy being released, which can be readily transmitted to more stable explosives. The ease with which primary explosives detonate makes them very useful in initiating devices, such as detonators, primers and blasting caps.[64] In general, primary explosives usually have a detonation rate of around 2000 to 5500 m/s.[65]

Secondary explosives have a very large rate of detonation, which is usually greater than 5500 m/s. Like primary explosives, on initiation the compound almost instantaneously dissociates into atoms, before reforming into more stable components, which are usually gases or liquids like water. However, unlike primary explosives, secondary explosives do not readily go from deflagration to detonation with external forces like friction and impact, usually requiring more energy to detonate. They are much less sensitive, and detonation can only be initiated by the shock produced from the explosion of a primary explosive, which is why primary explosives are so often used in initiating devices. The majority of the energy expelled in an explosive reaction is obtained from the oxidation process, therefore the amount of oxygen available is crucial. In general, most secondary explosives contain more oxygen than primary, making them more powerful, and the resulting detonation much larger. As secondary explosives are more powerful than primary explosives, they are often used in military, mining and demolition operations.

The three categories of explosives are shown in Table 1, which also contains examples of each category.

Table 1: Three categories of explosives with named examples for each category, and their detonation velocity.[66]

	Explosive Name	Detonation Velocity (m/s)
Propellant	Black powder	630
Primary	Mercury fulminate	4250
	Lead azide	4630
Secondary	Trinitrotoluene (TNT)	6900
	Pentaerythritol tetranitrate (PETN)	8400
	1,3,5-Trinitro-1,3,5-triazinane (RDX)	8750

Classification of chemical explosives can be accomplished in several ways other than their detonation velocity used in Table 1. Chemical explosives can also be separated based on source and use or application which is usually split into three categories; military, commercial and homemade explosives. Separating chemical explosives based on use and detonation velocity works well as in general the higher velocity explosives are used in the military and the lower velocity ones are used in industry. Several examples of these two categorising methods being combined can be found in R. Akhavan's "The Chemistry of Explosives"[57], in J.P. Agrawal's "High Energy Materials: Propellants, Explosives and Pyrotechnics",[62] and most recently in T. Klapötke's "Chemistry of High-Energy Materials".[67]

Another major way of categorising explosives is by their chemical composition. Van't Hoff originated this method in 1909 by suggesting separating explosives into groups depending on their molecular groups.[68] Many other scientists have further developed this idea by adding more groups, and now the list is quite specific. The grouping

focused on in this thesis are the nitro-explosives. Nitro-explosives, in general, are secondary explosives as they are highly energetic, and are therefore very dangerous.[69] The nitro-explosive group can be further divided into nitro-aromatic, nitro-aliphatic, nitrate esters and nitroamines, the names of which depend on which atom the nitro group is chemically bonded to.

Trinitrotoluene is a nitro-aromatic molecule, discovered in 1863 by Julius Wilbrand. In 1870, F. Beilstein and A. Kuhlberg identified the 6 different isomeric forms trinitrotoluene could exist in, the most common being 2,4,6-trinitrotoluene (shown in Figure 1.6), which is now the form generally known as TNT.

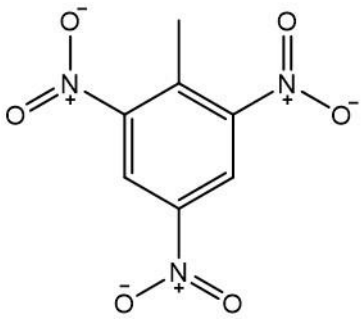

Figure 1.6: Structure of 2,4,6-trinitrotoluene (TNT)

TNT was used extensively as a yellow dye in the chemical dye industry, which was only just emerging at the time. In 1904 TNT was developed as an explosive,[70] and was widely used in the military before World War 1. It is an attractive explosive as, despite its low volatility and chemical stability, TNT has high explosive power. Upon detonation, TNT undergoes the following decomposition:

$$4\ C_7H_5N_3O_6 \rightarrow 6\ N_2 + 10\ H_2O + 7\ CO_2 + 21\ C \quad \text{or}$$

$$4\ C_7H_5N_3O_6 \rightarrow 6\ N_2 + 10\ H_2O + 14\ CO + 14\ C$$

It is understood that equilibrium favours the formation of gasses at high temperatures and pressure, therefore the driving force of the reactions above is the formation of

the gaseous products. At lower temperatures, the gaseous products are not favoured, and the slower release of energy usually produces solid carbon products like graphite and diamond.

Currently, TNT is still one of the most used explosives due to the many handling and manufacturing advantages. On top of its low volatility and chemical stability, TNT has quite a low cost of manufacturing and materials, is one the safest secondary explosives to handle because of its low sensitivity to impact and friction, and its low melting point makes it an ideal explosive for casting (where the explosive is melted, and the molten mixture poured into a form). TNT's purer, more crystalline form is currently used for military purposes in landmines, bombs, missiles, and guns[71] as the more crystalline form will contain larger explosive power. The less pure form is used for commercial use, such as underwater blasting.[72] TNT is also very compatible with other secondary explosives, making it an ideal explosive to put in mixtures other secondary explosives.

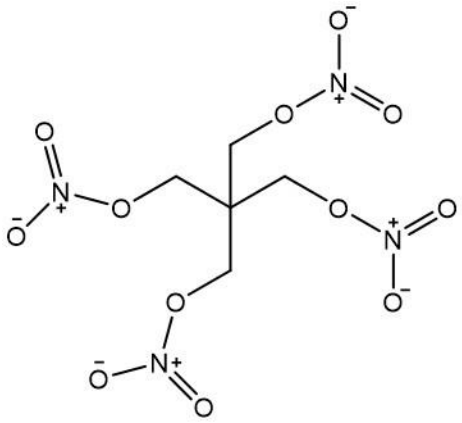

Figure 1.7: Structure of pentaerythritol tetranitrate (PETN)

Pentaerythritol tetratnitrate, known as PETN, is a nitrate ester molecule which was discovered and patented in 1894 by Bruno Thieme on behalf of an explosives manufacturing company in Germany.[73] It was first introduced as a commercial explosive with a shattering effect during World War 1, where it was used by the German military. PETN (shown in Figure 1.7) is one of the most stable and least reactive of the explosive nitric esters, which also makes it one of the most powerful

nitro-based explosives. Its stability and insensitivity to friction make PETN slightly more difficult to detonate in comparison to TNT, therefore stronger detonators are required to achieve the higher temperature and increased pressure needed for PETN detonation.[71] Upon detonation, PETN undergoes the following decomposition:

$$C_5H_8N_4O_{12} \rightarrow C_5H_8N_3O_{10}^- + NO_2$$

In the absence of water, is it assumed that the decomposition of aliphatic nitrate esters involves the reversible scission of the O-NO_2 bond, which results in a by-product of NO_2. However, 10 other by-products have been identified upon the high-temperature decomposition of PETN. These include CH_2O, N_2O, NO, CO_2, CO, H_2O, CH_3OH, HNO_2, CH_3NO_2 and $(O_2NOCH_2)_3C\text{-}CHO$.[74]

In its purest form, PETN is a colourless crystal that is still sensitive to friction and impact, and as the PETN detonation velocity is large, PETN crystals are usually desensitized with 5 % - 10 % paraffin wax, or by mixing with plasticisers or polymers. By desensitising PETN with other compounds, the energy from friction or impact will be absorbed first into the contaminant making it less likely that PETN will unintentionally react. PETN is very sensitive to initiation by other explosives and therefore the addition of other secondary explosives to PETN with other stabilising components can have a dual effect of desensitising PETN and thus increasing the stability for handling, whilst also allowing the PETN explosion to be more easily initiated by the detonation of other explosives, like TNT and RDX, which require less energy to initiate.[71] When mixed with TNT in a 50:50 ratio, a compound called pentolite is formed. Pentolite can be used for the loading of small calibre projectiles and grenades, as well as booster chargers.[62] Mixing PETN with RDX and the appropriate amount of solvent creates an explosive plastic mixture called Semtex. By mixing PETN with other components, the resulting plastic explosives are malleable and can therefore be moulded into any required shape, thus allowing great versatility on the use. However, this versatility also has its drawbacks as the easy moulding of the explosives means that it can be more easily concealed, thus making it a desirable

explosive for terrorist events.

One of the first major terrorist attacks involving PETN occurred in the Lockerbie bombing of 1988,[75] where a cassette recorder was filled with Semtex. One hour after the scheduled gate departure, the explosive was detonated in the main body of the aircraft resulting in the death of all 259 passengers and crew, and a further 11 people on the ground as sections of the aircraft crashed into a residential street in Lockerbie, Scotland. This tragic event killed a total of 270 people, and to date remains the deadliest terrorist attack in the history of the United Kingdom. There have also been several failed bombings involving PETN. One well-known example is the "shoe bomber" in 2001,[76] where PETN was combined with TNT and a fuse in the suspect's shoe. The suspect attempted to detonate the bomb using a lit match, however, this was unsuccessful as the suspect had excessively sweated, thus stabilising the explosive material. Another example of a failed bombing attempt is the previously mentioned "underwear bomber" in 2009, where the explosive was in liquid form containing a mixture of PETN and acid.[77,78]

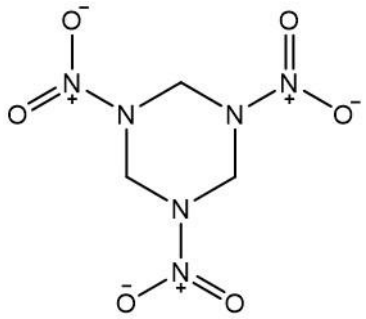

Figure 1.8: Structure of 1,3,5-trinitroperhydro-1,3,5-triazine, also known as Royal Demolition eXplosive (RDX)

1,3,5-Trinitroperhydro-1,3,5-triazine, or RDX, is a nitroamine molecule which is known by many other nicknames. In Europe, it is knowns as cyclonite or hexogen, whereas in the UK it is given the name Research Department eXplosive, Royal Demolition eXplosive or RDX for short. RDX was first prepared in 1898 for medicinal purposes by Friedrich Henning.[79] In 1920, Edmund von Herz discovered its potential

as an explosive[80], however, this was not fully explored until World War 2. RDX (shown in Figure 1.8) has high chemical and thermal stability which is not much lower than aromatic nitro explosives. RDX contains very high explosive power which is much greater than TNT and picric acid, making it an attractive explosive.[62] Currently, RDX is mostly used in military applications to fill all types of munition compounds, however, RDX can also be used in controlled demolition operations.[81]

Like other secondary explosives, RDX requires a detonator to provide the energy needed to initiate the explosion, and similar to TNT and PETN requires high temperatures and pressures to create the gaseous products as the driving forces of the reaction. Upon detonation, RDX undergoes the following decomposition:

$$C_3H_6N_6O_6 \rightarrow 3CO + 3H_2O + 3N_2$$

Like PETN, pure RDX crystals are very sensitive to impact and friction, so the crystals are generally mixed with wax, oils, grease, and other materials, which ultimately gives plastic explosives. RDX has a high melting point which can be lowered by mixing with TNT, thus allowing casting to be more easily performed. As previously mentioned, RDX can also be mixed with PETN, to create Semtex.

As RDX is both more stable and contains a greater detonation velocity than TNT, it is often used in terrorism. As previously mentioned, the Lockerbie bombing in 1988 was one of the first major terrorist events using Semtex, which contains RDX. In 1993, the Bombay bombings occurred where a series of 13 coordinated car bomb attacks killed 257 people and injured a further 1400.[82],[83] Most recently, in the 2019 Pulwama attack, a convoy of vehicles transporting Central Reserve Police Force personnel were attacked by a suicide bomber in a vehicle containing an estimated 80 kg of RDX, resulting in the death of 40 people.[84]

All three of the compounds introduced are nitro-based explosives commonly used as weapons in terrorist events. These explosives are of particular concern as

nitroaromatic compounds are released after the detonation and absorbed into the skin which is extremely dangerous as they have carcinogenic and mutagenic properties.[85] In the aftermath of the First World War, there were 475 deaths and 17,000 cases of poisoning relating to exposure to TNT. The deaths were due to toxic hepatitis or aplastic anaemia.[86]

The main focus of this thesis is to detect trace levels of PETN, however, RDX and TNT will also be briefly investigated in Chapter 4. Trace level detection of these explosives are very important as not only do they pose a security threat, but the compounds themselves are also toxic.

1.3.2 Current Methods for Detecting Explosives

With such an increase in security threats in recent years, it is extremely important to develop a fast and simple method of detecting trace amounts of secondary explosives such as TNT, PETN and RDX. Currently, the most common techniques that are relied upon in airports are X-ray diffracted computed tomography (X-ray CT)[87] or X-ray diffraction imaging,[88] ion-mobility spectroscopy[89] and, to a lesser extent, trained detection dogs.[90] However, the nitro explosives produce very small amounts of vapour pressure,[91] thus making it difficult to detect using vapour techniques such as ion-mobility spectroscopy and trained detection dogs.

After the attack on the World Trade Center on September 11th 2001, the American Federal Government passed an act requiring 100% of hold luggage to be inspected before boarding a flight.[87] As X-ray CT has the capability of scanning vast quantities of samples in a day, with real-time analysis, it was used as the primary first point of scanning. X-ray CT involves trained staff visually monitoring the densities in a sample and flagging suspicious samples for further inspection. This type of testing relies heavily on the training and capabilities of the staff operating the X-ray CT, as they must remain vigilant while screening a vast number of bags every day. An algorithm using density-based calculations are employed to aid the screening process,[88]

however staff must still be able to correctly interpret the results. As X-ray CT monitors densities, it is most successful detecting plastic explosives in bulk concentrations. However, the algorithm can flag anything with similar densities to explosives (including peanut butter, chocolate, and toothpaste) and any items which x-rays cannot penetrate, like electronics.[92] These results in false positives in the algorithm used to select the samples to be further investigated. While this technique is incredibly useful for its capabilities to test thousands of samples a day, there are several drawbacks such as the high cost of equipment, the fact it can only be used by trained staff and the bulky size making X-ray CT only suitable for airport use only, eliminating field applications where it could also be useful.

Another method used in bulk explosive detection is nanosecond neutron analysis (NNA), nicknamed the "neutron in, gamma out" technique on account of how it works.[93] This technique involves the irradiation of a suspicious sample with neutrons, measuring the resulting gamma radiation. This technique can identify material compositions as it can differentiate between different chemical elements as each will produce characteristic gamma radiation as a result of neutron capture, or inelastic scattering. This allows the sample to be identified as an explosive or not. Neutrons and gamma radiation are very high in energy, thus allowing explosives to be detected in barriers such as thick metal or concrete, as this intense energy gives high penetrating ability. Portable detectors can be built, thus allowing the instrumentation to be used in field analysis as well as in luggage screening. However, this technique was reported to detect 400 g of hidden explosives in 10 minutes, which is neither a small amount of explosives nor a very short time scale for the test.

Colourimetric Detection

Colourimetric testing is another method which can be used for explosive detection. Commonly used by the military, colour testing kits use chemistry discovered in the 1800s to create coloured complexes by reacting with explosives, therefore allowing it to be detected. In 1864, John Griess reported a method in which nitrite ions could

be detected.[94] This chemistry has been developed into the Griess test, where a nitrite reacts with sulfanilamide and an α - naphthylamine under acidic conditions to form an intensely coloured azo compound. The original Griess reaction has been modified many times[95] to increase properties such as sensitivity and total reaction time. The Griess reaction has also been modified to target specific types of explosives, like in the Franchimont test where nitro-amines are targeted. This test can be used to detect explosives containing both nitrates and nitrites, as it is very easy to reduce the nitrates.

Another test which is commonly used to detect explosives is the Meisenheimer complex, where a nucleophilic compound will react with a base acting as a nucleophile. In 1886, Jaroslav Janovski observed a colour change when mixing dinitrobenzene with an alcoholic mixture of an alkali.[96] In 1902 Jakob Meisenheimer further developed this technique into what is now known as Meisenheimer complex.[97] This test can be used to detect nitroaromatic explosives likes TNT. This technique can be used to identify and differentiate between different nitro-aromatic explosives, as different coloured complexes will be synthesised depending on the nitroaromatic compound and which base is used. The basic reaction of TNT to form a Meisenheimer complex is shown in Figure 1.9.

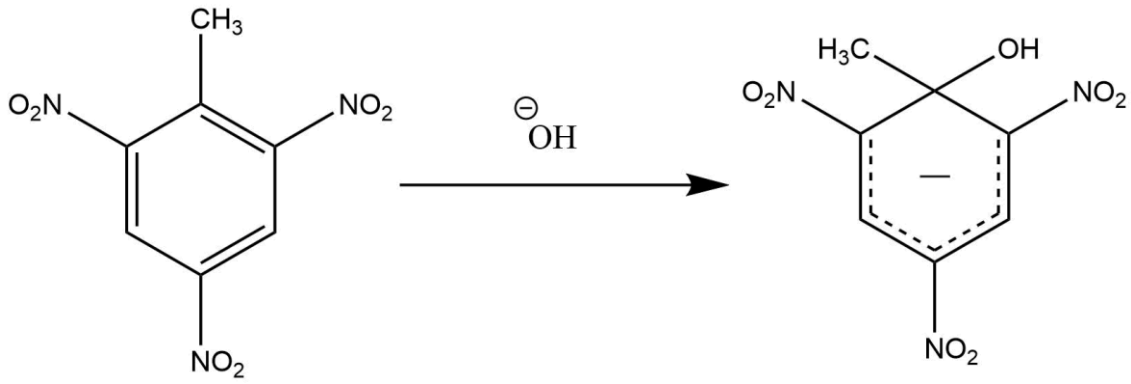

Figure 1.9: Schematic of the formation of a Meisenheimer complex from TNT.

One of the first reported field testing kits was developed in Israel in 1986 and was called an Explosive Testing Kit (ETK).[98] The kit worked in two different stages which were able to identify different types of compounds based on the two reactions explained above. In the first step, nitroaromatic compounds were detected by the formation of coloured Meisenheimer complexes, while the second step detected nitrates and nitroamines by a modified Griess reaction. The creation of a colourimetric testing kit was a ground-breaking discovery, as suddenly the test was portable. Today, colourimetric testing kits are easily bought online for an affordable price. These detection kits even boast of detection limits as low as 0.02 mg/L[99], which is comparable to some of the techniques previously mentioned.

There are a lot of positives to be gained from using colourimetric tests while examining potential explosive samples. All colourimetric tests are simple, portable, fast and require minimal interpretation from the examiner. They can be analysed by eye, or a more precise measurement can be obtained from the red-green-blue (RGB) values from digital photographs, which sometimes also allows for quantification of the sample. However, there are also quite a few disadvantages to consider. Specificity is low as most colour tests are unable to distinguish between different explosives of similar structure, only identifying groups of explosives. For example, the Griess test will react with nitrates and nitrites, but will not react to explosives without nitro groups. Another example is the Meisenheimer complex, which can only form

with nitroaromatic explosives as the aromaticity of the reacting compound is essential for the reaction to work. This lack of specificity also causes an issue with false positives, as the test will react with any compound similar in structure to the explosives, which are often found in cleaning products and pharmaceuticals. Lastly, it is hard to quantify an explosive sample using colourimetric tests and often the sample will need further testing if quantification is needed. There are a lot of advantages and disadvantages to using colourimetric tests, however, they are indispensable for preliminary testing, onsite, as they can identify samples which might need further investigation.

Spectroscopic Detection

One method which allows trace explosives detection is ion mobility spectroscopy. Ion mobility spectroscopy is a fast and simple technique often used in conjunction with X-ray CT in airport security. In this technique, a sample is swabbed, introduced into the system and then ionised. The samples' ions will become separated based on the ion's mobility in a buffer gas, and on the mass of the ion, lighter ions eluting faster than heavier ions. The results will then be compared with a library of documented materials, where it will flag a warning if it has tested positive for explosive material. This method can detect both vapours and residues of explosives, however, it does not perform particularly well for the secondary explosives focused on in this thesis, or on homemade explosives not containing nitro groups. While able to detect picogram (pg) values of TNT and RDX, PETN requires significantly greater activation energy to ionise and thus is much more difficult to detect using this method.[100] Furthermore, moisture and temperature also affect the quality of the samples and can lead to false positives.

Another common method used in vapour explosive detection is the use of detection dogs, where canines are trained to detect low concentrations of specific molecules such as narcotics and explosives.[101] While it is difficult to pinpoint an exact range, detection dogs have been able to detect certain compounds to the parts per billion,

and even the parts per trillion range for volatile compounds.[102] The performance of detection dogs can even increase when the soil moisture content is high, as the water molecules compete with the explosive molecule binding in the soil, thus releasing more explosive vapour. However, the time and cost taken to train the canines are vast and they require frequent breaks when working, otherwise, the number of false positives significantly increases due to being tired. Detection dogs are obviously unable to communicate the identity of the explosive, and therefore they should only be used for preliminary testing, despite their ability to detect trace concentrations.

Spectroscopic analysis techniques such as fluorescence have been shown to provide one way in which trace amounts of explosives can be detected. In 2007, Andrew et al[103] reported a fluorescent turn-on mechanism which selectively reacted to nitroamine and nitrate ester explosives over nitro aromatic ones. Using a photostable zinc compound, a concentration-dependent 480 nm intensity emission was found upon reaction with RDX and PETN, allowing for detection limits as low as 7×10^{-5} and 1.3×10^{-4} M respectively. Wang et al [104] also developed a fluorescent sensor molecule which quenched its fluorescent properties when reacting with NO_2 radicals and cations obtained from the UV irradiation of RDX and PETN. They also created a substrate which contained a large surface area capable of detecting RDX and PETN LODs of 0.2 nanogram (ng) and 0.3-3 ng respectively, and a spray kit which could be directly used for naked-eye detection.

One of the problems highlighted in the colourimetric testing section is the lack of specificity which is a result of some explosives having similar structures and functional groups. This can be solved by using antibodies which have highly specific binding ability and possess the capability to target analytes, which could be an explosive, at low concentrations.[105] Anderson et al. demonstrated a competitive bead-based fluid array immunoassay involving antibodies for PETN detection. Here, the fluorescence decreased with increased levels of free competitor PETN conjugates, thus making a negative assay.[106] Chaudhary et al developed an

immunochemical detection assay where PETN, RDX and TNT were immobilised on explosive specific antibody functionalised microtitre strips. UV induced photolysis of the bound explosives was performed, generating nitrite ions which reacted with a

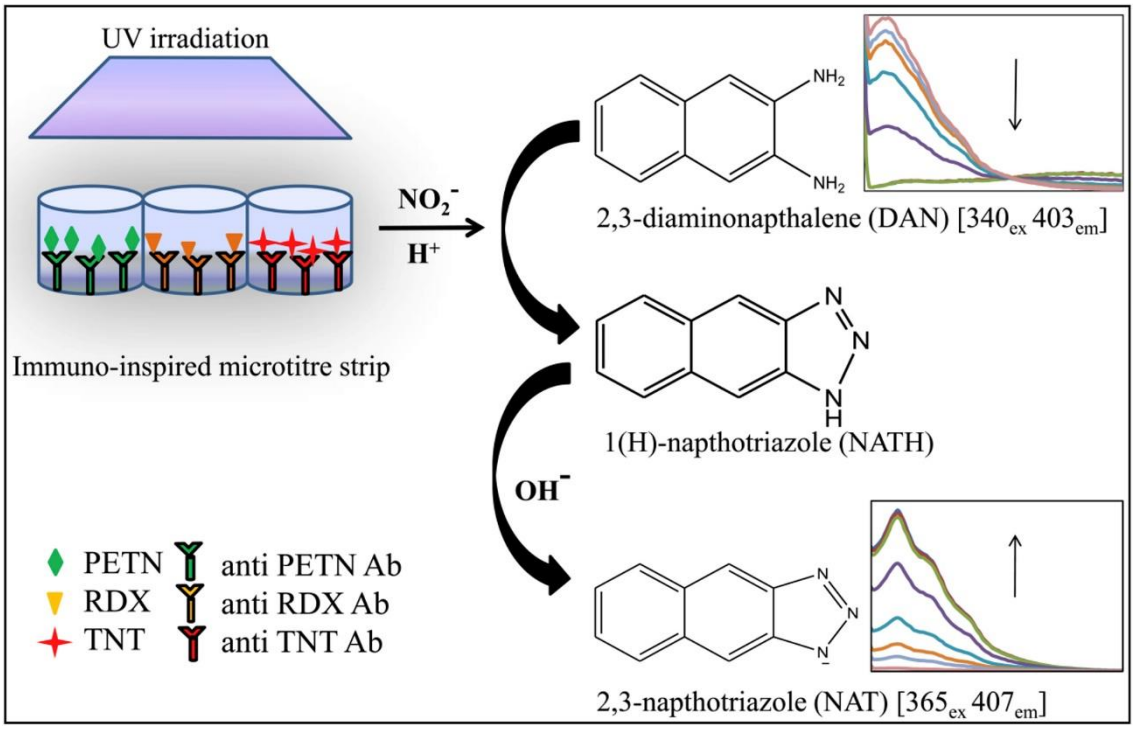

Figure 1.10: UV induced photo-fragmentation of PETN, RDX, and TNT into nitrite ions, and their subsequent reaction with DAN to form NAT in the fluorescence-based assay. [105] *Replicated with permission from* Anal. Chim. Acta, *2019,* ***1077****, 266–272. Copyright (2019) Analytical Chimica Acta.*

detector fluorophore, 2,3-diaminonaphthalene (DAN). By monitoring the decreasing levels of DAN and the increasing levels of the resulting product 2,3-naphthotriazole (NAT), detections limits of PETN, RDX and TNT were discovered to be approximately 10, 15 and 15 parts per billion (ppb) respectively (shown in Figure 1.10).[107]

Although the current methods used for detecting explosives work as well as screening methods, they often yield false positives or require bulky, expensive equipment. Therefore, it is important to research and develop methods of detecting trace amounts of explosives in a quick and reliable manner, using portable instrumentation so that in field analysis can occur.

1.3.3 Detecting Explosives using Raman Spectroscopy

As previously mentioned, Raman scattering is another spectroscopic technique which offers the advantage of producing a unique "fingerprint" spectrum for an analyte of interest. This allows the analysis of complex mixtures to be performed when more than one analyte of interest is present. However, Raman scattering is an inherently weak technique due to the fact that only 1 in 10^7 photons are Raman scattered.[37] Explosive molecules, in particular, are very small and the non-aromatic explosives have very poor Raman cross-sections, thus making it difficult to obtain Raman scattering from them. It has also been found that explosive materials experience significant resonance enhancement in the ultraviolet spectral range, therefore Raman spectra cannot be obtained without using high energy lasers. In 1994, McNesby et al used Fourier transform Raman spectroscopy to obtained Raman spectra from pure crystalline samples of the explosives PETN, TNT and RDX. Spectra were averaged from 500 spectrums taken over 18 minutes, using a Nd:YAG laser at 0.3 – 0.8 W.[108] Nagli et al discovered that the Raman spectra of certain explosives changed depending on whether the samples are interrogated in the UV spectral range, or the visible spectral range, showing a resonance Raman enhancement for the UV range.[109] Tuschel et al also showed a resonance Raman enhancement when using a 229 nm laser to interrogate TNT, PETN and RDX, where they managed to detect 100 ppb, 2200 ppb and 160 ppb, respectively.[110] However, to obtain these Raman spectra, relatively large amounts of pure samples (1 mg), high laser power and very long acquisition times were required, yet only weak spectral images were produced. The use of such high energy lasers and long acquisition times could cause laser heating of the explosives and the creation of subsequent hot spots, causing potential initiation of the explosives. However, this is more likely to occur with sensitive primary explosives than secondary ones.[111]

Advancements in Raman scattering, like SERS and SERRS, use micro and nanostructured surfaces (in solution or substrate form) and resonance to enhance

the surface plasmons of the analyte of interest, thus increasing the signal. This improvement allows Raman scattering to become a very desirable technique as it is fast, the results are reliable, it has the capability of multiplexing several analytes and the instrumentation can be portable.[112]

Often, nanoparticle solutions will be aggregated to provide a SERS enhancement to overcome the poor Raman cross-section of PETN, RDX and TNT. Jerez-Rozo et al presented a method of detecting the explosive TNT by aggregating gold and silver nanoparticle colloids. It was discovered that TNT could be detected as low as 10^{-15} g when using citrate stabilised gold and silver alloy nanoparticles.[113] Xu et al report a different method of aggregation where they attached thiol conjugated cyclodextrins (CD) to triangular gold nanoparticles. The plasmonic band of the nanoprisms experience a red-shift suggesting aggregation which created more hotspots. They focused on detecting 2,4-dinitrotoluene (DNT) which is trapped in the cavity of the CD and detections limits at the sub-ppb level were achieved.[114] Dasary et al[115] used gold nanoparticles conjugated with *p*-aminothiophenol to detect TNT at concentrations of 100 pM. The conjugated nanoparticles underwent aggregation in the presence of TNT as strong π-donor-acceptor interactions were formed, causing the size of the particles to drastically change. This change could be tracked via DLS and could also be visually monitored.

Another example of using SERS to detect trace amount of explosives is demonstrated by Milligan et al[116] who detected nano-molar concentrations in a multiplex of nitroaromatic explosives by creating a coloured Janowsky complex with the explosive and adding this complex to silver nanoparticles. The resulting unique SERS signal obtained from three different explosives are shown in Figure 1.11.

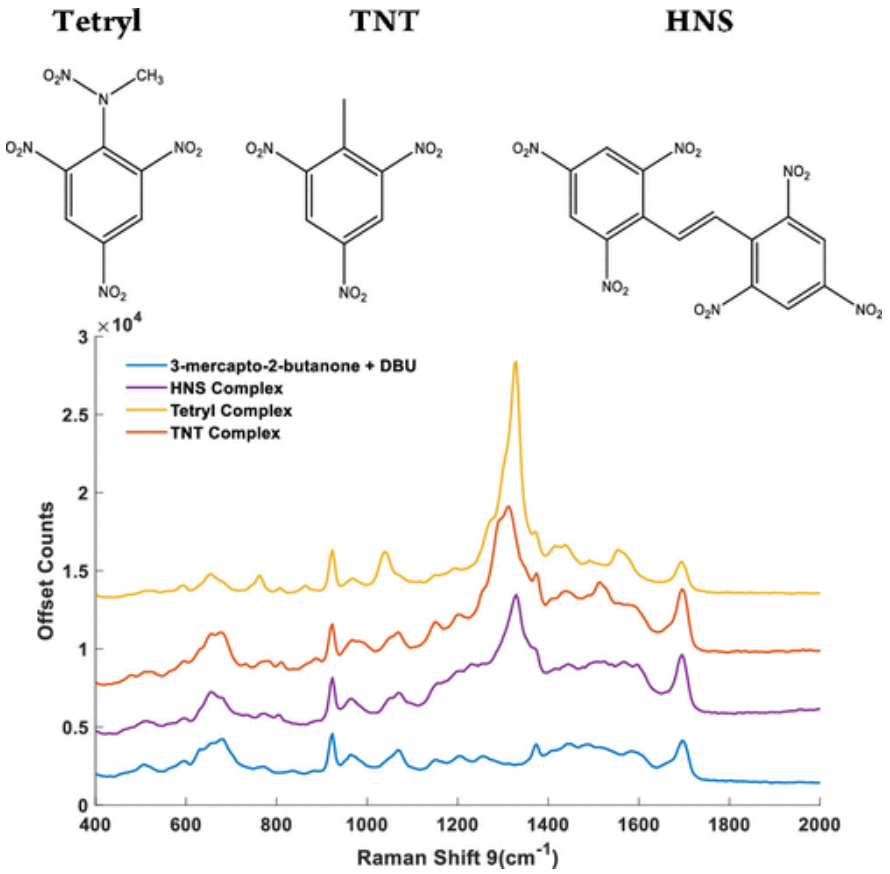

Figure 1.11: Structure of tetryl, TNT, and HNS and SERS spectra obtained from addition of TNT (red), hexanitrostillbene (purple), and tetryl (yellow) to a solution containing 3-mercapto-2-butanone and DBU (blue). [114] Replicated with permission from Anal. Chem. *2020, 92, 4, 3253–3261. Copyright (2020) American Chemical Society.*

It is clear from the examples above that to produce a strong SERS signal of explosives in solution, using nanoparticles, aggregation has to occur. An alternative method which also is capable of achieving sensitive SERS results from explosive samples is to use SERS substrates. On top of having poor Raman cross-sections, the explosives examined in this thesis also have low water solubility (PETN is averaged at 2.042 mg/L[117]). This causes problems for Raman spectroscopy, as the solvents the

explosives are soluble in (acetone and acetonitrile) have very good Raman cross-sections and can disrupt Raman signals of the explosives. Drying the sample onto a SERS substrate removes the solvent from the analysis, thus allowing analysis of relatively low concentrations.

A widely used commercial SERS substrate named Klarite™, which is no longer available, consisted of a surface fabricated by vapour depositing a thin layer of gold onto lithography etched square-based pyramids in a silica platform.[118] Botti et al[119],[120] published several papers proving that Klarite™ could be used to detect explosives such as PETN, however, they only managed to detect 0.1 mg/mL.

In recent years there has been a lot of research specialising on the synthesis of SERS substrates, especially to apply to explosives and narcotic detection. Dowgiallo et al reported a method of sputter depositing a gold-silver alloy onto a roughened glass surface. This 200 nm thick film allowed for adsorption of explosives onto the surface and was able to detect around 30 pg of PETN.[121] Liyanage et al[122] created a flexible SERS nanosensor capable of detecting PETN, RDX and TNT to 50, 50 and 900 parts pet quadrillion (ppq) respectively. The sensor was created by transferring a self-assembled layer of gold triangular nanoprisms onto a pressure-sensitive flexible adhesive film. This sensor allowed for two different sampling techniques, the traditional swabbing and drop-casting, and a new way of using the adhesive to directly pick up the explosive molecules from the sample. Another method of attaching nanoparticles to a surface to create a SERS sensor is to print them. Fierro-Mercado et al[123] created sensitive SERS substrates which could detect TNT at 94 pg by inkjet-printing gold nanoparticles on filter paper.

1.4 Introductory Conclusions

There are many methods currently used to detect highly energetic secondary explosives such as PETN, however, a large number of these tests require expensive and bulky instrumentation or trained personnel to interpret the results. This means

that these tests are usually not suitable for in-field testing. Colourimetric testing is another method often used for explosive detection which requires no instrumentation, resulting in a fast and inexpensive analysis of the explosive. However, these tests can only identify the class of the explosives, not the exact explosive, and often results in false positives for house hold items containing the same functional groups, making the test a presumptive one. Since the discovery of Raman spectroscopy, many technological advances have been made to develop miniaturised instrumentation. This makes Raman spectroscopy desirable for in-field detection of explosives as the miniaturised instrumentation makes this technique portable. Raman spectroscopic techniques can also boast specificity, able to identify the explosive molecules rather than the class of explosive, and can be made progressively more sensitive with techniques such as resonance Raman, SERS and SERRS.

1.5 Overview of Research Aims

The overall aim of this research was to develop a method of detecting PETN using Raman spectroscopic techniques such as resonance Raman and SERS. While Raman spectroscopy is desirable because of its sensitivity and specificity, PETN has a small Raman cross-section and therefore is difficult to detect using these techniques. However, advancements in this technique allow for the use of portable instrumentation and can be easily adapted for in-field analysis, making this method of detection desirable for rapid in-field analysis of explosives. . The ultimate goal of this research was to detect PETN using Raman spectroscopic techniques, gaining detection limits comparable to currently established techniques and spectroscopic techniques in literature.

Chapter 2 : SERS Detection of PETN using Klarite™

2.1 Introduction

With the increase in security threats in recent years, it is extremely important to develop a fast and simple method of detecting trace amounts of (high grade/military) explosives such as pentaerythritol tetranitrate (PETN). SERS has become a very attractive option for analysis as it is a very sensitive technique than can identify different explosives. Portable instrumentation can also be used, thus allowing for on-site analysis. PETN has a poor Raman cross-section as it is aliphatic, small in size and symmetrical. The low water solubility of PETN (averaged at 2.042 mg/L[117]) also causes issues for Raman spectroscopy as it is well known that water has minimal interference in Raman signal.[124] Nagli et al. and McNesby et al. have previously obtained Raman spectra of PETN, however, relatively large amounts of solid sample, high laser powers and very long acquisition times were required.[109,108] PETN is most soluble in solvents such as acetone and acetonitrile, which have good Raman cross-sections, therefore causing problems for detection by SERS using solution-based assays. SERS surfaces (or substrates), which are metal surfaces roughened to the nano-scale, can be used to detect explosives with poor Raman cross-sections.

SERS substrates generally consist of uniform nanostructured surfaces which are designed to enhance the Raman signal. Methods like electron beam lithography, nanolithography, chemical etching, electroplating and even immobilising gold or silver nanoparticles are often used to produce SERS substrates.[125,126,127,128,129] Fierro-Mercado et al[123] demonstrated a method of inkjet-printing gold nanoparticles onto filter papers for the detection of TNT. Spectra could be obtained using portable Raman instrumentation with a 785 nm excitation laser, a relatively low laser power of 19 mW and were able to detect TNT at 94 pg. Another example is an “optical nose” created by Chou et al[130] where a femtosecond laser created a nanostructured surface able to detect 0.05-15 mM concentrations of nitroaromatic vapours. These surfaces

experienced an eight-fold increase in Raman signal over that observed on the unstructured portion, however, signal intensity was dependent on the thickness of the gold coating and the structure of the surface. Botti et al[119] used a lithography etched silica substrate with a roughened gold surface called Klarite™ to detect trace level amounts, as low as tens of pg, of several explosives (TNT, RDX, PETN). While these explosives could be detected in a multiplex, a relatively long acquisition time of 10 s was required.

2.2 Chapter Aims

In this chapter, the detection of pentaerythritol tetranitrate (PETN) was investigated using the previously commercially available SERS substrate, Klarite™. The structure of PETN is shown in Figure 2.1.

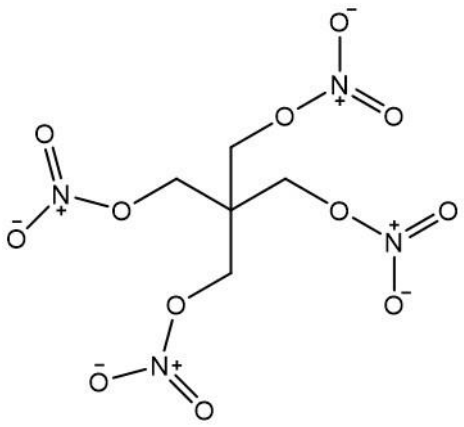

Figure 2.1: The structure of pentaerythritol tetranitrate (PETN).

Several experiments were performed to better understand which properties of Klarite™ cause the enhancement observed in these results, and how the explosive PETN deposits onto the surface of the SERS substrate. To investigate whether the enhancement in the PETN signal originates from the explosives concentrating in the Klarite™ pits, or a SERS enhancement from the roughened gold surface, the SERS signal on different sections of the substrate were compared (in-pit and side of the pit). It was found that while a larger signal was observed inside the pit, a decent signal

was still observed in the areas surrounding the pit, suggesting that both concentration and SERS affects the PETN signal. A cross-section SERS map of the sample area was also studied, and it was found that while a coffee ring effect was experienced, a large signal difference between each area was not observed, and therefore the explosive spread relatively evenly. PETN concentration studies were performed on Klarite™, flat silica, flat gold and uncoated Klarite (without the gold coating). It was found that PETN could be detected down to concentrations of 50 mg L^{-1} on Klarite™ but no PETN bands were observed on the flat silica or uncoated Klarite. From the results, it is clear that the signal enhancement experienced on Klarite™ is the result of both a SERS effect and a concentration effect on the PETN molecule in the pits.

2.3 Results and discussion

Klarite™ is fabricated by depositing a thin layer of gold onto a silicon wafer with ordered microstructures imbedded into the surface by electron-beam lithography.[118] The microstructures consist of a lattice of inverted square-based pyramids measuring 1.4 µm in width and 0.8 µm in depth,[131] with a fixed pit angle of 70.5°[119] and a roughened gold coating on the surface. These features can be visualised with progressively magnified SEM images in Figure 2.2, with (A) being the least magnified and (C) being the greatest.

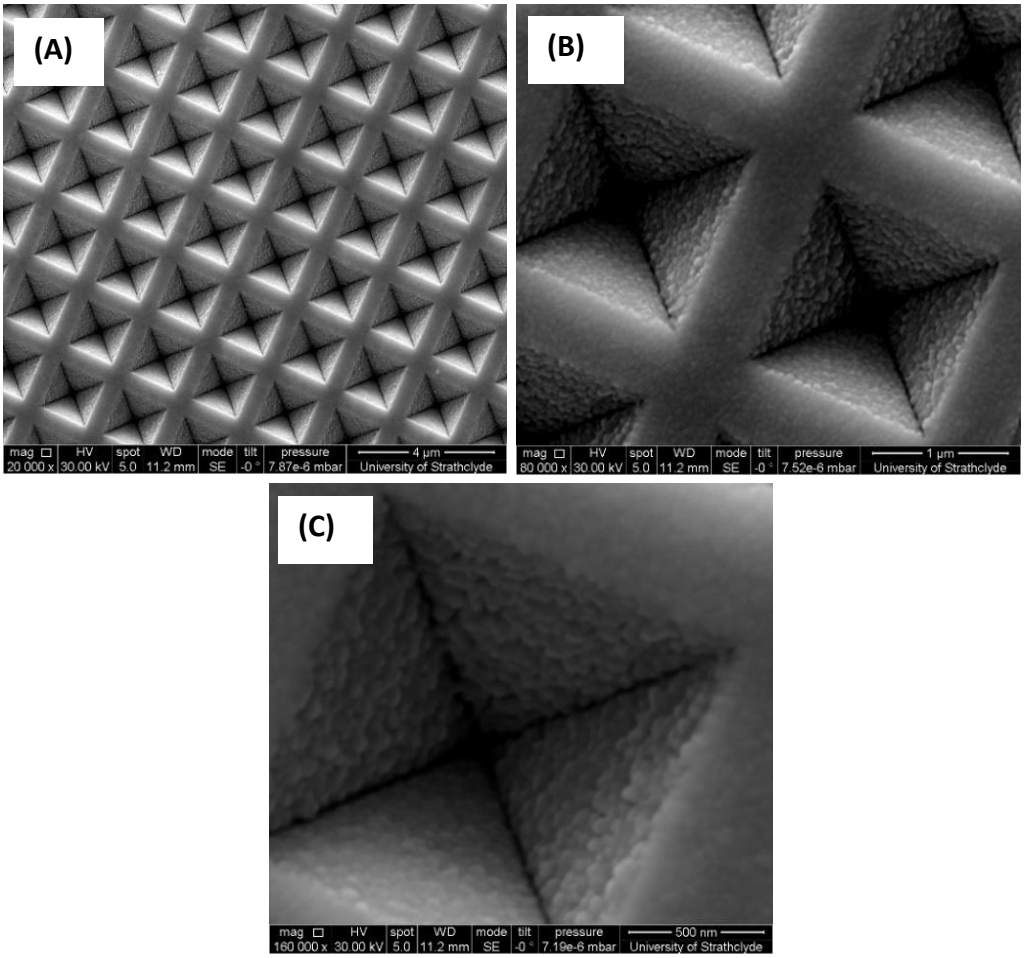

Figure 2.2: SEM images of Klarite™ at 20,000 x (A), 80,000 x (B) and 160,000 x (C) magnification. Each image was obtained used a 5 nm spot size, 30,000 keV beam energy, 0° tilt angle and a working distance of 11.2 mm. Roughened features in (C) were found to be between 40-70 nm in diameter.

Until recently, Klarite™ was commercially available and produced by Renishaw Diagnostics Ltd. The structure was designed to be uniform and to provide reproducible SERS results over the entire surface. The roughened gold surface provides SERS enhancement of the molecules adsorbed onto the surface and could be analysed using commonly available excitation wavelengths such as 633 nm and 785 nm. Gold was used as the plasmonic enhancer as it provided more reliable SERS signal and was more resistant to surface degradation, though the SERS signal would be smaller than those obtained from other metals.

Klarite™ has previously been used to detect small concentrations (100 mg L^{-1}) of explosives which are difficult to detect using SERS, such as PETN.[119] However, the

mechanism in which the enhancement of PETN is performed on the substrate is not very well known, as it is unsure whether it is fully a concentration effect of the PETN building in the pits, or a SERS enhancement from the roughened gold surface.

In order to determine the capability of Klarite™ to detect PETN, the explosive (0.5 µL, 1000 mg L^{-1} in acetonitrile (ACN)) was spotted onto the substrate surface and the solvent was allowed to evaporate (5 minutes). The substrate was then interrogated using excitation wavelengths of 633 nm and 785 nm. The resulting spectra were averaged and shown in Figure 2.3.

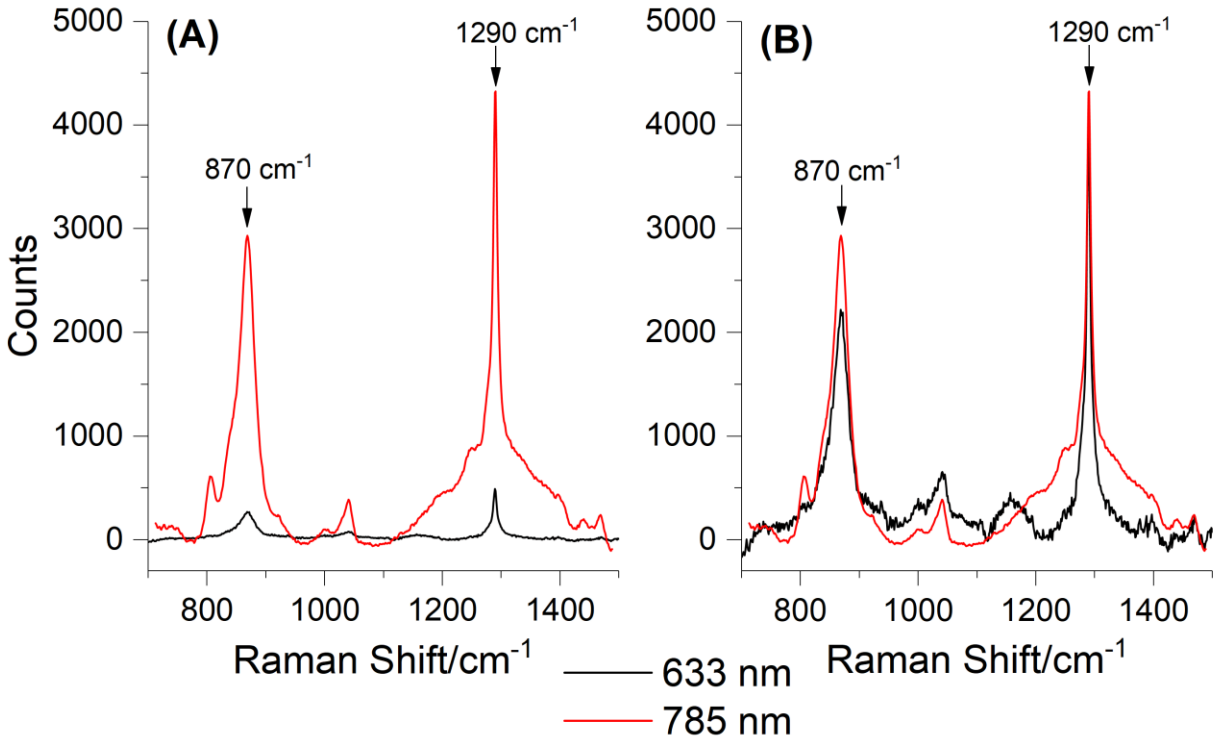

Figure 2.3: SERS of 1000 mg L^{-1} PETN dissolved in acetonitrile (ACN) on Renishaw Klarite™ at 633 nm (black) and 785 nm (red) excitation wavelengths. Each spectrum was the average of 5 replicate small maps with a map size of around 69 data points and step size of 1 µm. All spectra were collected using a Renishaw InVia Confocal Raman Microscope with a 10% excitation wavelength of 633 nm (4.9 mW) or 785 nm (20 mW), a 1s acquisition time, a 50 x objective lens and were baseline corrected using Matlab 2016 software. The spectra are shown before (A) and after (B) normalising to the ethanol standard at 10% laser power.

Figure 2.3 shows that signal was obtained from the PETN sample spotted onto the Klarite™ surface. The SERS spectra display strong bands at 870 cm^{-1} (O-N stretching) and 1290 cm^{-1} (symmetric stretching of the NO_2 groups).[132,133] As PETN was

suspended in acetonitrile (ACN), it was questioned whether the bands resulted from residual ACN which has failed to fully evaporate in the time given to dry the sample. However, the absence of bands at 924 cm^{-1} (C-C stretching), 1374 cm^{-1} (CH_3 deformation), 2258 cm^{-1} ($C \equiv N$) and 2945 cm^{-1} (C-H stretching) confirms that the bands observed were not due to residual ACN as these are bands commonly found in ACN spectra. The PETN bands at 870 cm^{-1} and 1290 cm^{-1} were also not observed when testing the surface before depositing the sample, and therefore they can be identified as belonging to PETN.

Figure 2.3 (A) shows the spectra as obtained after baseline correction, using 10% laser power for both excitation wavelengths. The signal experienced an increase of as 11.1 x for 870 cm^{-1} band and 8.8 x for 1290 cm^{-1} band when using a 785 nm excitation wavelength compared to a 633 nm wavelength. It was also observed that a new peak at 1040 cm^{-1} appeared when using a 785 nm excitation wavelength, which is another characteristic vibrational band of PETN belonging to the CH_2 torsion and C-C bending. However, when comparing the PETN signal from different laser excitation wavelengths, the laser power difference should also be considered. While both lasers were used at 10 % power, these came out at 4.9 mW and 20.0 mW for the 633 nm and 785 nm lasers, respectively. This difference in laser power would obviously contribute to SERS intensity differences. Figure 2.3 (b) shows the same data set after normalising to 20 mW laser power. It can now be seen that both excitation laser wavelengths result in very similar spectra with similar peak intensities. All three bands belonging to PETN can be identified, however, the 785 nm laser can be seen to produce a more resolved spectrum, as the 1040 cm^{-1} band was more defined. A lower signal to noise ratio was also observed in the spectra obtained from the 785 nm excitation laser.

The signal difference resulting from the features of Klarite™ were investigated next. As mentioned before, Klarite™ consists of a thin layer of roughened gold on a silicon substrate with embedded inverted square-based pyramids. (Figure 2.2) Here,

1000 mg L^{-1} PETN was deposited onto the Klarite™ surface and an area of 55x40 µm was interrogated using a 785 nm laser. Typical spectra obtained from the pit and the area surrounding the pit were then isolated. The intensity map at 1290 cm^{-1} and the isolated spectra are shown in Figure 2.4.

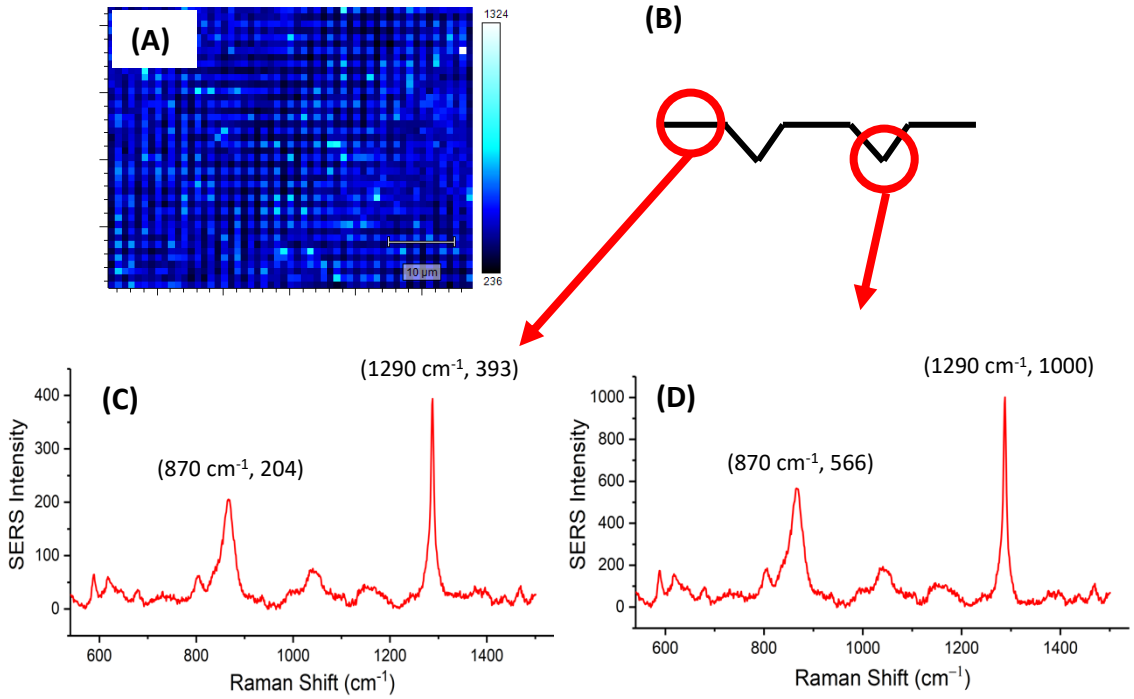

Figure 2.4: (A) SERS intensity map of the peak at 1290 cm^{-1} of PETN (1000 mg L^{-1}) dissolved in acetonitrile and spotted onto the surface of Klarite™. (B) Side profile diagram of Klarite™. Typical SERS spectra obtained from the area surrounding the pit (C), and the pit itself (D). All spectra were collected using a Renishaw InVia Raman Microscope with an excitation wavelength of 785 nm (20 mW), a 1s acquisition time and a 50x objective lens. The spectra were smoothed, baseline corrected, and a SERS intensity map was generated using Renishaw's WiRE 4.4 software to plot the intensity of the band at 1290 cm^{-1} for each map point. The peak position and intensity values of the peaks of interest have been identified on spectra (A) and (D).

It is theorised by the author that the pit angle helps the excited surface plasmons of the roughened gold by reflecting the oscillating plasmons. Constructive interference would then occur, amplifying the Raman signal, thus causing SERS. As the microstructure of Klarite™ is inverted pyramids (see Figure 2.2), it can be assumed that the concentration of the analyte would be greater in the bottom of the pit compared to the areas between the pits. From the results obtained a difference of around 600 counts was observed when comparing the signal obtained from these two different areas on the substrate (Figure 2.4 (C) and (D)), thus demonstrating that the pits in Klarite™ increase analyte signal. It is still uncertain whether the

concentration effect of the molecules (Raman), or the reflecting plasmons (SERS) in the pits is responsible for the increase in signal observed. Both may have an effect as if the signal was only coming from the concentration effect then no PETN vibrational bands would have been observed from the areas between the pits.

These results also demonstrate that a signal can be obtained from anywhere on the surface of Klarite™ that has been spotted with the sample, and that the specific inverted pyramid features do not need to be targeted to get a readable measurement. This is because the roughened surface of Klarite™ (see Figure 2.2 (C)) can be observed to extend to all areas of the Klar Klarite™ ite chip, therefore allowing for SERS enhancement to occur across the whole substrate. The roughened surface would make the substrate useful for onsite analysis as specific features would not need to be targeted. While a mapping instrument was used for this work, it would be simple to use handheld Raman instrumentation, as the laser spot size for handheld instrumentation is likely to be larger than the substrate features, therefore obtaining an average signal of all the Klarite™ features.

Another important issue for sampling data on the Klarite™ chip is the distribution of PETN on the surface. PETN is insoluble in water and, as stated earlier, is soluble in very few solvents such as acetone and ACN. In this study, PETN was dissolved in ACN. It was assumed that the dried sample would experience a coffee ring effect, where there would be a large signal difference from the outer parts of the droplet compared to the centre of the droplet. Solvents generally evaporate in the less concentrated regions first and so the ACN would first evaporate from the edge of the droplet. As the solvent evaporates at the edge of the droplet, the liquid is replenished from the centre, occurring until the centre of the droplet is dry. This would lead to the accumulation of PETN molecules in the edges of the droplet, resulting in an increased concentration and therefore a larger signal.[134]

In order to test this theory, 1 µL of PETN (1000 mg L^{-1}) was deposited onto the substrate surface, and a map of the cross-section of the dried droplet, from the middle to the droplet edge, was performed. The spectral map is shown in Figure 2.5.

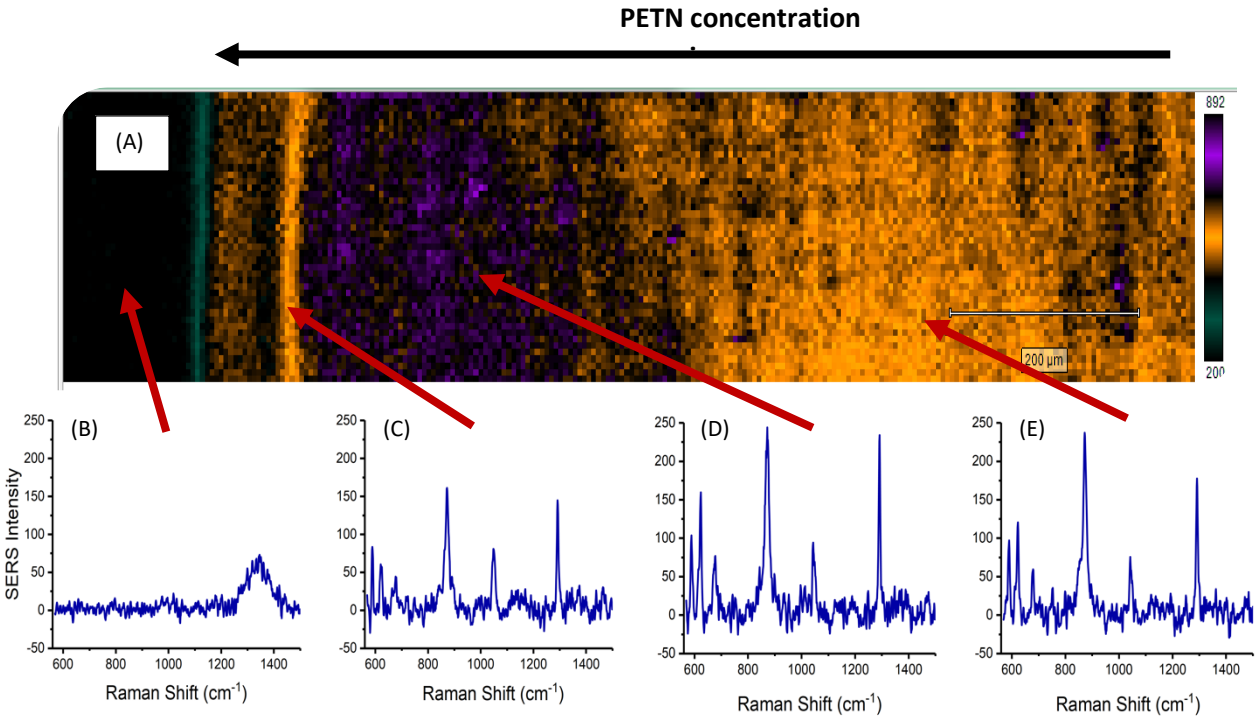

Figure 2.5: SERS intensity map of a cross section of a 1 µL droplet of 1000 mg L^{-1} PETN on Renishaw Klarite™ (A), SERS spectra from outside (B), the edge (C), the outer third (D) and the centre of the sample droplet (E). Spectra were collected using a Renishaw InVia Confocal Raman Microscope with an excitation wavelength of 785 nm (2 mW), a 1s acquisition time, a 5 µm step size and a 5 x objective lens. Spectra (B), (C), (D) and (E) were typical spectra found in their specific areas. The spectra were smoothed, baseline corrected and the SERS intensity map was generated using Renishaw's WiRE 4.4 software to plot the intensity of the peak at 1290 cm^{-1} for each map point.

Figure 2.5 shows the SERS cross-sections of the dried droplet of PETN. Typical spectra from outside the droplet (A), the edge of the droplet (B), the outer third (D) and the middle of the droplet (E) have been isolated and shown in Figure 2.5. It was found that the resulting spectra from the experiment contradicted the expected results. While some variation was found when comparing the different areas of the substrate, the difference was only around 100 counts, which is negligible when some Klarite™ chips yielded a response of up to 10000 counts for a 1000 mg L^{-1} solution of PETN. Using PETN dissolved in ACN worked in our favour as it was found that the volatile nature of this solvent allowed for the sample to spread uniformly, thus leaving a

relatively even distribution of the analyte on the substrate surface. It should be noted than a lower magnification (5 x) was needed to obtain a cross-section of sample droplet. This resulted in lower laser power, and therefore the PETN signal was poor in comparison to the intensity observed in Figure 2.3.

While the SERS intensity maps do not show a huge amount of variation, the white light images of the substrates show something quite different at the higher concentration of PETN tested in this work. In some Klarite^{TM} samples, PETN crystals and droplet like features were observed in many areas of the sample. These features can be seen in the white light images in Figure 2.6.

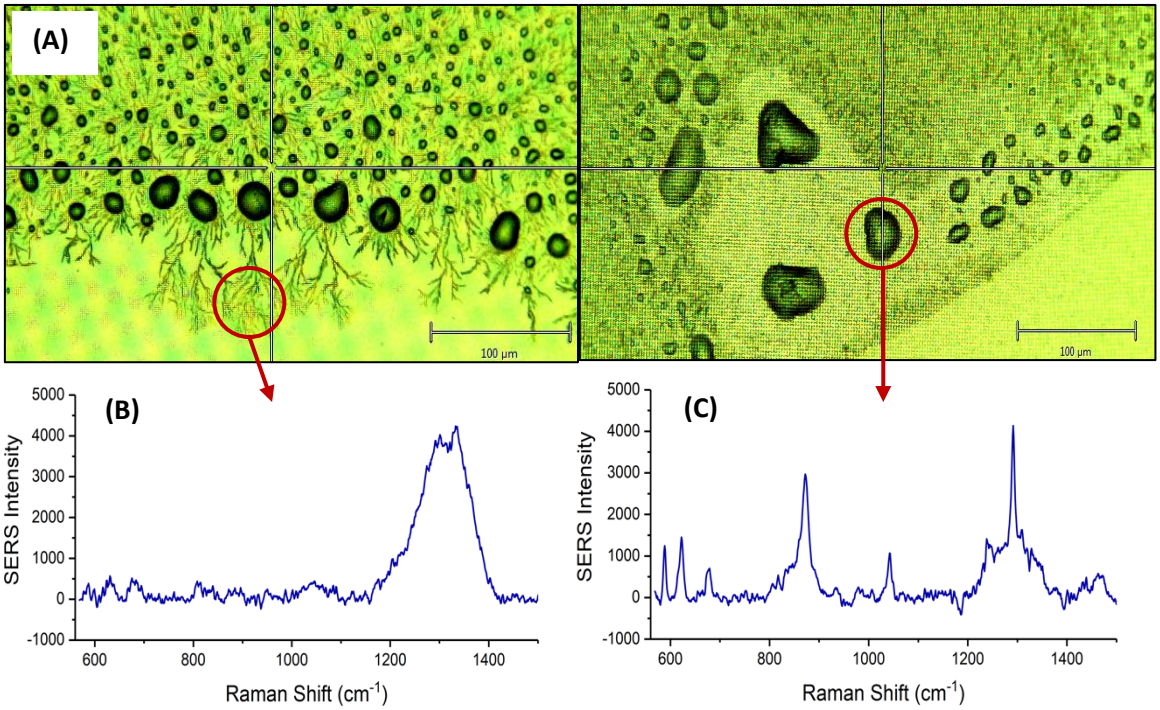

*Figure 2.6: **(A)** White light images of PETN drying patterns on 1.4 µm pitted Renishaw Klarite^{TM} using a 20x lens objective. The scale is 100 µm. The spectra of the crystal **(B)** and droplet **(C)** features were collected using a Renishaw InVia Confocal Raman Microscope with a 10% excitation wavelength of 785 nm (10 mW), a 1s acquisition time and a 1 µm step size. The spectra were smoothed and baselined using Renishaw's WiRE 4.4 software. Crystals (left) and a droplet (right) have been circled in red.*

When looking at these features separately from the rest of the map, a few things were discovered. While not entirely clear from the images above, the crystals were small, thin, needle-like and were generally found in clusters, with a width measuring

less than 0.5 µm. These crystals did not result in a PETN SERS signal (Figure 2.6 (B)) as they were too thin for the laser to properly focus on. As the step size of the map and the laser diameter were both around 1 µm, this would have been too large an area to pinpoint the crystal. The droplet features were reminiscent of solvent droplets which had not fully evaporated in the 5 minutes allotted, however, it was discovered that the droplet features resulted in a PETN signal (Figure 2.6 (C)) rather than the expected ACN signal, and so it was proposed that the droplets contained the majority of the PETN sample. In fact, it can be observed from the crystal patterns in the left white light image (Figure 2.6 (A)) that it appears as if the crystals were originating from the droplet, supporting the theory that the majority of the PETN sample was contained in the droplet. However, the crystal and droplet features were not always observed, and samples without them also gave a good PETN response at this concentration.

These features, especially the PETN crystallisation, disappeared at concentrations lower than 1000 mg L^{-1}. The droplet features were observed in several of the flat substrates tested in this work, and therefore the substrate pits cannot be solely responsible for these interesting drying patterns. However, there was much less crystallised PETN on the untextured substrates (without pits or a roughened metal surface) so this cannot be ruled out fully without further testing. The crystallisation patterns of PETN could not be studied more in-depth in this work as there was a low number of Klarite™ samples available for testing. However, despite the lack of further testing, the crystallisation patterns are worth mentioning as it could potentially affect the SERS signal obtained from PETN at higher concentrations than those studied in this work.

To examine PETN concentrations lower than 1000 mg L^{-1}, a study was performed on the concentration range 10 mg L^{-1} – 1000 mg L^{-1}. The same experimental procedure

as repeated, using 0.3 µL PETN at those concentrations and the average spectra are shown in Figure 2.7.

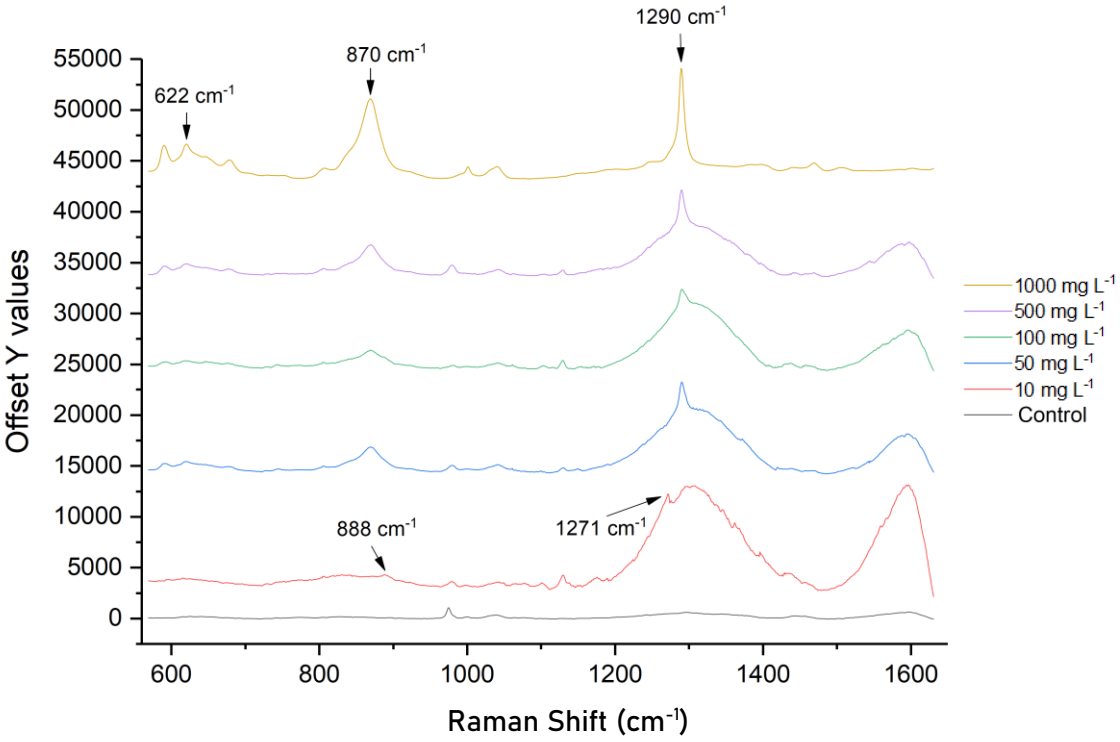

Figure 2.7: SERS spectra of PETN at 5 different concentrations (10 mg L^{-1} – 1000 mg L^{-1}) on Renishaw Klarite™. PETN was dissolved in acetonitrile, and therefore the control was acetonitrile spotted onto the substrate. Each spectrum is the average of 3 maps, with 300 map points each, collected using a Renishaw InVia Confocal Raman Microscope with a laser excitation wavelength of 785 nm (20 mW), a 1s acquisition time, a 1 µm step size, a 50 x objective lens and was averaged and baseline corrected using Matlab 2016 software.

The SERS spectra in Figure 2.7 are the results of several averaged maps for each concentration. Mean averages were calculated so the maps could be compared to single spectra which would be obtained from portable instrumentation. The SERS spectra display strong bands at 622 cm^{-1} (ONO_2 rocking), 870 cm^{-1} and at 1290 cm^{-1}.[132,133] These bands were not observed when testing the surface before sample preparation, or from ACN spiked onto the surface, and can therefore be attributed to PETN. The signal observed at 50 mg L^{-1} (blue) is quite strong, and therefore it was thought that the detection limit could go lower, however, at 10 mg L^{-1} (red), the bands disappeared. The bands identified in Figure 2.7 at

10 mg L^{-1} (red) show a signal shift of the peaks from 870 cm^{-1} and 1290 cm^{-1} to 888 cm^{-1} and 1271 cm^{-1}, suggesting that PETN was no longer detected at this concentration. The band observed at 970 cm^{-1} in the Klarite™ control is seen in all the Klarite™ samples. The broad bands observed in the lower concentrations of PETN at ~1300 cm^{-1} and ~1600 cm^{-1} were not visible in the average of the control spectra (bare Klarite™ or ACN spotted onto Klarite™), therefore suggesting that these bands might belong to a contaminant in the explosive solution. However, on average, less than 10 map points out of 300 contained these broad bands. It is also possible that minute solvent droplets did not evaporate, focusing the laser beam and burning the substrate, therefore, creating the broad bands observed. These broad bands most likely increase in strength when there is less PETN to compete with.

It should also be noted that while the spectra in Figure 2.7 were obtained using 20 mW laser power, signal could also be obtained from the higher concentrations of PETN at 180 mW laser power. At lower concentrations of PETN, the signal obtained from 180 mW and 100 mW laser power saturated the detector, and therefore a laser power of 20 mW was used in this study. It can be suggested that the more concentrated the PETN sample the more disordered the PETN molecules would settle on the surface, thus creating multilayers and resulting in a Raman signal. It is possible that destructive interference of the surface plasmons could occur, therefore dampening the SERS signal. If the PETN concentration is less, it creates a thinner, more ordered monolayer of the PETN molecules and this could cause constructive interference of the surface plasmons, thus resulting in SERS and an increase in signal.[135]

It was found that the 1290 cm^{-1} band resulted in similar intensities at each of the concentrations investigated (ranging between 7.7 to 11 thousand counts) and therefore it can be concluded that there is no correlation between PETN concentration and signal intensity. This suggests that Klarite™ substrates can be used for qualitative PETN detection, rather than quantitative.

To provide an estimation of the sensitivity of the Klarite™, the mass of PETN and the number of molecules interrogated by the laser beam in a single measurement was estimated. The lowest concentration of PETN detected was 50 mg L^{-1}. A droplet of 0.3 µL of this concentration was estimated to dry over an area of 7.07 mm^2, calculated using the diameter of the droplet. The laser beam had a diameter of around 1 µm, which has an area of around 7.85 $x10^{-10}$ mm^2. By calculating the ratio of interrogation to sample areas, it was estimated that 1.7 ag, or 3.2 thousand molecules of PETN were interrogated by the laser at any one point in the map. This value would only be accurate if the molecules were evenly distributed across the whole drying area. While it was shown that a coffee ring effect was not fully experienced in these samples (Figure 2.5), it is unlikely that the whole sample was evenly distributed.

In order to better understand what enhances the Raman signal of PETN on Klarite™, the same concentration range of 10 mg L^{-1} – 1000 mg L^{-1} was investigated on three

different substrates similar in morphology and material type to Klarite™: flat silica, flat gold and uncoated Klarite with a well size of 1.4 µm (see Figure 2.8).

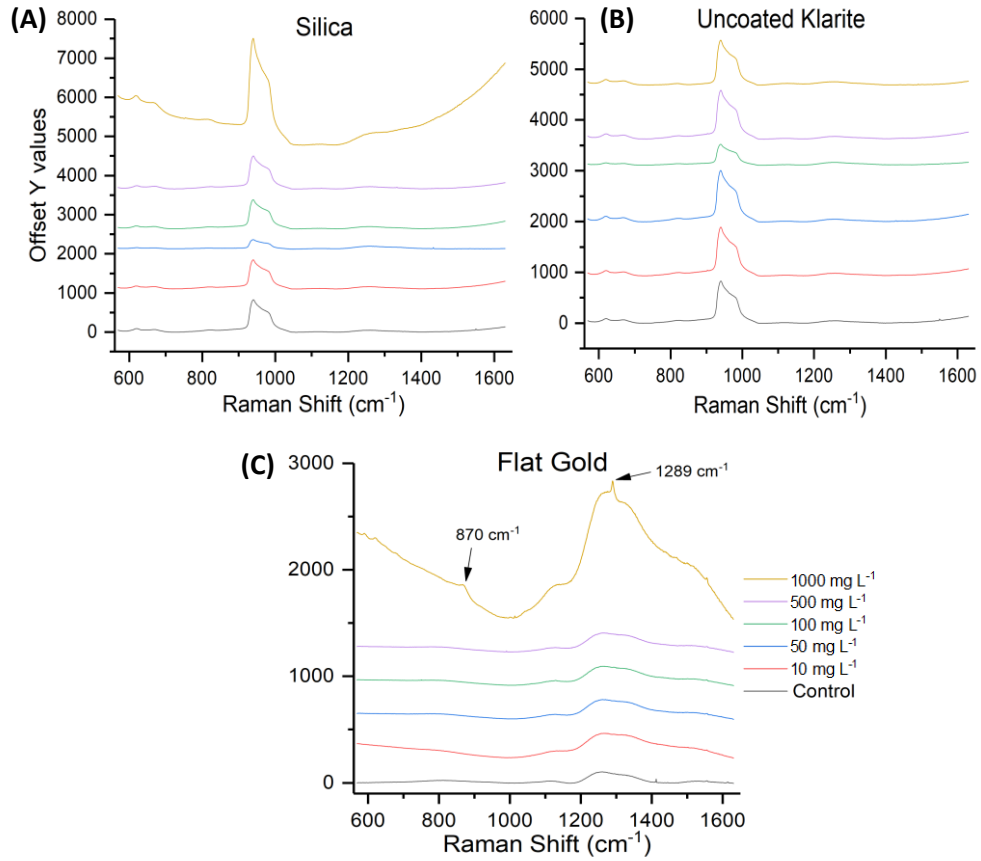

*Figure 2.8: SERS spectra of a 0.3 µL droplet of PETN at 5 different concentrations (10 mg L^{-1} – 1000 mg L^{-1}), on 3 different substrates (silica **(A)**, uncoated Klarite **(B)** and flat gold **(C)**). Each spectrum (except 1000 mg L^{-1} PETN on flat gold) is the average of 3 maps, with 300 map points each, collected using a Renishaw InVia Confocal Raman Microscope with a 10% excitation wavelength of 785 nm (20 mW), a 1s acquisition time, a 1 µm step size, a 50 x objective lens and was baseline corrected using Matlab 2016 software. 1000 mg L^{-1} PETN on flat gold was collected using 100% excitation wavelength of 785 nm (180 mW)*

Figure 2.8 shows that no PETN signal was obtained on both the flat silica substrate (A) and the uncoated Klarite (B) for the PETN concentration range tested in this work. This suggests that the enhancement seen on Klarite™ could not be solely attributed to the PETN concentrating into the pit of the substrate. If this was the case, then a Raman signal would have been obtained from the uncoated Klarite. At concentrations of 1000 mg L^{-1}, using 100% laser power, a Raman signal of PETN can be detected on flat gold by the bands observed at 870 cm^{-1} and 1290 cm^{-1}. These

vibrational bands were quite weak and difficult to pinpoint, even after baselining the data. This signal is only visible for the highest concentration of PETN and the strongest laser power, at lower concentrations the Raman signal would be too weak to identify any bands. The PETN bands that are found in the flat gold substrate were most likely visible due to the gold contribution to the signal, the gold surface providing an electrical field enhancement, thus increasing the intensity of the Raman signal.

Reusability of the Klarite^{TM} chips was also briefly investigated as the high cost of producing the substrates encourages the analyst to use them multiple times to offset the cost. Used Klarite^{TM} chips were sonicated in isopropyl alcohol (IPA) for 10 minutes and then in acetonitrile for another 10 minutes to remove PETN from the surface of the Klarite^{TM}. While no signal was seen before adding PETN to the surface, the signal obtained from the different concentrations tested were at least 2x more intense than the first tests performed on the chip, therefore suggesting that PETN was not completely removed. It is possible that the second PETN sample built onto the first, causing constructive interference on the surfaces plasmons and thus increasing the signal. This also proves that the chips are single-use only, unless a technique such as plasma cleaning was employed to remove impurities. This additional step would cost time and money, and if the analyte in question is so difficult to remove properly, then this could tamper with results. Therefore, it can be concluded that these substrates are very expensive to make because they can only be used once.

Finally, Dr Stacey Laing supplied some Klarite substrates made inhouse with two different pit sizes (1.5 µm and 0.5 µm), which were tuned to the 785 nm and the 633 nm lasers, respectively. These substrates were fabricated by depositing a thin layer of gold onto a silicon substrate with ordered microstructures imbedded into the surface by electron-beam lithography, similar to how they were originally made in industry. These substrates were spotted with 1000 mg L^{-1} PETN and investigated using 10% laser power (4.9 mW for 633 nm laser, 20 mW for 785 nm laser) and 1 s acquisition time for the two laser wavelengths previously mentioned (see Figure 2.9).

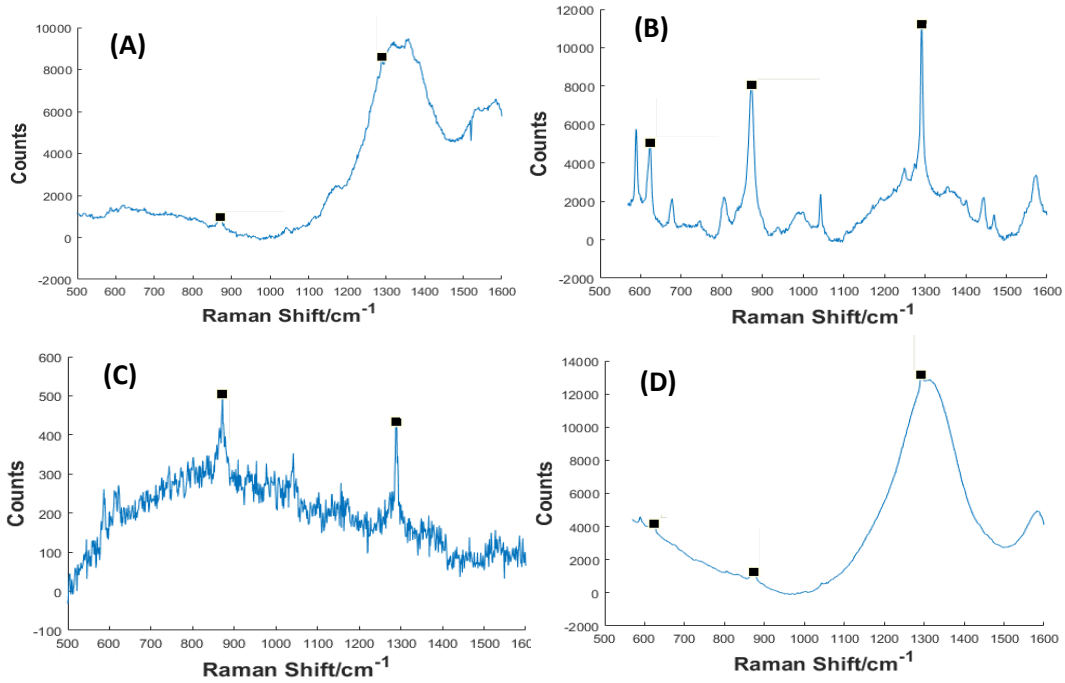

*Figure 2.9: Small (0.5 µm) and large (1.5 µm) pitted Klarite substrates made inhouse with 1000 mg L^{-1} PETN spiked on top. The inhouse Klarite was made by depositing a thin layer of gold onto a silicon substrate with ordered microstructures imbedded into the surface by electron-beam lithography. The large pitted substrates were interrogated with a 633 nm excitation laser **(A)**, and a 785 nm excitation laser **(B)** and the small pitted substrates with a 633 nm excitation laser **(C)**, and a 785 nm excitation laser **(D)**. Each spectrum is the average of 3 maps collected using a Renishaw InVia Confocal Raman Microscope with a 10% excitation laser strength (3.9 mW for 633 nm, 20 mW for 785 nm), a 1s acquisition time, a 1 µm step size, a 50 x objective lens and was baseline corrected using Matlab 2016 software.*

The large pitted inhouse Klarite chips performed well with the 785 nm laser, yielding a very strong SERS response for PETN (See Figure 2.9 (B)). Previously identified bands (623 cm^{-1}, 870 cm^{-1}, 1044 cm^{-1} and 1290 cm^{-1}) were observed in this spectrum as well

as weaker PETN bands, including the band at 1573 cm^{-1} which is due to the NO_2 asymmetric stretching of the PETN molecule. This was the first time in this work that so many PETN bands were observed in a PETN spectrum, proving that the large pitted inhouse Klarite was very efficient as it gave a clear signal at this excitation wavelength. It is possible that the large pitted inhouse Klarite chip produced a clear spectrum as the substrates were recently fabricated, whereas the other Klarite™ chips examined in this work were several years old. It was found that the 633 nm excitation generated very poor response for 1000 mg L^{-1} PETN on the large pitted substrates, but this was expected as the pit size was not tuned to this wavelength of laser (Figure 2.9 (A)).

The small pitted substrates (0.5 µm) resulted in very poor signal in comparison to the large pitted substrates (1.5 µm). As this size of pit was tuned to 633 nm laser excitation, it was expected to obtain a reasonable response from this laser wavelength, however, the resulting spectrum was much less resolved than the large pitted counterpart. While both characteristic bands used as PETN indicators in this work (870 cm^{-1} and 1290 cm^{-1}) can be identified from both lasers, the 785 nm excitation laser (Figure 2.9 (D)) did not yield a good response, as the bands characteristic of PETN were hard to distinguish from the background in the spectrum. It is unknown why the smaller welled substrates did not perform as well as they should have, especially with lasers tuned to the right wavelength to provide resonance enhancement. It is possible that changing the pits to a smaller size does not allow the PETN molecule or solvents of high volatility, to settle on the surface or in the pits as it does in the larger sized wells.

In both the large and small pitted substrates, broad bands at ~1300 cm^{-1} and ~1600 cm^{-1} were again observed in the spectra obtained from the 785 nm excitation laser. As explained earlier, these bands are most likely due to a contaminant in the PETN solution, or as the result of burning of the substrate through unevaporated droplets, as the bands were not observed in either the plain inhouse Klarite chips, or in the spectra obtained from ACN on the chips. Interestingly, these broad bands seem to

have a wavelength dependence, as they were not as apparent in the 633 nm spectra. This dependence can support both suggested explanations for the broad bands observed. The 785 nm laser was stronger in power than the 633 nm laser, therefore burning would be achieved easier with the higher laser power. It is also possible that the PETN solution contaminant is more in resonance with the 785 nm laser, therefore resulting in a stronger signal. It is impossible to tell which explanation is correct from the data obtained in our experimentation.

2.4 Conclusions and Further Work

In conclusion, this work has shown that PETN can be detected on SERS substrates such as Klarite^{TM}, to a concentration of 50 mg L^{-1}, which is two times lower than previously reported in literature.[119] It is uncertain whether the signal obtained from PETN is a result of the molecules concentrating in the pits features, or from the roughened gold coating on Klarite^{TM}. The vibrational band intensities from different regions of the Klarite^{TM} were investigated and it was found that while a more intense signal was obtained from the pits, the area surround the pits also resulted in a signal, suggesting that both theories affected the PETN signal intensity obtained on Klarite^{TM} substrates. The drying pattern of the sample was also investigated to see if a coffee ring effect was experienced, where a higher concentration of the sample would be found at the sample edge. However, it was found that by using PETN dissolved in acetonitrile this effect was negated as a similar signal intensity was found throughout the sample area. These results showed that specific areas of the substrate were not needed to be targeted to obtain measurable results, and therefore the substrate could be used with handheld instrumentation in future. Crystal and droplet features were observed on the substrate after sample addition, appearing as if the crystals were originating from the droplets. It was found that the droplet contained reasonable high PETN signal and the crystals were too small to interrogate. Further work should be done to examine the effect of different drying times on the appearance of these droplets and crystals, and the resulting SERS signal.

Finally, this work also performed PETN concentration experiments on flat silica, flat gold and pitted silica (Klarite without the roughened layer of gold). No signal was found on the flat or pitted silica, suggesting that the PETN signal enhancement experienced by Klarite™ is effected by SERS, and the signal is not solely due to a concentration effect when the sample solvent rapidly evaporates, causing the PETN molecules to settle into the bottom of the pit feature.

Chapter 3 : Colourimetric and Resonance Raman Detection of PETN

It was demonstrated in Chapter two that SERS detection of the explosive PETN, of concentrations down to 50 mg L^{-1}, was achieved using a SERS substrate such as Klarite^{TM}. This was a lower concentration than previously reported in the literature.[119] However, this substrate is no longer commercially available, and is expensive to synthesise, as it uses electron-beam lithography. The SERS enhancement of the substrate is still not fully understood, and the reusability is poor, thus making them single use only. The detection limit of 50 mg L^{-1} was accomplished on SERS mapping instrumentation, and while there is evidence suggesting that handheld instrumentation would achieve similar results, work had yet to be performed to confirm this. The expense of the substrate makes them impractical for on-site detection despite their ability to detect relatively low concentrations of PETN and alternative detection methods need to be investigated.

In this chapter, an alternative solution-based approach was demonstrated which involved the hydrolysis of PETN and the reaction of the subsequent products to make an azo complex. This approach allowed for the quantitative detection of PETN in the 2-50 mg L^{-1} concentration range using UV-Visible spectroscopy, with the potential of achieving lower concentrations using resonance Raman and SERS spectroscopy, with portable instrumentation. Different molecules were investigated in the reaction, allowing for faster detection and stronger signals from the PETN than discovered in the original research by Üzer et al.[136]. While this approach was primarily used for PETN detection in the chapter, any nitro-based explosive could be detected, thus making this method ideal for simple preliminary testing of explosives.

3.1 Introduction

As previously mentioned in Chapter 1, Section 1.3.2, colour testing kits using azo chemistry are commonly used by the military to detect nitrite explosives, and are easily purchasable from online suppliers such as Merck[99]. This chemistry was discovered in the 1800s by John Griess, thus coining the name of the reaction – the Griess Reaction[94]. In the Griess reaction, a nitrite ion reacts with sulfanilamide then an α-naphthylamine under acidic conditions, where it will form a coloured azo compound that can be detected using absorption spectroscopy. The modern version of this reaction now uses a diamine instead, as α-naphthylamine is a potent carcinogen. This reaction is shown in Figure 3.1.

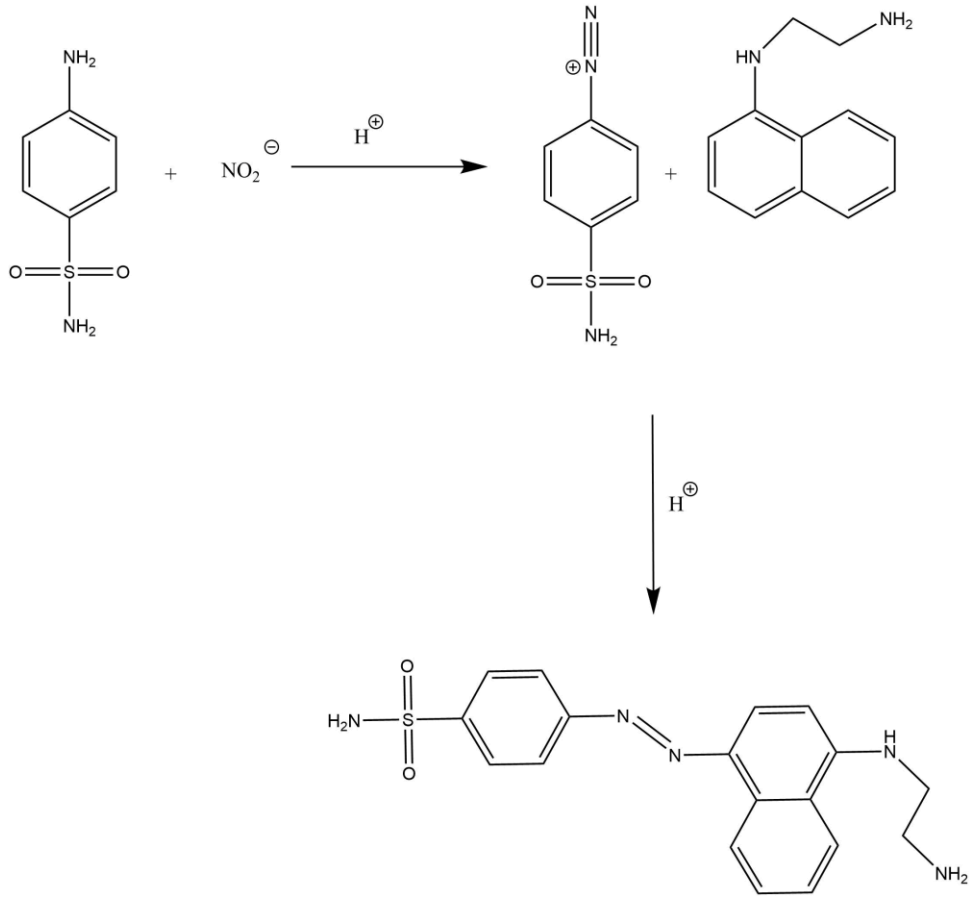

Figure 3.1: Schematic of the modern Griess reaction, where an azo complex is formed from the reaction of sulfanilamide and N-(1-naphthyl)ethylenediamine (NED) with a nitrite ion under acidic conditions.

While this reaction targets nitrite ions, some commercially available kits even include a precursor reaction to reduce nitrate ions to nitrites, thus allowing this reaction to detect most nitro-based compounds. However, these kits are expensive, and often only include enough enzyme for the nitrate detection of 1/5 of the assays in the kit, and so are not cost-effective, especially when dealing with nitro-based explosives.

Peters et al.[137] developed a five lane microfluidic paper-based analytical device capable of detecting multiple explosives with detection limits in the range of 0.39-19.8 µg. Each channel contained reagents for specific colourimetric reactions, thus allowing for specificity of the reaction. Analysis could occur 5 minutes after sample addition, however only colourimetric detection was used.

To the best of the author's knowledge, the most recent work on detecting nitro-based explosives using an azo reaction has been performed by the Apak group in Turkey.[136,138] They have published several papers over the past 5 years detailing the detection of RDX, HMX and PETN and compared the original Griess reaction (method 1) to a modified reaction that functionalised the azo product on a gold nanoparticle or nanorod (method 2).

While Üzer et al. methods can detect micromolar (µM) concentrations of the previously mentioned explosives, only absorption spectroscopy was investigated when testing for PETN, as the resulting product was a strongly coloured azo compound. While the Griess reaction completes after a few seconds, the work required to extract the nitrite ions from the explosive adds 45 minutes to the reaction. The preparation of the functionalised gold nanoparticles used in their second method is also time-consuming, and the resulting nanoparticles do not remain stable for a long period of time. These additional procedures make the reaction very time consuming, especially for presumptive tests. This creates an opening for research to be performed to reduce the total time needed for the reaction and to modify the assay for resonance Raman, allowing for portable instrumentation to be used for monitoring the reaction.

3.2 Chapter Aims

The aim of this research was to recreate the solution-based assay of Üzer et al. for detecting mg L^{-1} concentrations of PETN and to improve the sensitivity using resonance Raman. In this work, both methods in the paper were altered to increase the sensitivity of the assay, resulting in lower limit of detection (LOD) values when detecting PETN, and to make a more favourable reaction which proceeds faster and is more reproducible than the original Griess reaction. By replacing NED with 3,5-dimethoxyaniline (DMA), two additional assays were developed by altering the original two, making a total of 4 assays. Each assay was analysed by either absorption spectroscopy or a combination of absorption and resonance Raman spectroscopy. The reactions were then optimised to obtain a lower LOD and a faster reaction by investigating the medium solvent used, the temperature, the pH of the reaction at different steps and the conjugated gold nanoparticles. This work aimed to develop sensitive, presumptive tests using azo chemistry to detect the explosive PETN using either absorption or resonance Raman spectroscopy.

3.3 Results and Discussion

To indirectly detect PETN via a coloured azo reaction two slightly different methods based on the work by Üzer et al were investigated. The methods begin the same way by hydrolysing PETN and then the resulting NO_3 ions are reduced to NO_2 ions, so an azo reaction can occur. In the paper, they used a 20% hydrogen peroxide (H_2O_2) solution for 20 minutes at room temperature to hydrolyse PETN, then reduced the resulting NO_3^- to NO_2^- with successive additions of 0.25% $CuSO_4.5H_2O$, 0.1 M NaOH and 0.208% hydrazine sulfate, before leaving for a further 15 minutes and heating in a water bath at 65°C. These reactions are shown in Figure 3.2.

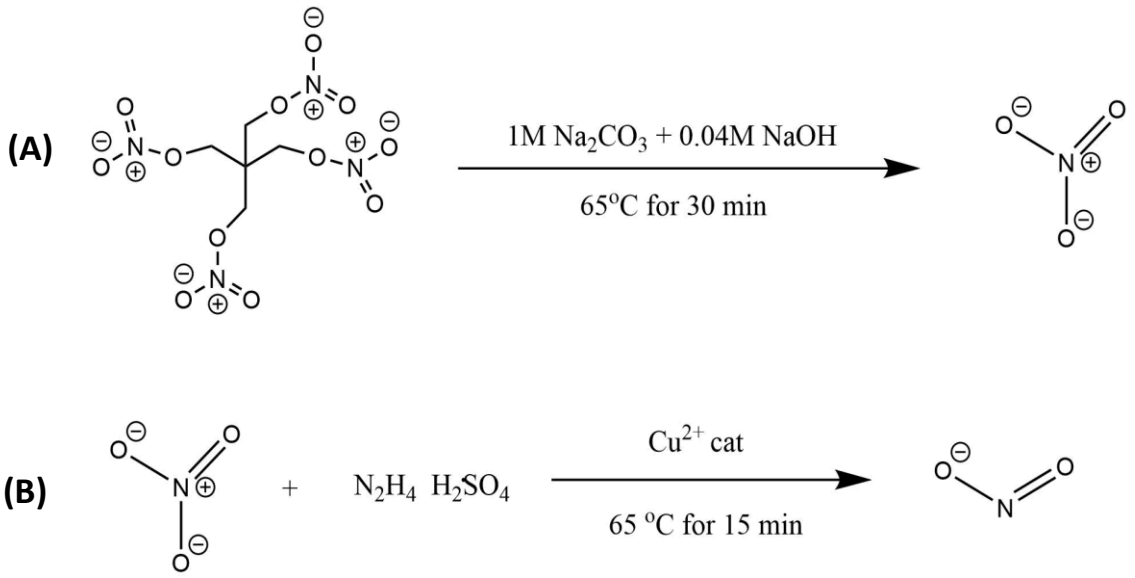

*Figure 3.2: Reaction schemes for the hydrolysis of PETN **(A)** and the reduction of nitrate to nitrite ions **(B)**.*

Alkaline solutions of hydrazine have been shown to reduce nitrate to nitrite with varying success (50-85% yield). Small concentrations of copper catalyses this reaction, however, excess amounts could result in cuprous oxide.[139]

After the hydrolysis and reduction of the explosive PETN, the two proposed methods in the paper began to differ slightly. The first method is the original Griess reaction, which is found in Figure 3.1.

In the Griess reaction, a reagent containing 4% (w/v) sulfanilamide solution in 10% phosphoric acid solution and a 0.2% NED solution (w/v) in distilled water was made beforehand. These two solutions were then mixed in equal amounts to make the Griess reagent, before being added to the hydrolysed and reduced PETN sample. The colour change observed (clear to pink) happened within 10 seconds of the addition of the reagent.

The second method added 4-aminothiophenol (4-ATP) functionalised gold nanoparticles to the hydrolysed and reduced solution of PETN, before adding 0.1 M

HCl and 20 mM NED. The sample was then left for 30 minutes for a colour change to develop. This reaction is shown in Figure 3.3.

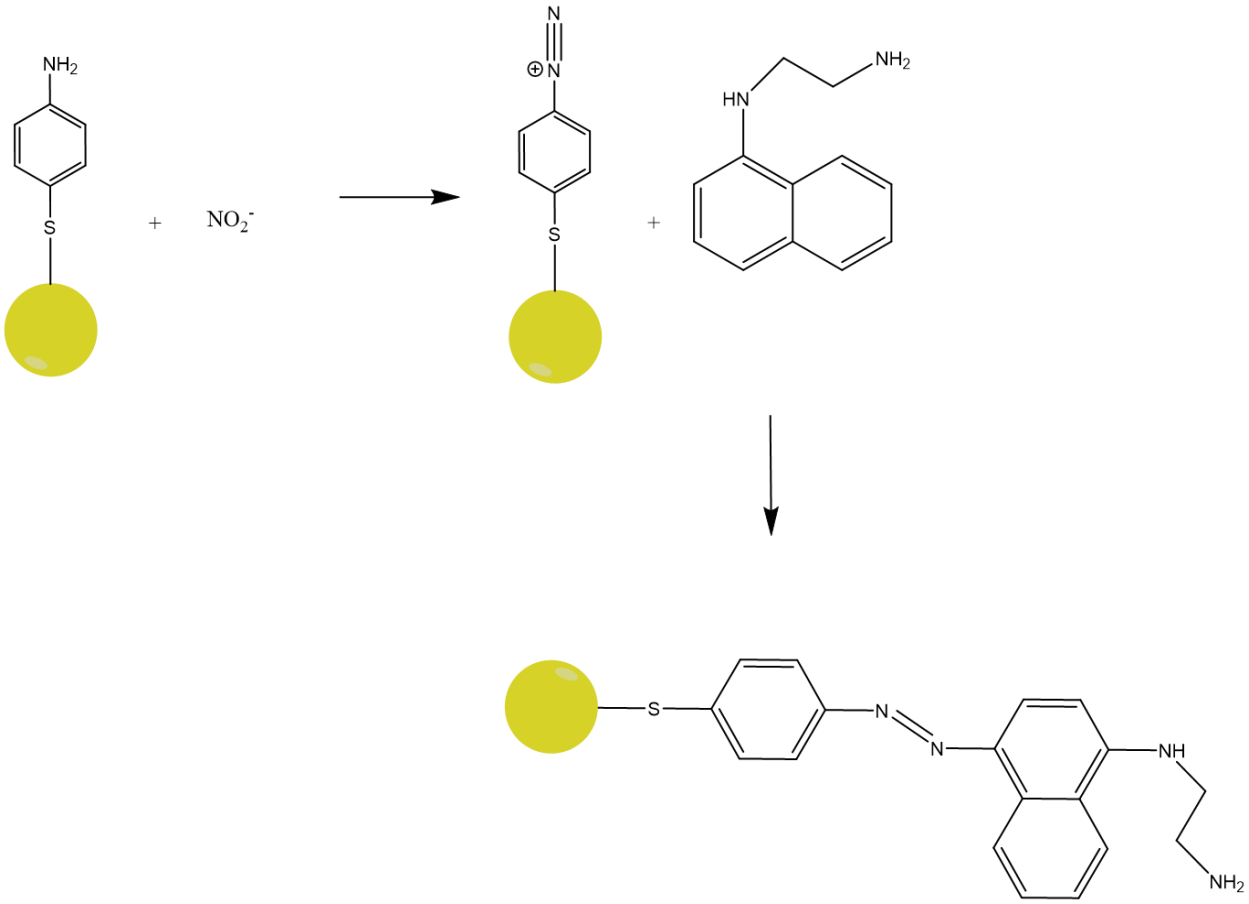

Figure 3.3: Schematic of the nanoparticle reaction based on the Griess reaction, where an azo reaction occurs between 4-ATP functionalised gold nanoparticles and NED, in the presence of NO_2^-. The yellow ball represents the gold nanoparticle.

3.3.1 Recreating the Griess reaction

As a starting point for this chapter, the Griess reaction (Figure 3.1) and the nanoparticle version (Figure 3.3) from Üzer et al. work with PETN were carried out. The same concentration ranges used in the previous work (2-10 mg L^{-1} for Griess, 10-50 mg L^{-1} for nanoparticle version) were investigated, using the strongest concentration for the following preliminary test. Control (with no PETN) and spiked samples were prepared for each method, taking care to use the correct ratio of acetone: water for each one (4:1 for Griess, 1:1 for nanoparticle version). Both reactions preceded as described in experimental section 6.4.4 and the visual results from the test are shown in Figure 3.4.

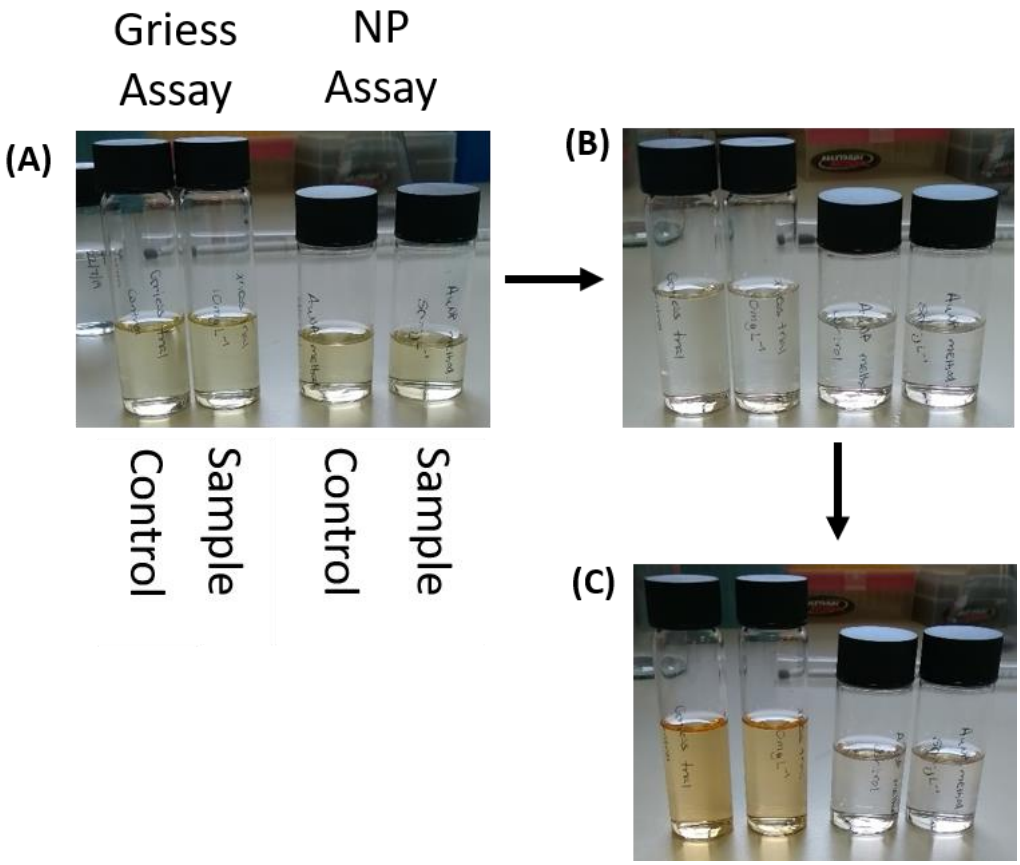

*Figure 3.4: Pictures taken of the samples after the addition of NO_3^- reduction agents **(A)**, directly **(B)** and 30 minutes **(C)** after the addition of the Griess reagent, or nanoparticle equivalents (4-ATP conjugated nanoparticles and NED). Original Griess samples were conducted in the tall vials, and the nanoparticle version was in the short vials. In each vial set, the control (lacking NO_2^-) can be found on the left, and the spiked sample on the right (annotated on picture **(A)**).*

The original Griess samples were performed in the tall glass vials, whereas the shorter vials were used for the nanoparticle version. In each vial set, the control sample was found on the left, and the spiked sample on the right. This is annotated in Figure 3.4 (A), and the annotations can be applied to the other two images. The nanoparticle assay used 4-ATP conjugated gold nanoparticles which did not have any colour. The preliminary tests for both methods failed as both the control and spiked samples resulted in the same colour change. It was observed that all samples changed colour (colourless to yellow) after the addition of the reagents needed for NO_3^- reduction (Figure 3.4 (A)). All the samples returned to colourless after the addition of the Griess reagent, or the nanoparticle equivalents (Figure 3.4 (B)). After 30 minutes, both sample sets had changed colour (colourless to orange/yellow), the change was more evident in the Griess reaction samples than the nanoparticle version (Figure 3.4 (C)).

Despite a colour change being observed in both sample sets, this trial failed as the controls were the same colour as the spiked samples. It was also noted that the speed of the reaction was poor, as azo compounds are usually fast to form. The received colour change was also not the expected one, as if the reaction had succeeded then a pink colour should have been obtained.

The lack of colour difference observed between the control and spiked sample suggests that the reaction failure likely occurred in either the hydrolysis step or the nitrate ion reduction step. To address this issue, the original Griess reaction had to be investigated and performed successfully, before moving onto the nanoparticle version.

3.3.2 Altering the Griess reaction

The failed reaction could be due to a number of possibilities, however the most plausible was that H_2O_2 was not oxidising the PETN, and therefore there was no NO_3^- available to reduce to NO_2^-, hence the azo reaction could not proceed. The fact that H_2O_2 was used in the paper was strange, as it is a weak acid and it is known that PETN fragments in alkaline conditions (see Figure 3.5).

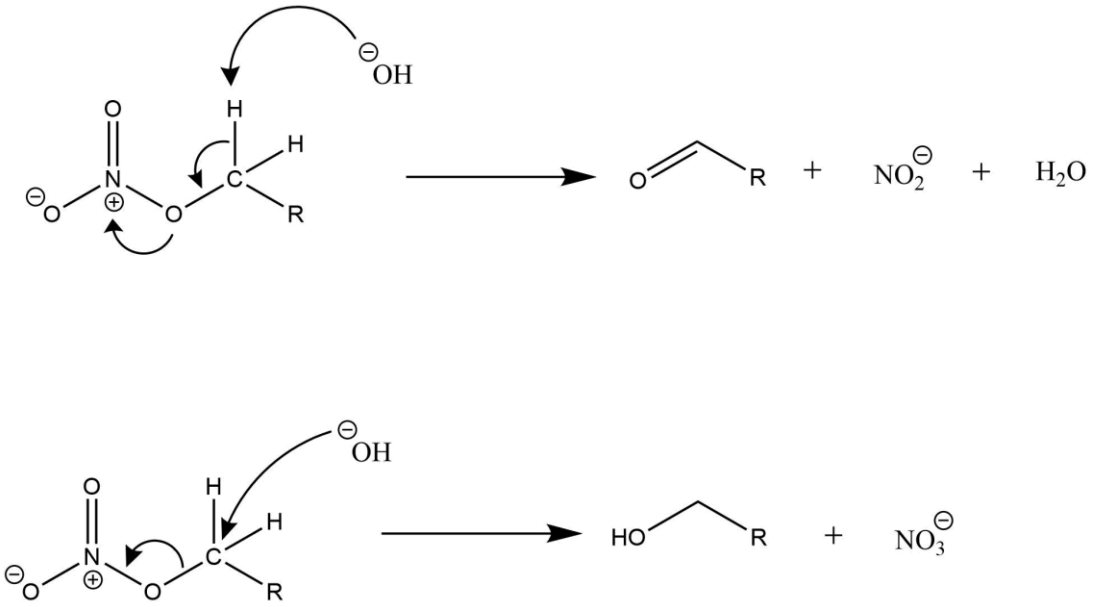

Figure 3.5: Two methods of PETN fragmentation under basic conditions. For simplicity, R represents the rest of the PETN molecule. Movement of the electrons are shown by the arrows.

Two experiments were performed to investigate both the PETN hydrolysis step and the nitrate ion reduction step. To investigate the hydrolysis step, the brown ring test was attempted. In this test, iron(ii) sulfate was added (in excess) to a solution of nitrate, then when concentrated sulfuric acid is added slowly, a brown ring ($[Fe(H_2O)_5(NO)]SO_4$) should form between the two layers if nitrates are in solution.[140] This test is best performed in a test tube so the two layers are made more apparent. The chemistry of this test is shown below;

$$2HNO_3 + 3H_2SO_4 + 6FeSO_4 \rightarrow 3Fe_2(SO_4)_3 + 2NO + 4H_2O$$

$$[Fe(H_2O)_6]SO_4 + NO \rightarrow [Fe(H_2O)_5(NO)]SO_4 + H_2O$$

This test failed to result in the formation of a brown ring, therefore confirming the theory that H_2O_2 did not hydrolyse the PETN.

Potassium iodide starch paper was used to examine the nitrate ion reduction step. In this reaction, nitrite ions oxidise potassium iodide to form iodine. This elemental iodine then reacts with starch to form a blue-violet complex. This test was also unsuccessful, though this is most likely due to the low PETN concentration examined. While it is difficult to calculate the amount of nitrite ions present in the sample, it can be roughly estimated. If 100% of the PETN hydrolysis and nitrate ion reduction were experienced, then it could be expected that the nitrite ion concentration would be around 130 µM. While this concentration is slightly higher than the limit of sensitivity for the paper, it can be expected that the concentration of nitrite ions in the lab test was below this, and therefore beyond the sensitivity of the test.

The same group published another paper similar to this work in 2013, where their target was RDX and octahydro-1,3,5,7-tetranitro-1,3,5,7-tetrazocine (High melting eXplosive, or HMX). In this paper, their hydrolysing solution comprised of a mixture of 1M Na_2CO_3 + 0.04 M NaOH. As the brown ring test confirmed that the PETN molecule was not being hydrolysed by the H_2O_2 hydrolysing solution, it was decided to switch to a basic solution. By using an alkaline hydrolysis system instead of an acidic one, the formation of the by-products nitric oxide, nitrogen and ammonia was prevented.[141]

By combining the different methods into the one, the Griess reaction was successful in detecting 10 mg L^{-1} PETN. The reaction was carried out at room temperature and 65 °C with a control and a spiked sample. The visual results from this test are shown in Figure 3.6.

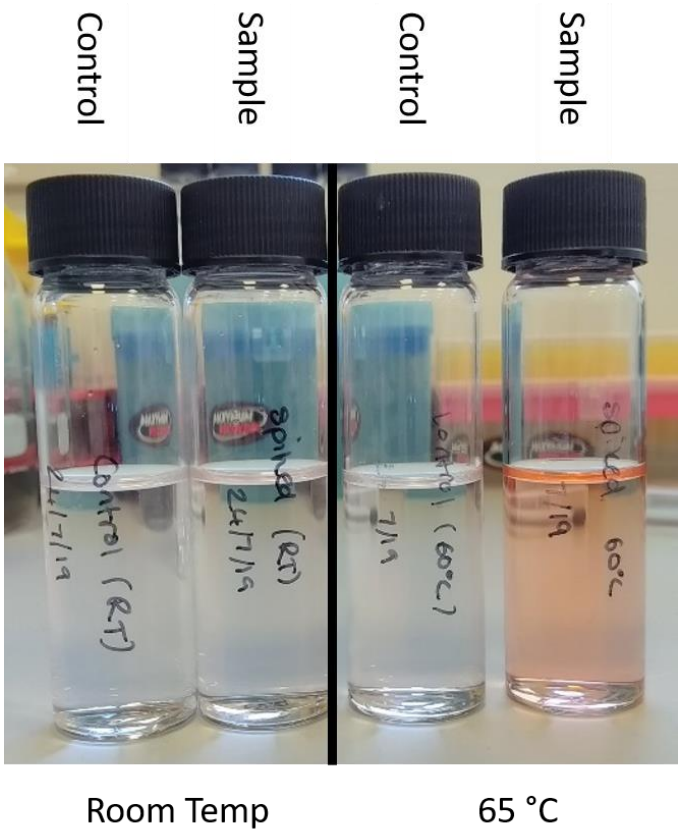

Figure 3.6: Pictures taken from the reaction of 10 mg L^{-1} PETN with the Griess reagent. The reaction was performed at room temperature (left) and 65 °C (right). The controls contained no PETN.

It was observed that both the control samples stayed colourless, whereas the spiked samples are both coloured, the room temperature sample being only slightly coloured at the meniscus. As the product is more visible in the heated sample, a simple conclusion can be drawn that the reaction is more successful (or perhaps just faster) when the sample is heated, rather than at room temperature. It was therefore decided that heating the samples would be a requirement for this reaction to be successful for PETN.

3.3.3 Scaling down the reaction

With the success of the alterations of the Griess reaction for the detection of PETN, it was decided to scale down the original volumes as the large volumes were not needed for UV analysis. It was decided to scale the reaction from 9 mL to around 2 mL, giving more than enough product for analysis by absorption spectroscopy and leaving a volume for error.

A concentration study (2-10 mg L^{-1}) was performed using the Griess reagent, following the experimental procedure listed in section 6.4.6. Two separate colours were observed if the sample was not agitated (pink) or agitated (peach) during the final step of the reaction (addition of the Griess reagent). This is shown in Figure 3.7.

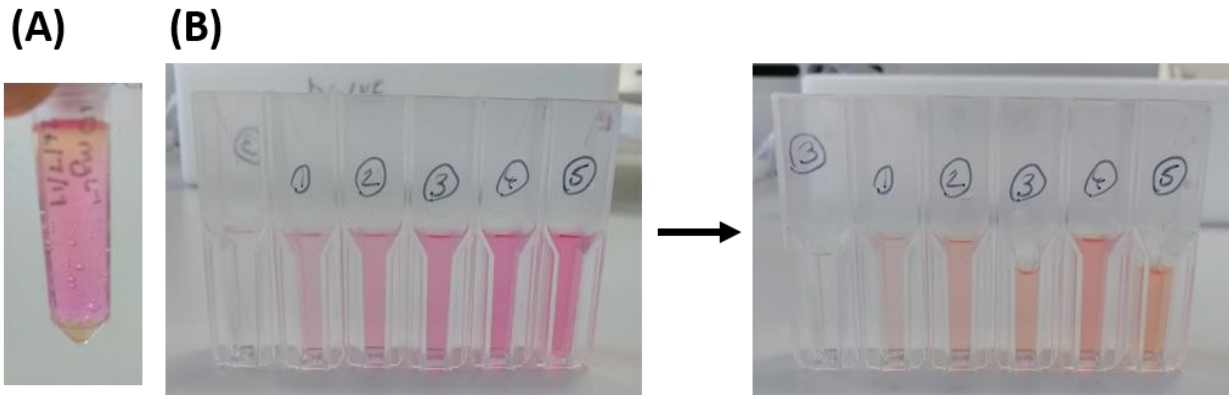

*Figure 3.7: Picture of a PETN sample reacted with the Griess reagent before sample agitation **(A)**, and the two different colours separated before and after sample agitation **(B)**.*

Before mixing the sample, a pink colour dominated containing an absorbance maximum of around 530 nm. After agitating the sample, the whole solution turned into a peach colour with an absorbance maximum of around 500 nm. It can also be observed that there is a small volume at the bottom of the Eppendorf which does not incorporate into the solution until after sample agitation.

These different coloured solutions were analysed by carefully removing the pink part of the solution, without agitating the bottom layer of solvent, and analysing by absorption spectroscopy. The pink solution was then returned to the sample holder and mixed to produce a peach colour, which was analysed for a second time by absorption spectroscopy. The spectra produced are shown in Figure 3.8, and absorbance maximum values are detailed in Table 1.

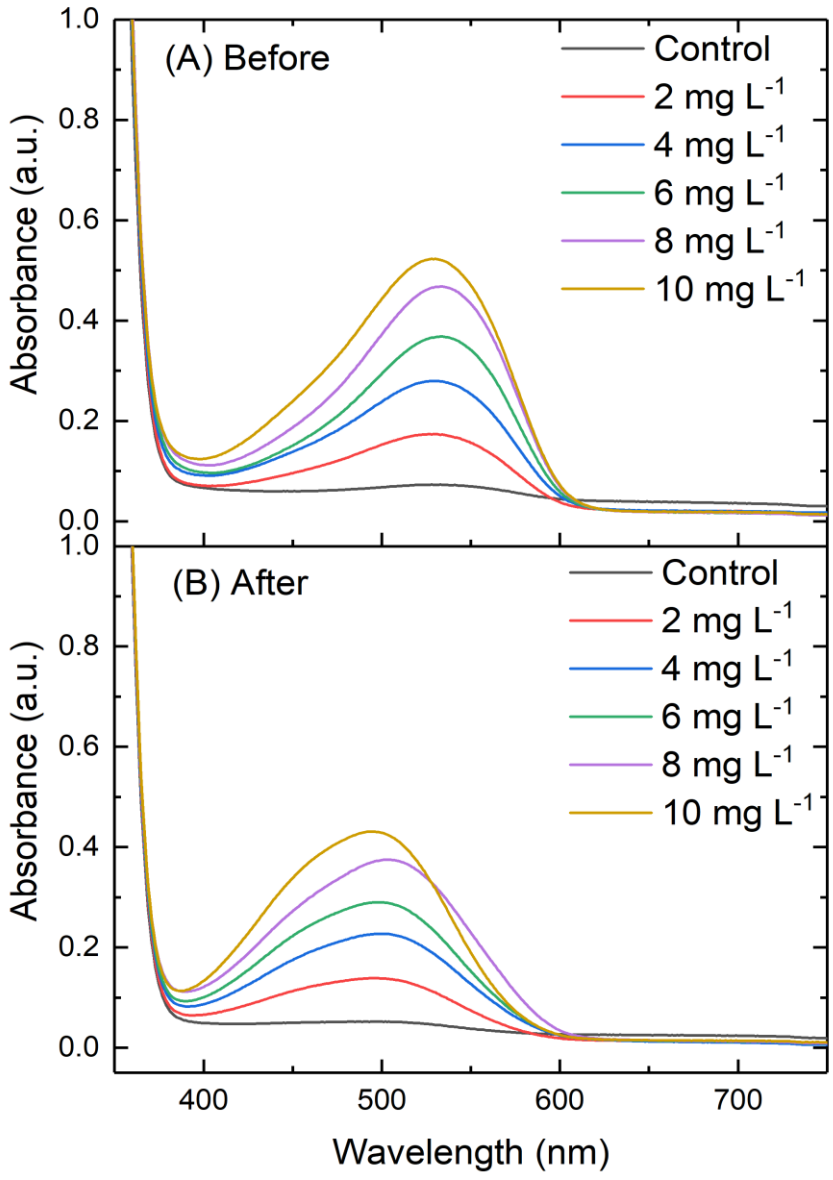

*Figure 3.8: Absorbance maximum profiles obtained from the reaction of 2-10 mg L^{-1} PETN with the Griess reagent before agitating the samples **(A)** and after **(B)**.*

Table 1: Absorbance maximum values obtained from the reaction of 2-10 mg L^{-1} PETN with the Griess reagent before and after agitating the sample.

	UV before	**UV after**
Control	528 nm, 0.073 abs	-
2 mg L^{-1}	530 nm, 0.174 abs	497 nm, 0.139 abs
4 mg L^{-1}	528 nm, 0.280 abs	500 nm, 0.227 abs
6 mg L^{-1}	533 nm, 0.368 abs	498 nm, 0.290 abs
8 mg L^{-1}	533 nm, 0.468 abs	504 nm, 0.375 abs
10 mg L^{-1}	530 nm, 0.523 abs	496 nm, 0.431 abs

The UV-Vis data supports that there is a colour change occurring before and after agitating the sample. Before agitation, the absorbance maximum ranged between 528-533 nm, which is very similar to the desired azo absorbance expected at 540 nm. The product after agitation appears to have blue-shifted and contains an absorbance maximum ranging between 496-504 nm. This peak shift implies that the molecules have gone from being more aromatically conjugated to less.[142] It can be suggested, as sulfanilamide was in excess, that the product molecule that dominates the sample was sulfanilamide self-coupling. This is supported by the UV-Vis data as the combination of two sulfanilamide molecules bound together are less aromatically conjugated than sulfanilamide and NED. While this potential self-coupled product is not the desired one from this reaction, it can still be used to detect the presence of PETN in the sample solution.

3.3.4 pH analysis of Griess reaction

As a change in pH can affect an azo reaction, the pH's were also investigated at each of the following stages of the experiment;

1- Sample after adding base hydrolysing solution → pH 10-11
2- Sample after adding solutions needed for nitrate conversion → pH 10-11
3- Final product – pink → pH 0-2
4- Final product – peach (lower layer) → pH 5-6
5- Final product mixed – peach → pH 2-3

Looking at the pH of the solution at each of these stages is very interesting. Unsurprisingly, the pH of stage 1 was around 10-11. This was to be expected as a base solution was added to hydrolyse the PETN sample. In stage 2, copper sulfate (Cu^{2+}), HCl and hydrazine sulfate were added, however, it can be seen that the pH of the solution does not change. This suggests that the HCl is either too weak a concentration (0.1 M) or too little was added to change the pH of the solution, therefore making the HCl addition redundant. In stage 3, after the addition of the Griess reagent, it can be seen that the pink azo product is extremely acidic, between pH 0-2. The bottom layer of the sample, which was peach colour was more neutral, at around pH 5-6. The final combined/mixed product was peach in colour and had a pH of 2-3.

Comparing the three pHs of the products might help to further explain the colours visible for each. At sample 3, the product has an acidic pH which would facilitate the diazotisation reaction as H^+ ions are needed in excess. At sample 4, the pH of the sample is much more basic, leaning towards neutral. As explained before, the diazotisation reaction requires an excess of H+ ions which is found at acidic pH's. A less acidic pH or a more neutral one could hinder the process, halting the reaction before the formation of the desired product. By mixing the acidic pink and the less acidic peach layer, the pH of the solution shifts to a slightly less acidic one. The pKa's

of each molecule (sulfanilamide and NED) should also be taken into consideration, as it was 10.4 for sulfanilamide[143] and was predicted to be 9.4 for NED[144]. However, these values cannot be fully relied upon, as they were the pKa values calculated in water, whereas the solvent used in this experiment was a mixture of acetone and water. Usually, pKa values are calculated or measured in either water or dimethyl sulfoxide (DMSO) and therefore the addition of a different solvent could shift these pKa values.[145] It is unknown how much these values would shift in a mixture of acetone and water, however, it can be estimated that NED will protonate faster at lower pH's and when the pH increases the reaction will favour sulfanilamide. This helps explain the pink colour observed in sample 3 (pH 0-2) which would result from sulfanilamide coupling with NED. The peach colour observed in the mixed sample has a higher pH (pH 2-3), suggesting that sulfanilamide could be self-coupling. However, both azo compounds only react in the presence of a nitrite ion, and can therefore be used for analysis, meaning that the final azo product is not too important.

It also appears that the absorbance is less strong for the sample after agitation. The absorbance intensity could depend on how well the sample was mixed, and on making sure no sample was lost in the reaction or the sampling process. The reaction vessels used were Eppendorfs, which, despite being tightly closed, popped open during the heating steps. This is presumably because of the building pressure of the acetone evaporating, as the water bath's temperature was above the boiling point of acetone. The opening of the reaction vessel could have contaminated the sample, and at the very least would have inserted additional water into the sample and allowed for some acetone to be lost to the environment. Instead of using Eppendorfs as a reaction vessel, later experiments used 5 mL glass vials with screw-on lids. These proved to be much more reliable as the lids never popped open.

3.3.5 LOD values for Original Griess reaction

To obtain an LOD value for the detection of PETN using the original Griess reaction, the assay was performed in triplicate using PETN in the concentration range of 2-10 mg L^{-1}, following the experimental procedure listed in section 6.4.6. The solutions were analysed by absorption and Raman spectroscopy in an attempt to see if the product gave a Raman signal, and the result can be found in Figure 3.9. The original Griess reaction scheme can be found in Figure 3.1.

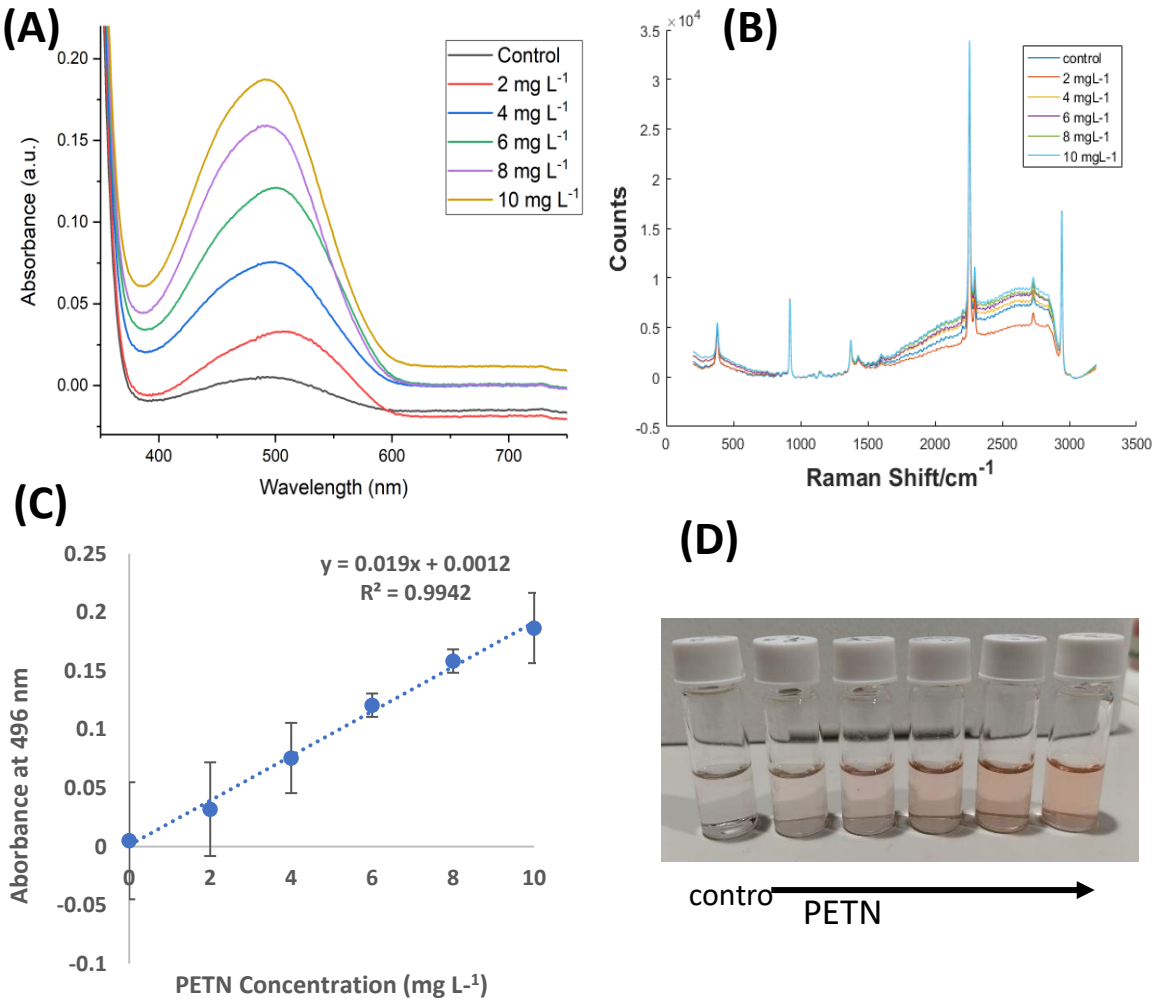

*Figure 3.9: Absorbance **(A)** and Raman **(B)** spectra obtained from the reaction of 2-10 mg L^{-1} PETN in the Original Griess assay. Raman spectra were collected using a Snowy benchtop instrument with an excitation wavelength of 532 nm (40 mW) and an acquisition time of 1s. **(C)** Plot of absorbance of 496 nm peak against PETN concentration (mg L^{-1}) shows a linear relationship in the range of 2-10 mg L-1 (R^2 = 0.99). Error bars indicate standard deviation on 3 replicate samples. A visual picture **(D)** was taken of the sample colour gradient observed.*

From Figure 3.9 (A) it can be observed that the absorbance response to the Griess assay performed on a PETN concentration range of 2-10 mg L^{-1} was poor and an absorbance maximum of 0.17 was achieved. As discussed, the experiment was performed in 5 mL glass vials and the sample was thoroughly mixed during synthesis, resulting in the peach colour. This affected the absorbance profile obtained from the samples, broadening the peaks which therefore made the absorbance peak maximum differ slightly in each sample.

From Figure 3.9 (C) it can be observed that the absorbance displayed a linear dependence on PETN concentration, for the range investigated of 2-10 mg L^{-1}. The LOD was calculated using three times the standard deviation of the blank divided by the gradient of the line obtained and was calculated to be 7.89 mg L^{-1} which was higher compared to the 0.033 mg L^{-1} obtained in Üzer et al's work.[136] Water contamination and degradation of the reacting molecules caused very large error bars which was the cause of the high LOD found in this concentration study.

The samples were interrogated using a 532 nm excitation wavelength to try and be in resonance with the molecules. This spectrum is shown in Figure 3.9 (B). Other than the increasing fluorescence signal, only solvent vibrational bands were identified in the spectra, making this assay unable to use resonance Raman spectroscopy as an analytical method. It is possible that the concentration of the product was too low, and therefore the resonance Raman signal was undetectable.

The original Griess assay investigated in this work was able to detect PETN to a LOD value of 7.89 mg L^{-1}, which was larger than found in previous work. This reaction was modified in an attempt to increase the absorbance response and obtain lower LOD values.

3.3.6 Modifying the Original Griess reaction

As the original Griess reaction had been modified to successfully detect PETN, one of the first changes to the original reaction to increase the absorbance response was to switch the NED molecule for 3,5- dimethoxyaniline (DMA). The pKa value for DMA is around 3.6[146] whereas the pKa for NED was 9.4. Using DMA instead of NED should increase the speed of reaction as it is more favourable for sulfanilamide to couple with DMA than NED in acidic pH's. The molecular structure for both these molecules can be found in Figure 3.10. The version of reaction where DMA is used instead of NED shall be referred to as the "modified Griess" reaction, or the "mod Griess" for short. It should be noted that this reaction differs from the modified Griess test used to detect gunpower residue[147], however for simplicity this modified reaction is labelled "mod Griess" during this thesis.

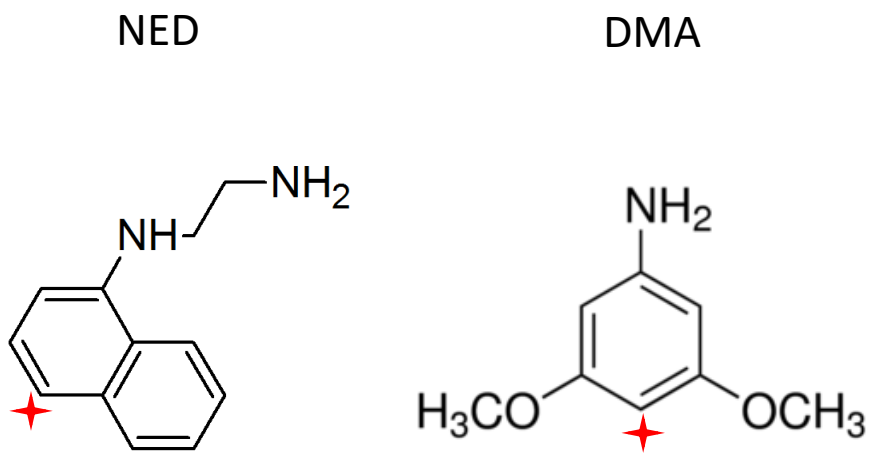

Figure 3.10: Molecular structures of N-(1-naphthyl)ethylenediamine (NED) and 3,5-Dimethoxyaniline (DMA). The azo attachment area has been highlighted with a red star.

Both original and modified Griess reagents were prepared as explained in experimental section 6.4.1, keeping the concentrations of NED and DMA the same (0.2% w/v). Initial experiments found that by changing NED to DMA, the wavelength of the resulting azo dye unsurprisingly also changed, from ~500 nm (original Griess after sample agitation) to ~435 nm (modified Griess using DMA), as a result of a

reduction of conjugation between the two molecules. It was also observed that the resulting sample from the Modified Griess reaction did not change colour depending on sample agitation, as was observed for the original Griess reaction.

The ratio of water to acetone varies in the original paper depending on which test was being used, either the original Griess or their nanoparticle version. As PETN was dissolved in either acetone or acetonitrile, the effect of different solvents on the resulting product was investigated. For this, samples made of 100 % Milli-Q water, 100% acetone and 100% acetonitrile (ACN) were examined. To simplify this reaction, a 10 mg L^{-1} solution of sodium nitrite replaced PETN as it is a more readily available nitrite source that does not require hydrolysis or reduction steps. These absorbance spectra are shown in Figure 3.11 (A) and a picture of the samples are in Figure 3.11 (B).

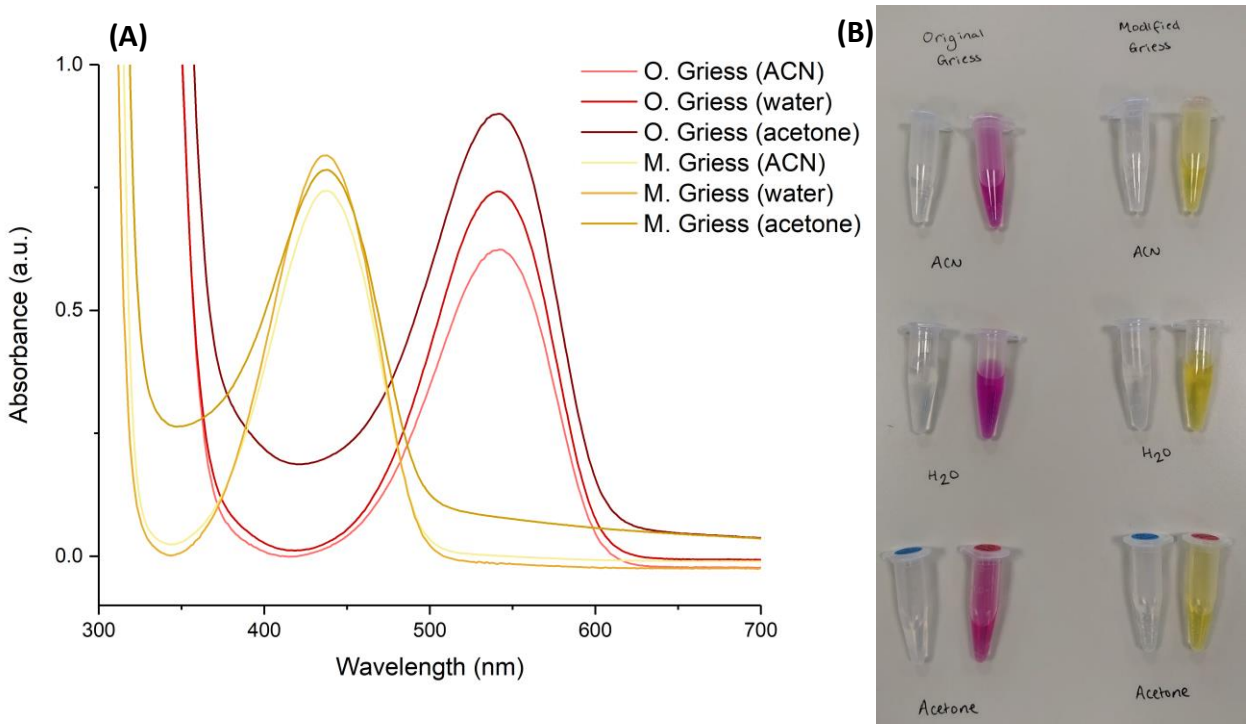

*Figure 3.11: Absorbance spectra for the original Griess (red) and modified Griess (yellow) reactions performed in either 100% acetonitrile (ACN), water or acetone **(A)**. Picture of the resulting samples **(B)**.*

It was found that changing the solvent used for the reaction slightly altered the perceived colour of the Griess reaction product. The Griess reaction in pure water obtained a wavelength of 535 nm, whereas the pure acetone or acetonitrile samples had a wavelength of 540 nm. This shifting of the wavelength shows the resulting azo dye from the original Griess reaction experiences a solvation effect depending on the solvent used, which could cause problems for the reactions involving explosives, as a mixture of water and acetone (or ACN) is used in varying amounts for the different assays. No solvation effect was observed for the modified Griess reaction product, where all three solvents gave wavelengths of 435 nm. Interestingly, the λ_{max} of the modified Griess product was the same as the λ_{max} for GM19, another azo dye made by this research group containing DMA.[148]

The same dilution factor was applied to all the samples, so the comparison was fair. It was observed that the absorbance of the modified Griess reaction products was very consistent, whereas the absorbance for the original Griess reaction varied depending on the solvent used. The acetone samples for both versions of the Griess reaction contained raised background levels, which were observed in both the $NaNO_2$ spiked samples and the controls (containing solvent only).

It should be noted that by using 10 mg L^{-1} sodium nitrite in pure acetone (the highest concentration examined for the Griess reaction with PETN), the expected wavelength of the resulting azo dye from the original Griess reaction (540 nm) which was stated earlier was found, whereas this wavelength was not found for PETN. This was due to the lack of base in the sample, which was needed to hydrolyse PETN in the explosive samples. This is further evidence that the two different wavelengths found for the PETN samples are most likely due to the pH of the sample at certain stages. While a basic pH is needed for the hydrolysis of PETN, an acidic one is needed for the azo product to form, this is why the Griess reagent is made up in 10% phosphoric acid. The nitrite ions would also be more concentrated in the sodium nitrite sample than in the PETN one, making the azo reaction easier/ more successful.

The variation of the λ_{max}, and the inconsistency of absorbance when using different solvents for both experiments performed with NED and the colour change observed upon sample agitation for reactions involving explosives made the Original Griess reaction less desirable when considering future experiments. This prompted further work to be performed on the modified version of the assay as these disadvantages were not seen.

The second change to the reaction was to replace the solvent (Acetone used in the paper) with ACN, as the high, sloping background observed in the Griess samples was undesirable. While the background observed for the $NaNO_2$ sample is the worst-case scenario (as it used 100% acetone), the possibility of a background affecting the sample, by masking a signal or by increasing the absorbance observed, should be avoided.

Therefore, the Mod Griess reaction substituted NED for DMA, and was performed in a 4:1 acetone-water medium.

3.3.7 LOD values for Modified Griess reaction

To obtain an LOD value for the detection of PETN using the modified Griess reaction, the assay was performed in triplicate using PETN in the concentration range of 2-10 mg L^{-1}, following the experimental procedure listed in section 6.4.6. The solutions were analysed by absorption and Raman spectroscopy. The modified Griess reaction scheme and all spectra can be found in Figure 3.12.

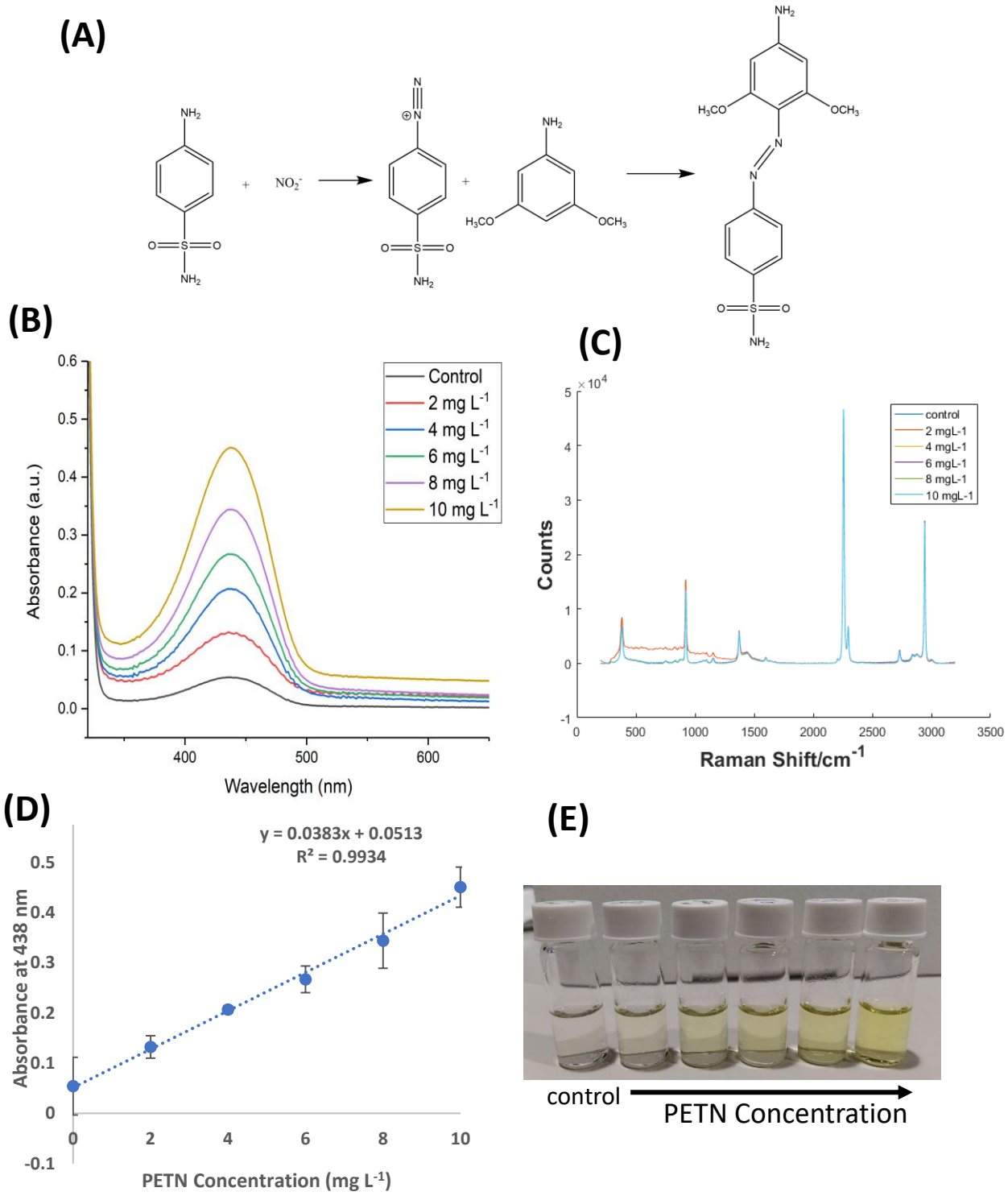

Figure 3.12: ***(A)*** *Reaction scheme of the Modified Griess assay. Absorbance* ***(B)*** *and Raman* ***(C)*** *spectra obtained from the reaction of 2-10 mg L^{-1} PETN in the modified Griess assay. Raman spectra were collected using a Snowy benchtop instrument with an excitation wavelength of 532 nm (40 mW) and an acquisition time of 1s.* ***(D)*** *Plot of absorbance of 496 nm peak against PETN concentration (mg L^{-1}) shows a linear relationship in the range of 2-10 mg L-1 (R^2 = 0.99). Error bars indicate standard deviation on 3 replicate samples. A visual picture* ***(E)*** *was taken of the sample colour gradient observed.*

The modified Griess assay obtained a higher absorbance response than the original assay, reaching an absorbance maximum of 0.45 compared to the 0.17 found in the original Griess assay. The absorbance profiles were also sharper, and the maximum wavelength only varied by 1-2 nm.

The absorbance obtained from the modified Griess assay displayed a linear dependence on PETN concentration, for the range investigated of 2-10 mg L^{-1}. The LOD was calculated to be 4.7 mg L^{-1} which is better than the LOD for the original Griess assay, however, is still not comparable to the LOD of 0.033 mg L^{-1} obtained in the original work.

Again, the samples were interrogated using a 532 nm excitation wavelength to obtain the Raman signals observed in Figure 3.12 (C). This assay only resulted in solvent bands, completely lacking the fluorescence signal observed in the original Griess assay as the excitation laser was further removed from the λ_{max} of 435 nm. The PETN concentration range investigated would still not be strong enough to be seen using Raman, especially as the absorbance maximum was 435 nm and therefore the excitation laser would not be in resonance with the azo product.

The original Griess reaction was successfully recreated, and a modified version developed which resulted in a stronger absorbance and a lower PETN LOD value than those found in the original Griess reaction. The modified version was unaffected by different solvents, resulting in the same absorbance and wavelength maxima, making the reaction more reliable than the original Griess reaction.

3.3.8 Recreating the Nanoparticle assay

The second part of the original paper used a nanoparticle reaction for the detection of the explosive PETN, analysing only by absorption spectroscopy. In this section, their detection method was repeated however SERS analysis was applied in a bid to lower the limit of detection of PETN. For the nanoparticle synthesis, gold

nanoparticles were synthesised using a citrate reduced method and then conjugated with 1.11 mM 4-ATP (4-ATP-NP). In this reaction, 4-ATP was used instead of sulfanilamide, as the structures were very similar, however 4-ATP contains a thiol functional group, instead of a SO_2NH_2 functional group, which allows for easy and strong attachment onto a gold or silver nanoparticle surface.[149] Thiol functional groups are often utilised when functionalising nanoparticles with Raman resonant dyes as they contain strong metal complexing properties and the attachment is ideal as SERS is a distance-dependent phenomenon. The extinction spectrum of the nanoparticles before and after 4-ATP functionalisation is shown in Figure 3.13.

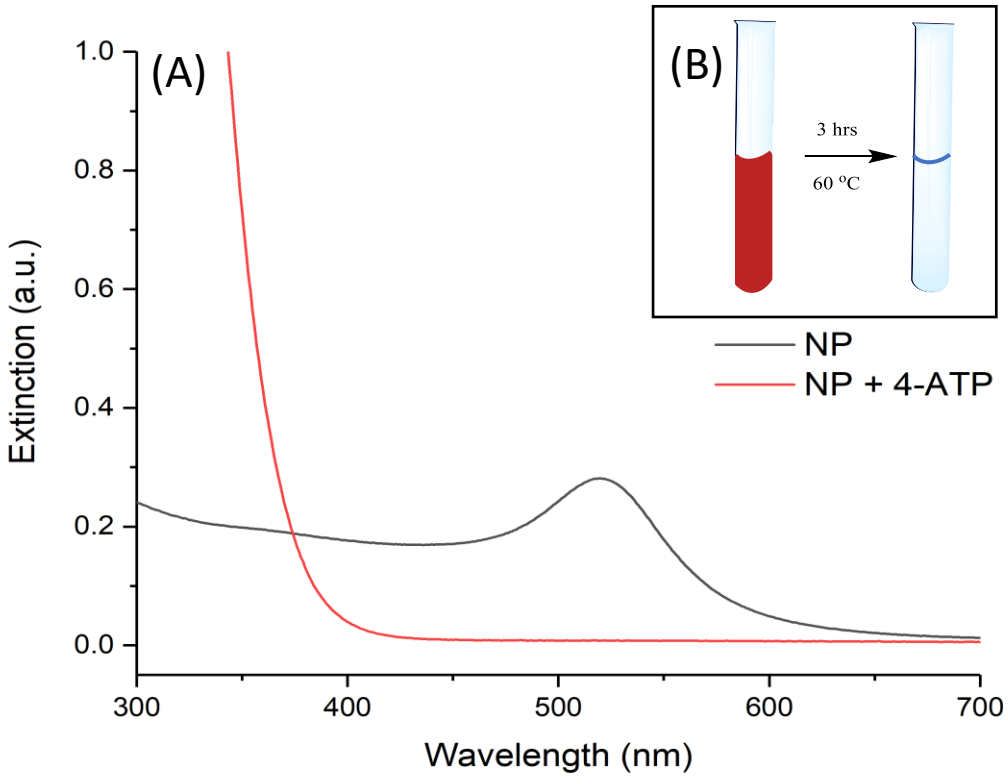

*Figure 3.13: Extinction spectra of gold nanoparticles before (black) and after (red) conjugation of 4-ATP **(A)**. Nanoparticles before 4-ATP addition displayed an excitation maximum of 519 nm. **(B)** displayed the colour change experienced before and after 4- ATP addition in a visual format.*

A colour change (red to clear) was visually observed during the heating stage of the 4-ATP conjugation, which suggests that the nanoparticles have completely aggregated out of solution due to the high concertation of 4-ATP. This result was

supported by the extinction spectra in Figure 3.13 (A), where a spectrum was taken before (black) and after (red) the 4-ATP functionalisation. The extinction maximum of the nanoparticles at 519 nm disappears after the conjugation, which was also observed in the original paper. DLS measurements taken of the NP before and after 4-ATP conjugation told of an apparent size increase from 26.6 ± 0.6 nm (before) to 157.6 ± 36.3 nm (after). Both the lack of an extinction profile and the size of the conjugated NP suggested severe aggregation had occurred, therefore calling into question whether the nanoparticle assay from the paper actually included nanoparticles. While the lack of the nanoparticles LSPR would not matter in the original paper (as they only used absorption spectroscopy analysis), this chapter is attempting to develop a SERS test and therefore nanoparticles are very important as they provide the roughened NP surface to enhance the azo product.

In order to examine whether the 4-ATP had successfully conjugated to the nanoparticle, the Raman spectrum of 4-ATP at the sample concentration was taken. To do this, 4-ATP was diluted in water to be the same concentration as would be found on the nanoparticle (1.11 mM). Raman and SERS analysis were then performed on both samples and then compared. These spectra are shown in Figure 3.14.

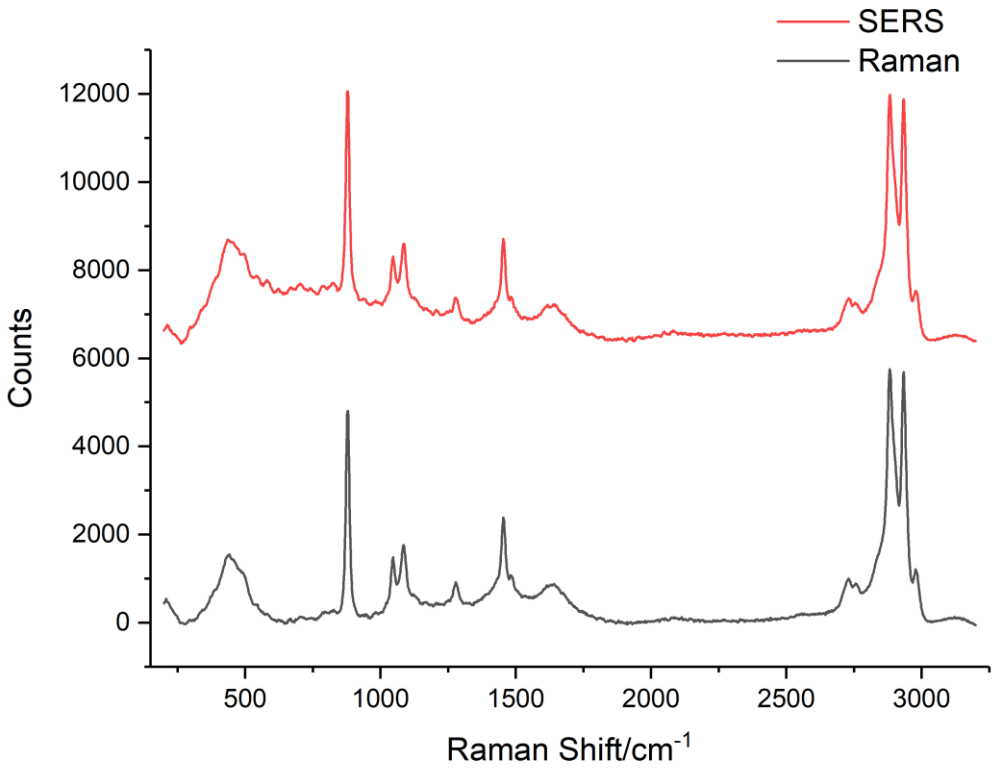

Figure 3.14: Raman and SERS spectra obtained from the 4-ATP solution (black) and the 4-ATP-NP solution (red) solution. Spectra were obtained using a Snowy benchtop instrument with an excitation wavelength of 532 nm (40 mW) and an acquisition time of 1s. Spectra were baselined corrected and offset for clarity.

Comparing both the 4-ATP-NP SERS (red) and the 4-ATP Raman (black) spectra, it can be observed that the spectra of the 4-ATP molecules were completely the same. When overlapping the spectra, it was even found that there was no intensity difference between both samples. This confirms the theory that the 4-ATP conjugated nanoparticles were unstable and aggregated out of solution therefore not taking part in the SERS.

Despite the aggregated NP, the assay with them included was used to detect PETN and compared with an assay with just 4-ATP solution. In this comparison, DMA was used instead of the suggested NED for the reasons described in the previous section. The reaction preceded as described in experimental section 6.4.6 and was analysed by absorption spectroscopy and by using 532 nm laser excitation. These spectra can be found in Figure 3.15.

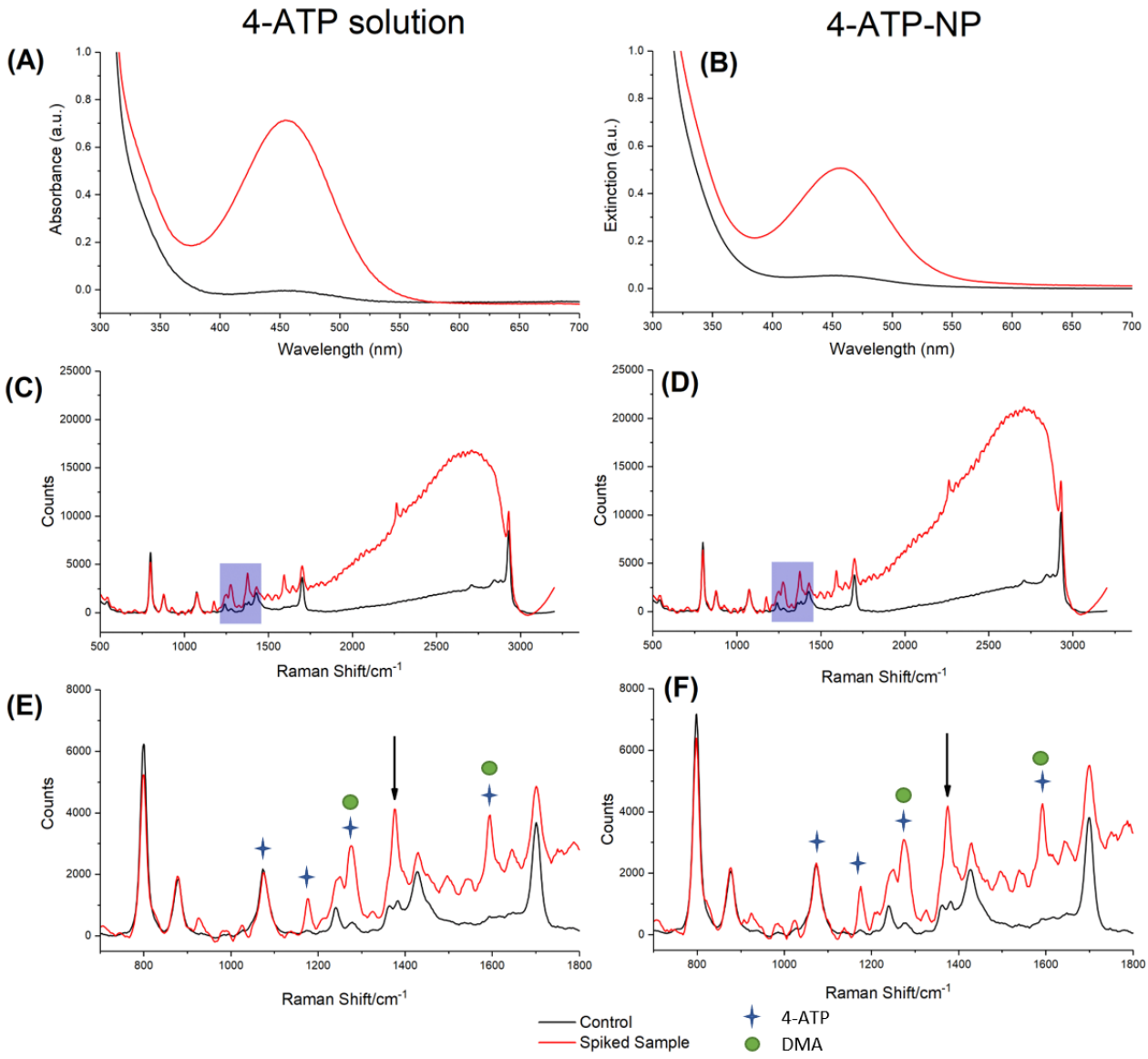

*Figure 3.15: UV-Vis spectra and Raman/SERS spectra from the nanoparticle assay performed with 50 mg L^{-1} PETN. **(A)** and **(C)** are the absorbance and Raman spectra from the assay performed with the "Mock" 4-ATP-NP solution, **(B)** and **(D)** are the extinction profile and SERS spectra from the assay performed with the 4-ATP-NP solution. **(E)** and **(F)** and the enhanced spectra of the peaks of interest found in the purple boxes in **(C)** and **(D)**. Raman/SERS spectra were obtained using a Snowy benchtop instrument with an excitation wavelength of 532 nm (40 mW) and an acquisition time of 1s. The spectral peaks belonging to 4-ATP have been identified with a blue star, DMA with a green circle, and the azo peak has been identified with a black arrow.*

Comparing the spectra obtained from the 4-ATP solution (left column, spectra (A), (C) and (E)) and the 4-ATP-NP (right column, spectra (B), (D) and (F)), it can be observed that both UV-Vis spectra and resonance Raman/SERS spectra are very similar to each other. The absorbance (A) and extinction (B) profiles both had

absorbance maxima of around 456 nm, and though the maximum absorbance differs slightly. It can be suggested that the nanoparticle version would result in a weaker absorbance as some of the 4-ATP would aggregate out of solution on the nanoparticle, therefore being unavailable for the azo reaction. For both the Raman (E) and "SERS" (F) spectra, while the spectra are very similar for each sample, several spectral properties belonging to the spiked sample of both can be discussed. Despite both sample sets resulting in the same signal, this was a good result as it was the first time different spectra had been observed in the control and spiked samples. Tentative peak assignments have been made in Table 2.

Table 2: Tentative peak assignment of azo product from reaction 4-ATP and DMA with 50 mg L^{-1} PETN. [150, 151, 152, 153]

Wavenumber (cm^{-1})	Assignment
800	C-H stretch (acetone)
1076	C-S stretch (4-ATP)
1176	b_2 C-H bending mode of benzene (4-ATP)
1250	C-C stretch (acetone)
1276	C-H in benzene ring (4-ATP and DMA)
1370	N=N (azo) stretch
1595	C-C ring stretch (4-ATP and DMA)

The first property which is apparent is the large broad background across most of the wavenumber range examined in spectra (C) and (D), which is due to the fluorescence

of the sample. This is another piece of evidence supporting the lack of nanoparticles in the 4-ATP-NP solution as if the solution contained nanoparticles, then the fluorescence would be quenched due to energy transfer between the molecule and the metal.[37] Basic post-processing of the data to remove the fluorescence background by baseline correction in Matlab was not particularly successful, as fluorescence was still observed at higher wavenumbers in the spiked sample spectra in (E) and (F).

From Figure 3.15 (E) and (F) vibrational bands at 1176 cm^{-1} (C-H bend in benzene), 1276 cm^{-1} (C-H stretch in benzene) and 1595 cm^{-1} (C-C stretch in benzene) can also be identified which only appear in the spiked samples. While the intensity values of 1276 cm^{-1} and 1595 cm^{-1} are unreliable due to the fluorescence background, it can be observed that the ratio between the acetone peak at 1250 cm^{-1} and the benzene peak at 1276 cm^{-1} has switched, suggesting a change in bonding has occurred. These bands are most likely occurring due to the combined vibrations of the benzene rings of both DMA and 4-ATP when combined to form the azo product. The last peak to identify is the N=N azo band at 1370 cm^{-1}. This experiment yielded good results, as while it proves that the nanoparticles in 4-ATP-NP have precipitated out of solution, the azo band also confirms that the reaction was successful and that it could be monitored for the first time using Raman spectroscopy. The 1370 cm^{-1} peak was used as the main indicator in Raman analysis that the azo product has formed and was one of the bands used to quantify the formation of the final product in this chapter.

An attempt was made to wash the excess 4-ATP from the conjugated nanoparticles by centrifugation, however, the results were the same as shown in Figure 3.15. This suggests that it was quite difficult to remove the excess 4-ATP from the nanoparticle solution if there were any nanoparticles in the solution in the first place.

Free 4-ATP molecules should experience a greater rate of reaction than it's nanoparticle conjugated counterpart as the latter would have reduced diffusion, resulting in a slower reaction. However, little difference was found in the vibrational

band wavenumbers and the intensity of the signal obtained from the two different samples, again suggesting the 4-ATP solution and the 4-ATP-NP were the same.

From these results, a conclusion was drawn that the signal seen from the azo reaction with the 4-ATP conjugated nanoparticles was from the resonance Raman of the synthesised molecule, rather than a SERS enhancement from the gold nanoparticle. The original nanoparticle assay from the paper shall now be referred to as the "NED RR (or resonance Raman) assay" and the modified version will be known as the "DMA RR assay". The detection of PETN with both assays will be compared in section 3.3.10.

3.3.9 Investigating solvent effect on resonance Raman assays

In both the original and modified Griess reactions, the molecules were prepared together in an acidic medium, which helps to facilitate the reaction. However, in the resonance Raman assays, the solutions of 4-ATP, NED and DMA are not particularly acidic. In this section, both the solvation and pH (acidic and neutral) effect on the products from both resonance Raman assays were investigated in a similar way to the study on the solvent effect for the Griess and modified Griess reactions in section 3.3.6. This experiment was performed to identify which solvent obtained the strongest absorbance of the azo product, if the absorbance maxima changed with different solvents and to observe if acidic pH's were required.

10 mg L^{-1} sodium nitrite replaced PETN and the azo reaction was tested in 100% ACN, H_2O and acetone. Three samples were prepared instead of the original two investigated in section 3.3.6 (control and spiked sample). These three samples were a control sample without sodium nitrite, a spiked sample with an acidic pH (pH 3) and a spiked sample with a neutral pH (pH 7). The sample preparations have been detailed in experimental section 6.4.6, removing the addition of the acids for the neutral sample. The absorbance spectra obtained from these samples can be found in Figure 3.16.

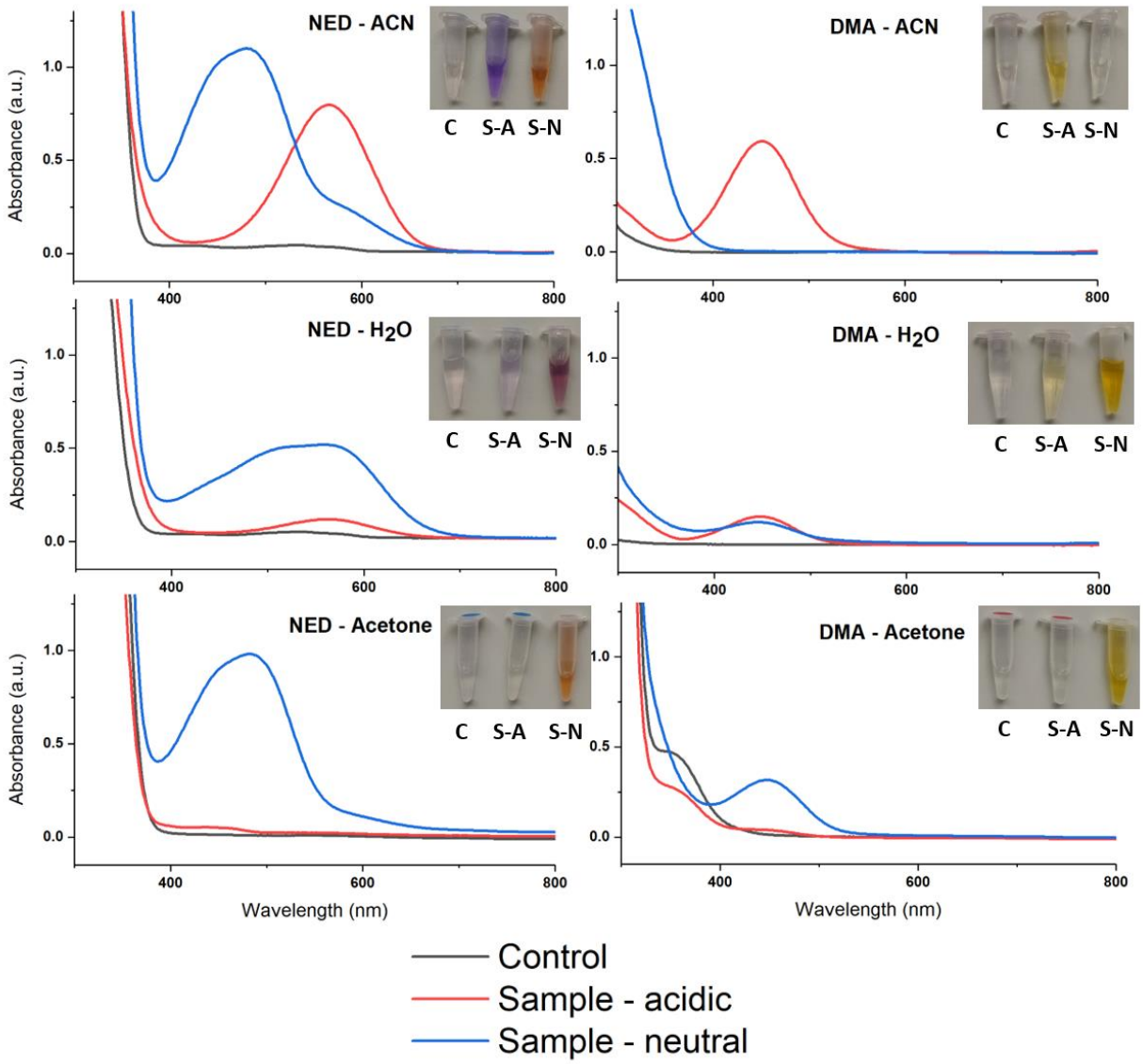

Figure 3.16: Absorbance spectra for the original NED (left column) nanoparticle reaction and the modified DMA version (right column) performed in either 100% ACN, H_2O or acetone. Each spectrum contains 3 samples, a control which lacked nitrite ions (C), a spiked sample which was acidly pH adjusted (S-A) and a spiked sample which was kept at a neutral pH (S-N). Pictures of each sample set 48 hours after samples were made have been attached to the appropriate absorbance spectra.

The general pattern observed from Figure 3.16 was that the NED resonance Raman assay resulted in very differently coloured compounds depending on both the solvent used and the pH of the solution, whereas the DMA version varied less. As discussed for the previous data set of the Griess reactions, the different coloured products for the NED reaction can be explained by the solvation effect, where a compound appears a different colour depending on the solvent used. Again, this solvation effect

was not observed for the DMA samples. The difference between the acidic (pH 3) and neutral (pH 7) samples are less easy to explain. The results are summarised in Table 3.

Table 3: Summary of the results from the NED and DMA resonance Raman assay with different solvents, and different pH.

		Azo product formed	Expected λ_{max}
NED – ACN	Control	✗	-
	Sample – Acidic	✓	✗
	Sample – Neutral	✓	✓
NED – H_2O	Control	✗	-
	Sample – Acidic	✓	✗
	Sample – Neutral	✓	✗
NED - Acetone	Control	✗	-
	Sample – Acidic	✗	-
	Sample – Neutral	✓	✓
DMA – ACN	Control	✗	-
	Sample – Acidic	✓	✓
	Sample – Neutral	✗	-
DMA – H_2O	Control	✗	-
	Sample – Acidic	✓	✓
	Sample – Neutral	✓	✓
DMA - Acetone	Control	✗	-
	Sample – Acidic	✗	-
	Sample – Neutral	✓	✓

It can be observed that the NED-acetone reaction only produced its coloured complex in a neutral pH. This result was strange, as it is known that H^+ ions are needed to facilitate the azo reaction, and therefore usually an acidic pH is required. This unusual result was similarly seen in the NED-H_2O samples. The absorbance peak observed for the neutral sample was also undesirably broad. This could potentially

affect the absorbance obtained from explosive samples, as they would be performed in a medium partially made up of H_2O. Both the acidic and neutral samples in ACN produced coloured compounds, however, the resulting λ_{max} differed greatly (acidic = 567 nm, neutral = 481 nm).

For the DMA samples (right column), it should first be mentioned that the neutral samples for H_2O and acetone changed in intensity after UV-Vis analysis. Where before the samples were only slightly coloured, after analysis they became a vibrant yellow. It was also observed that the DMA-ACN samples only reacted at an acidic pH, whereas the NED counterpart reacted for both a neutral pH and an acidic one. This can be explained by examining the pKa values of each NED and DMA. As previously mentioned, the pKa value for NED was ~9.4 and was ~3.6 for DMA, meaning that this reaction will favour the coupling of DMA in acidic conditions, whereas the coupling of NED is possible in neutral pH's. It was also observed that the resulting absorbance obtained from the H_2O and acetone samples were less intense than those for the ACN sample.

Similar to the Griess and modified Griess reaction, a conclusion from these results can be drawn that the DMA RR assay was more reliable as the λ_{max} did not vary and the width of the absorbance peak was the same in each solvent case. The solvent ACN resulted in the highest absorbance for the acidic sample and the majority of the colour change occurred within 10 minutes. The acidic samples performed in H_2O and acetone required additional time to form an azo complex, but resulted in a less intense absorbance spectrum. The relationship between the absorbance intensity and reaction time is important as the absorbance directly relates to the concentration of the azo product being formed. Presumptive tests should be designed to complete in a reasonable time frame, as they are commonly used for in-field analysis and further testing can be required to specify the explosive.

One advantage to the DMA RR assay is that the azo product has a λ_{max} closer to the extinction wavelength of silver nanoparticles, which can result in a better SERS

enhancement than gold nanoparticles.[154] The adaptation of these resonance Raman assays to their SERS counterpart is investigated in Chapter 4.

3.3.10 LOD values for resonance Raman assays

NED Resonance Raman

To obtain an LOD value for the detection of PETN using the NED resonance Raman reaction, the assay was performed in triplicate using PETN in the concentration range of 10-50 mg L^{-1}, following the experimental procedure listed in section 6.4.6. The solutions were analysed by absorption and Raman spectroscopy to compare the LOD values obtained from each technique. The NED RR reaction scheme and resulting absorbance spectra can be found in Figure 3.17.

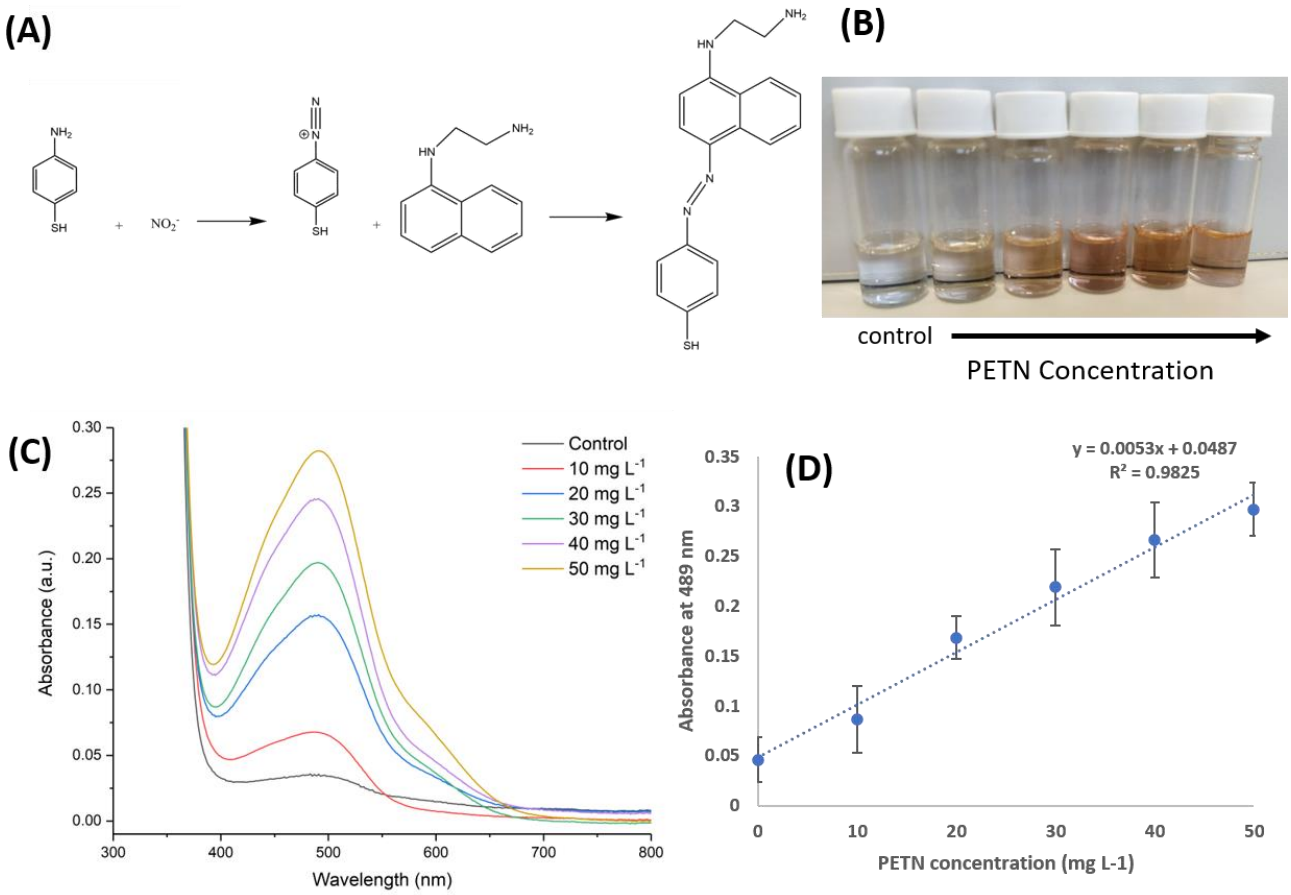

*Figure 3.17: **(A)** Reaction scheme of the NED Resonance Raman Assay with a visual picture **(B)** of the reaction of 10-50 mg L^{-1} PETN in the assay. Absorbance spectra **(C)** and the plot of absorbance of the 489 nm peak against PETN concentration (mg L^{-1}) shows a linear relationship in the range of 10-50 mg L^{-1} (R^2 = 0.98). Error bars indicate standard deviation on 3 replicate samples.*

From Figure 3.17 (C) it can be observed that the absorbance response to the NED RR assay performed on a PETN concentration range of 10-50 mg L^{-1} was poor, reaching a maximum of 0.30. Again, this assay had a linear relationship with the PETN concentration. Using graph (D) the LOD was calculated to be 11.3 mg L^{-1}, whereas the LOD in the original paper was 0.15 mg L^{-1}. While the alterations performed on this assay meant that a direct LOD comparison could not be made, it was still observed that the LOD resulting from the work in this chapter was larger by a factor of 10.

Both the original Griess and the NED RR assays were similar to each other, as they both contained NED as a reactant. When comparing the original Griess and NED RR assays, it was observed that the Griess reaction resulted in both a lower LOD and a

better R^2 value. However, this lower LOD value does not necessarily mean that the Griess reaction was superior. As both assays examined different concentration ranges, a direct comparison cannot be made as the LOD for the NED RR assay could be reduced if the concentration range of 2-10 mg L^{-1} was investigated. Time restrictions meant that this additional concentration study could not be performed.

However, while the Griess reaction could only be monitored using absorption spectroscopy, the NED RR assay could additionally use resonance Raman spectroscopy. (Figure 3.18)

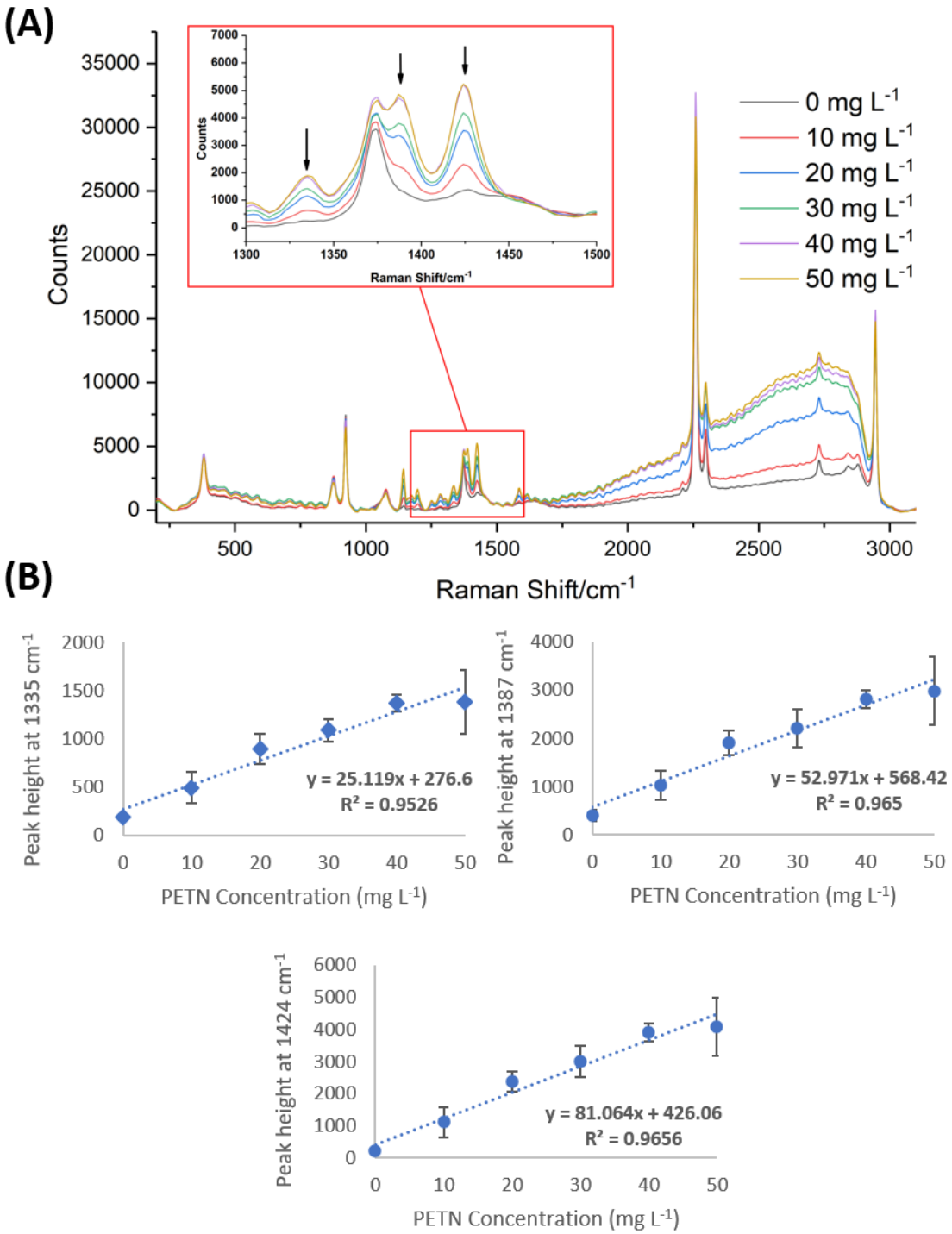

Figure 3.18: ***(A)*** *Resonance Raman spectra obtained from the reaction of 10-50 mg L^{-1} PETN in the NED RR assay. Spectra were collected using a Snowy benchtop instrument with an excitation wavelength of 532 nm (40 mW) and an acquisition time of 1s.* ***(B)*** *contains the plot of peak heights of four different bands (1336 cm^{-1}, 1387 cm^{-1} and 1424 cm^{-1}) against PETN concentration (mg L^{-1}). Error bars indicate standard deviation on 3 replicate samples.*

It was observed that several bands (and the fluorescence background) in the

resonance Raman spectra increased with increasing PETN concentration. Three main bands of the product molecule have been identified at 1336 cm^{-1} (ring stretch), 1387 cm^{-1} (azo stretch) and 1424 cm^{-1} (quadrant stretches of the aromatic rings).[153,151,152] As this reaction investigated the NED RR assay, the identified bands are slightly different from those identified in Figure 3.15 and Table 2, which belonged to the DMA RR assay. The peak height of these Raman bands have been plotted against the PETN concentrations in Figure 3.18 (B) by subtracting the height of the trough from the height of its adjacent peak, and the LOD's calculated. When considering the three bands, multiple LOD values were calculated ranging from 1.7-6.4 mg L^{-1}, which is a superior value than found when using absorption spectroscopy. While both the azo peak at 1387 cm^{-1} and the band at 1424 cm^{-1} were observed to experience a large increase in intensity over the concentration range studied, the LOD calculated using the azo band resulted in the highest LOD in the three (6.4 mg L^{-1}). This is likely due to the second peak occurring at 1370 cm^{-1}, which was influenced by the ACN solvent peaks due to CH_3 deforming vibration.[155] Acetone also contains bands at 1370 cm^{-1} and 1426 cm^{-1} which interfere with two of the indicator peaks in this reaction. While this ACN peak is undesirable for this reaction, it was decided that the benefits of a more reliable coloured assay which proceeds under different pH conditions, and the lack of second ACN band at 1424 cm^{-1} outweighs the drawback of the peak.

This assay had a linear relationship with the PETN concentration, however, it appears that the peak height begins to plateau at the higher concentrations, suggesting that the assay is reaching its higher limit of detection. This suggests that the assay can be used as a preliminary test for a wide range of concentrations but can only be used as a quantitative assay for concentrations below 40 mg L^{-1} of PETN. However, it is possible that this detection limit could be widened if the reactant solutions contained a higher concentration of amines (4-ATP and NED), as the plateau of the resonance Raman intensity is likely due to the lack of available amines for the increased nitrate/nitrite ion concentrations obtained from PETN.

DMA Resonance Raman

The second resonance Raman assay investigated replaced NED with DMA. To obtain an LOD value for the detection of PETN using the DMA RR reaction, the assay was performed in triplicate using PETN in the concentration range of 10-50 mg L^{-1}, following the experimental procedure listed in section 6.4.6. The solutions were analysed by absorption and Raman spectroscopy. The DMA RR reaction and resulting absorbance spectra can be found in Figure 3.19.

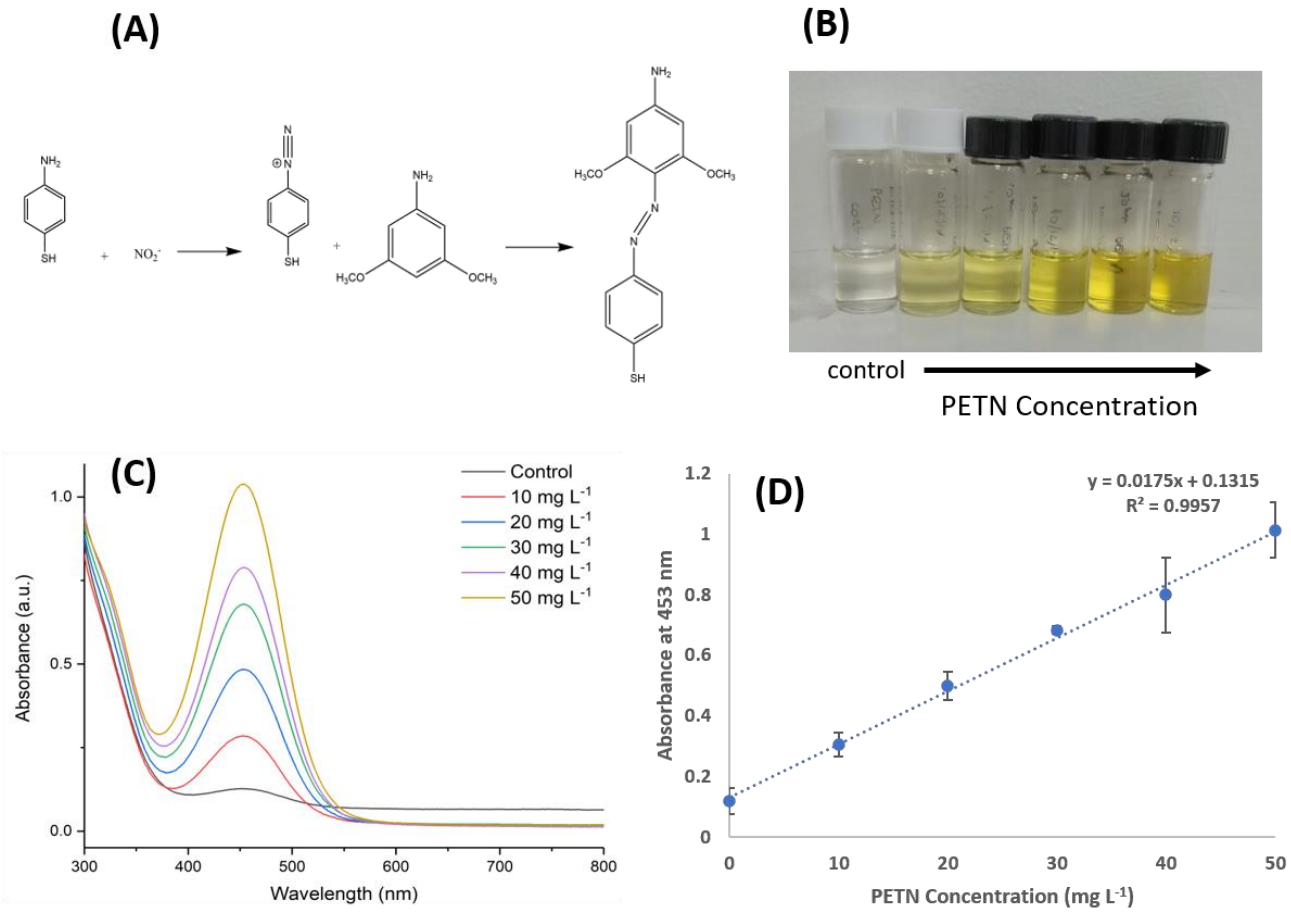

*Figure 3.19: **(A)** Reaction scheme of the DMA Resonance Raman Assay with a visual picture **(B)** of the reaction of 10-50 mg L^{-1} PETN in the assay. Absorbance spectra **(C)** and the plot of absorbance of the 453 nm peak against PETN concentration (mg L^{-1}) shows a linear relationship in the range of 10-50 mg L^{-1} (R^2 = 0.99). Error bars indicate standard deviation on 3 replicate samples.*

From Figure 3.19 (C) it can be observed that the absorbance response to the DMA RR assay performed much better than the NED RR assay, with the maximum absorbance

reached 1.01 abs. Like the other three concentration studies, Figure 3.19 (D) shows that this assay had a linear relationship between absorbance and PETN concentration, with an R^2 value slightly better than the NED RR assay. The PETN LOD using UV-Vis analysis was calculated to be 6.86 mg L^{-1}. It was also observed that the standard deviation in Figure 3.19 (D) were smaller than those seen in the NED RR assay. This error increased at higher concentrations but stayed relatively small for lower concentrations. This is a positive result as it suggests that a lower LOD might be obtained in future experiments. The DMA RR assay was also analysed using a 532 nm laser excitation and the resonance Raman results are shown in Figure 3.20.

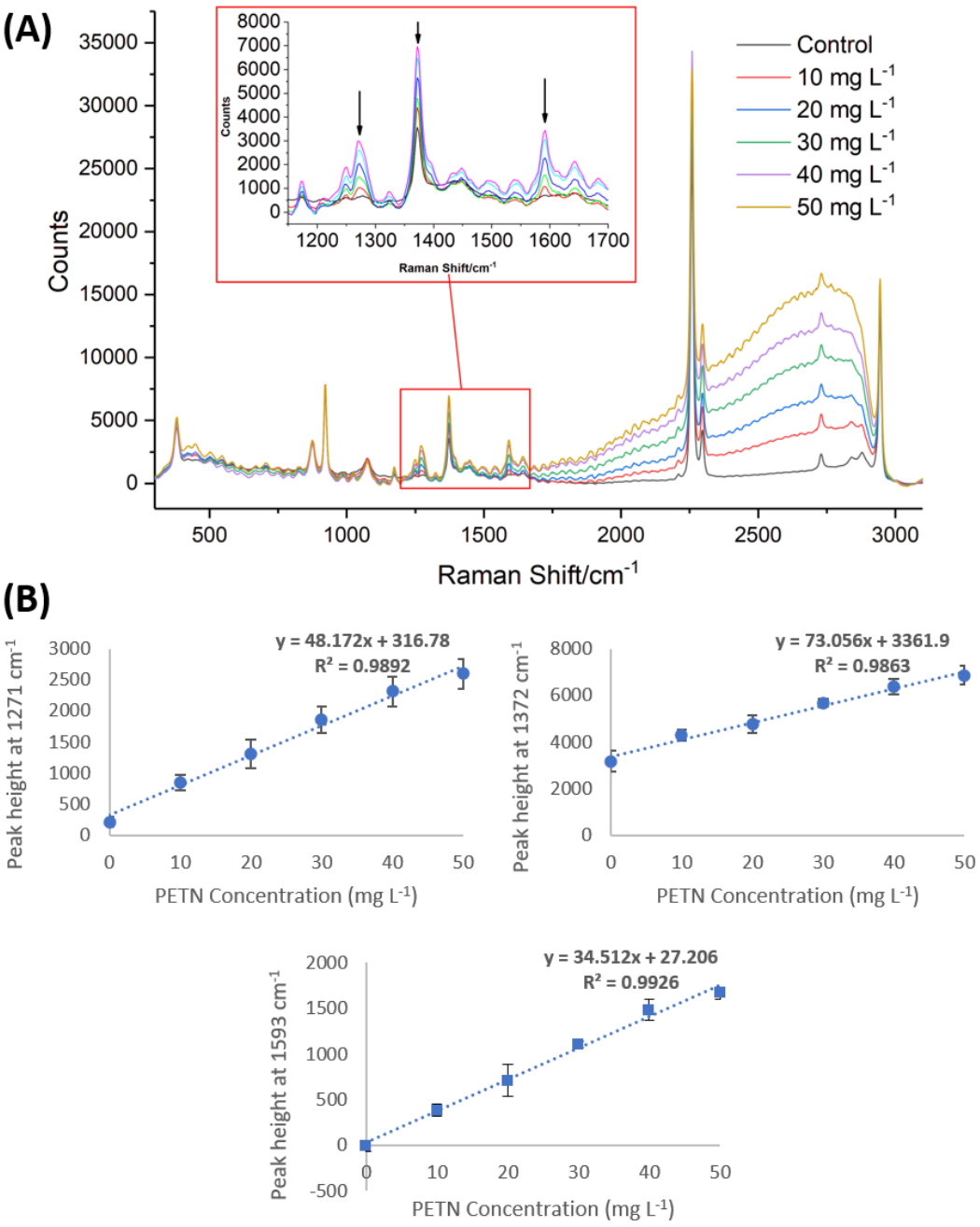

Figure 3.20: ***(A)*** *Resonance Raman spectra obtained from the reaction of 10-50 mg L^{-1} PETN in the DMA RR assay. Spectra were collected using a Snowy benchtop instrument with an excitation wavelength of 532 nm (40 mW) and an acquisition time of 1s.* ***(B)*** *contains the plot of peak heights of three different vibrational bands (1271 cm^{-1}, 1372 cm^{-1} and 1593 cm^{-1}) against PETN concentration (mg L^{-1}). Error bars indicate standard deviation on 3 replicate samples*

It was observed that several bands (and the fluorescence background) in the resonance Raman spectra increased at higher concentration. Three main bands of the product molecule have been previously identified in Table 2. The peak height of

these Raman bands have been plotted against the PETN concentrations in Figure 3.20 (B), and the LOD's calculated. Two of the indicator peaks (1271 cm^{-1} and 1593 cm^{-1}) yielded LOD values of 4.9 mg L^{-1}, which was superior to the LOD calculated from the UV-Vis results. The R^2 values were also slightly higher than those found for the NED RR assay, suggesting that the measurement was more reliable and accurate. However, the azo band yielded an LOD of 18.5 mg L^{-1}, which is quite high for this assay. As explained in the NED RR assay, ACN contains a peak at a similar Raman shift to the azo band, so while this peak could be used to confirm if the reaction was successful at higher PETN concentrations, the other two indicator peaks would be more useful at lower concentrations.

Again, this reaction had a linear relationship with the PETN concentration but did not plateau at higher concentrations. The standard deviation observed in this reaction was also quite small, implying that there was little variation between the three replica samples. These observations suggest that the DMA RR assay can be used quantitatively for this concentration range and perhaps beyond it.

3.4 Chapter Conclusions

In conclusion, it has been demonstrated that an azo reaction can be successfully used to detect PETN. The assay from Üzer et al[136] involved the detection of PETN using a hydrolysis step, a nitrate ion reduction step and the subsequent azo reaction. This chapter details how this reaction was recreated and improved upon. Modifications were made to the assay to ensure PETN hydrolysis occurred, and the resulting absorbance was more intense and reproducible. These modifications resulted in two additional assays, creating a total of four assays which could be analysed by absorption and/or resonance Raman spectroscopy. The Raman instrumentation used in this chapter was portable, therefore making the assay portable and able to be used in field detection.

Modifying the original nanoparticle reaction to exclude the 4-ATP-NP resulted in lower LOD values for the resonance Raman assays than those for the Griess and modified Griess assays. While the LOD values obtained in this chapter were larger than those in Üzer et al's work, it was discovered that the resonance Raman assays resulted in lower LOD values than the Griess assays. This suggests that the reaction has successfully been improved from the version in the paper as they found that the original Griess reaction resulted in the lowest LOD.

Although the NED RR assay yielded a lower calculated LOD value (1.7-6.4 mg L^{-1}), the assay was more temperamental compared to the DMA RR assay (4.9-18.5 mg L^{-1}), as it did not give as strong an absorbance value and the LOD was more varied. While the LOD obtained from the 1372 cm^{-1} band in the DMA RR assay was larger, the other two peaks both yielded an LOD of 4.9 mg L^{-1}, therefore making the assay more consistent. It was found that by changing the solvent from a mixture of acetone: water to ACN: water the resulting absorbance of the coloured product was both more intense and did not experience the solvation effect for the DMA RR assay. However, when using ACN, a solvent peak at 1370 cm^{-1} interfered with the azo band, making it unreliable as an indicator peak at it appeared strongly in the control sample (no nitrite ions). Acetone also contained bands which interfered with the product signal, and so it was decided that ACN was the preferred solvent as it resulted in a better signal. The LOD findings in both resonance Raman assays suggest that the assay could easily detect lower concentrations than those used in the concentration range, perhaps obtaining a lower LOD than found in this work.

3.5 Further work

One method of obtaining a lower PETN LOD would be to change the resonance Raman assay into a SERS or SERRS assay. Severe background correction is needed to remove the fluorescence signal from the spectra affecting the peak intensities, however, this correction would likely reduce the overall signal of the indicator band

peaks. One way of reducing the fluorescence signal is to change the resonance Raman signal to SERS, where the fluorescence is quenched. The development of a SERS assay is discussed in Chapter 4.

Further work on these assays would be to improve the PETN hydrolysis and the nitrate ion reduction step, to achieve the most intense signal possible from the sample. Improving the efficiency of these steps would allow for more accurate detection of PETN, rather than just the resulting nitrite ions. The concentration of the reaction components used in the resonance Raman assays should also be investigated as a more rapid or efficient assay could be developed. Lastly, further work should also be done on testing dirty samples, as in field analysis of real-life samples rarely consist of pure explosives.

Chapter 4 Indirect SERS Detection of PETN

In Chapter three it was demonstrated PETN could be detected using azo chemistry by hydrolysing PETN and converting the nitrate ions to nitrite. This was achieved by modifying the Griess assay to develop three additional assays which could detect PETN with an LOD as low as 1.7 mg L^{-1}. These assays could be analysed by absorption and/or resonance Raman spectroscopy, making the assay portable and therefore can be used in field detection.

In this chapter, the resonance Raman assays in chapter three were shortened to an assay which could quantitatively detect PETN though an indirect SERS assay. Both absorption spectroscopy and SERS spectroscopy using portable instrumentation could be used to detect the lower LOD's of 1-2 mg L^{-1}. This assay was further modified to reach completion within 10 minutes, making it a useful presumptive test able to detect nitro-based explosives for in field detection.

4.1 Introduction

The indirect detection of PETN using colourimetric analysis has previously been demonstrated by Üzer et al.[136] They showed that PETN could be hydrolysed, the resulting nitrate reduced to nitrite which was then used to form an azo compound, however, only UV-Vis analysis was used.

SERS analysis could use portable instrumentation, thus increasing the portability of the assay, and could potentially reach lower LOD values. N. Xiao et al[156] developed a system that used 4-aminothiophenol (4-ATP) conjugated gold nanorods that underwent a coloured reaction in the presence of nitrite ions. In this reaction, the 4-ATP molecule underwent deamination by heating the conjugated nanorods in an ethanol solution with nitrite ions. This led to aggregation of the particles, where the colourimetric response could be used quantitatively to detect nitrite ions. While this

work was not used to detect any explosives, they managed to develop a fast assay that could detect less than 1 ppm of nitrite.

Milligan et al.[116] developed a SERS test which created a coloured Janowsky complex with nitroaromatic explosives. This assay was capable of detecting a multiplex of nitroaromatic explosives in the same sample as it modified the original explosive, allowing it to be conjugated to a silver nanoparticle which then produced unique SERS signals.

PETN, the focus of this thesis, is an aliphatic explosive with a poor Raman cross-section, suggesting that it cannot be modified to give a SERS signal in a solution-based assay. One successful way to obtain a SERS signal from PETN is to hydrolyse the molecule and create a Raman reporter from it.

4.2 Chapter Aims

The aim of this research was to take the assays developed in the previous chapter and modify them to obtain a SERS response, thus making this a sensitive and portable technique when analysed with a portable spectrometer. The second aim was to maximise the resulting SERS signal and to shorten the experiment from the original 75 minutes required.

4.3 Results and Discussion

The previous chapter demonstrated that the 4-ATP "functionalised" gold nanoparticles were not stable and could not be used for the SERS enhancement of the azo products. In this chapter silver nanoparticles were used due to their enhanced scattering when compared to gold. The azo product would be functionalised to the silver nanoparticle surface and provide superiors scattering over gold nanoparticles.

4.3.1 Nanoparticle characterisation

Silver nanoparticles were synthesised using a method by Leopold and Lendl[19], where hydroxylamine hydrochloride was used to reduce silver nitrate at an alkaline pH. These nanoparticles were chosen as the synthesis was relatively simple, the resulting nanoparticle size and shape were easily reproducible, and they were stable for a long period of time. This method resulted in the formation of silver nanoparticles with an extinction maximum (λ_{max}) of 407 nm. The extinction spectrum obtained is shown in Figure 4.1.

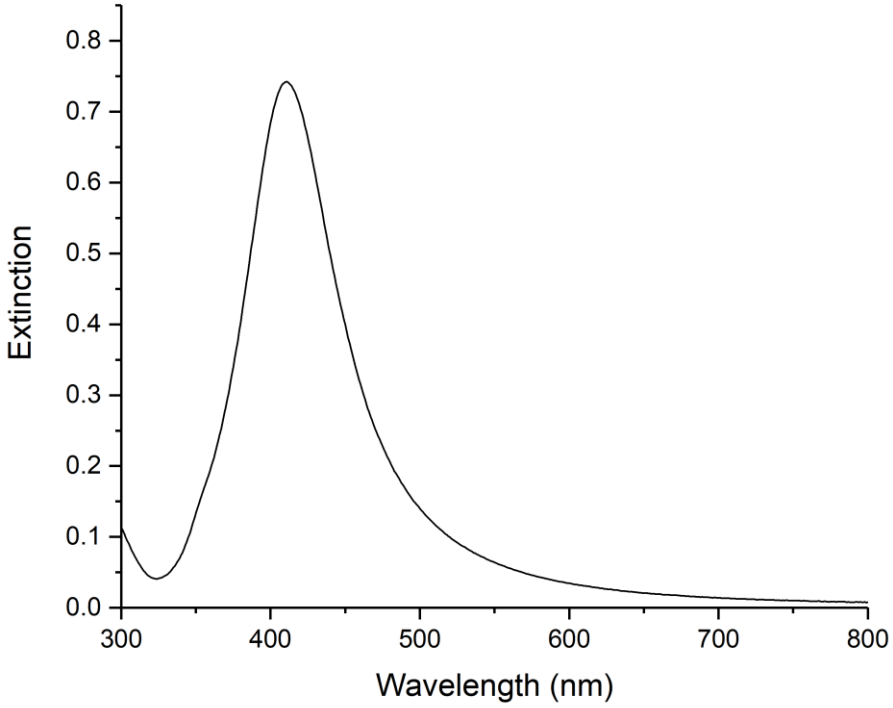

Figure 4.1: Extinction spectrum of hydroxylamine reduced silver nanoparticles. The nanoparticles were diluted 50 x in water and had an extinction maximum of 407 nm, which is characteristic of silver nanoparticles with a diameter of approximately 40 nm.

As shown in Figure 4.1 the silver nanoparticles contained an LSPR of 407 nm which was characteristic of particles with a diameter of approximately 40 nm. Size and zeta potential measurements were performed using dynamic light scattering (DLS). The

size was found to be around 49.3 ± 3.1 nm, the zeta potential was -38.72 ± 1.3 mV and the pH was 7.6. These values were typical for non-aggregated nanoparticles as DLS measures the hydrodynamic diameter of the nanoparticle, and therefore usually gives a larger value than the actual size[157]. The zeta potential indicated that the nanoparticles were stable in solution as nanoparticles below -30 mV or above +30 mV exhibit enough repulsion to not aggregate due to Van der Waals inter-particle attractions [158].

4.3.2 Development of the SERS assay

4.3.2.1 First attempt

Section 3.3.8 demonstrates that the 4-ATP conjugated nanoparticle assays resulted in a resonance Raman signal, rather than the expected/ anticipated SERS signal due to unstable NPs. Although satisfactory, resonance Raman is comparatively weak and it was hoped that by functionalising the azo product to silver nanoparticles that an intense SERS signal of the azo product would be obtained, allowing for a more sensitive assay.

To assess the SERS of the azo product, 100 µL sample (with azo product) was added to 200 µL of hydroxylamine silver nanoparticles and interrogated using an excitation wavelength of 532 nm. A control (no NO_2^-) and a spiked sample (50 mg L^{-1} of PETN) was synthesised using the DMA RR assay described in experimental section 6.4.6. The Raman signal of the samples was also analysed by adding 100 µL sample to 200 µL

H_2O. The Raman and SERS spectra of the samples obtained are shown in Figure 4.2 below.

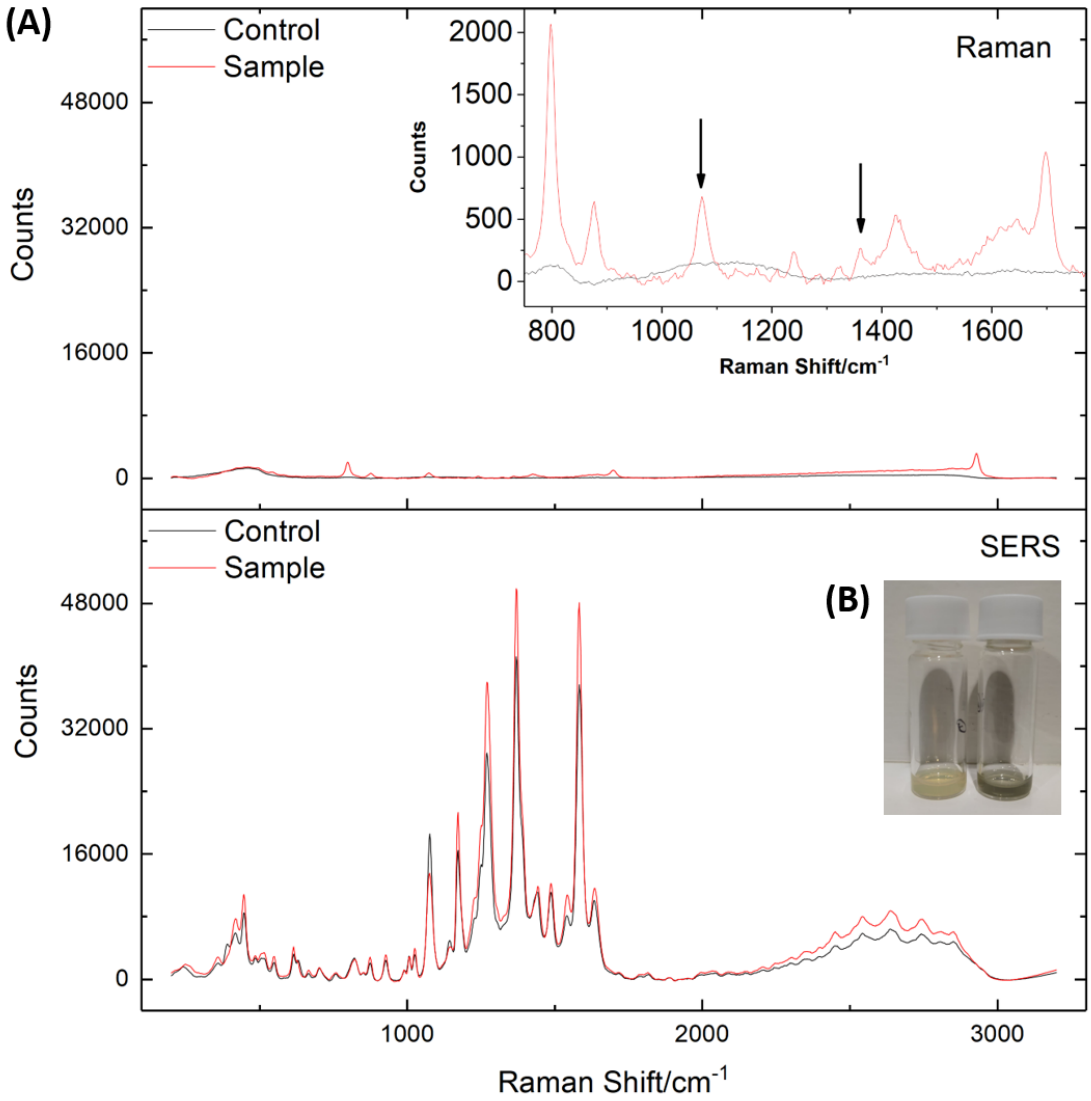

Figure 4.2: ***(A)*** *Raman (upper) and SERS (lower) spectra obtained from the addition of the 100 µL azo product from the DMA RR assay to 200 µL of either H_2O (Raman spectra) or hydroxylamine silver nanoparticle (SERS spectra). Control samples (black) were performed without the presence of a NO_2^- donor and spiked samples (red) used 50 mg L^{-1} PETN.* ***(B)*** *is a visual picture of the nanoparticles before (left) and directly after (right) addition of the sample. Spectra were obtained using a Snowy benchtop instrument with an excitation wavelength of 532 nm (40 mW for Raman spectra, 15 mW for SERS) and an acquisition time of 1s. All spectra were baselined and plotted so the axes would be the same. Indicator peaks for the azo product have been pointed out in the inserted spectrum.*

In the spectra in Figure 4.2, a weak signal was obtained from the resonance Raman spectra of the control and spiked samples and a much stronger signal was obtained from the SERS spectra. The power of the laser had to be reduced from 40 mW to

15 mW as the signal reached saturation. It was visually observed in Figure 4.2 (B) that the nanoparticle solution aggregated (yellow/brown to a green/brown) directly after the addition of the samples. This aggregation created electromagnetic hotspots between the nanoparticles when the particle gap is less than 1 nm. These are highly confined areas containing enhanced local electromagnetic fields which result from the interparticle plasmons coupling. The molecular vibrations of any analyte found within this hotspot will increase, therefore enhancing the SERS signal.[39]

However, when you compare the signal for the control and spiked SERS samples there was very little difference observed and both samples resulted in the same signal. This was problematic as it was impossible to distinguish the control from the spiked sample.

The vibrational bands observed in the SERS spectra appear at similar positions as the corresponding RR spectra, albeit differing by a few wavenumbers. These peaks are identified in detail in Table 1 in Chapter 3. The band at 1176 cm^{-1} is due to the CH_3 in-plane bending vibrations, 1276 cm^{-1} to the C-H stretching vibration in benzene and 1595 cm^{-1} is due to the C-C stretching vibrations in benzene. While the most intense peak now seems to be the azo band at ~1390 cm^{-1}, this matters little if the spiked sample cannot be differentiated from the control. Further investigation was needed to understand why such a strong signal was obtained from the control, and how to reduce this.

4.3.2.2 Examining controls

In an attempt to identify why there was no difference in control and spiked samples, the Raman and SERS signals obtained from each compound in the reaction were examined. To do this, solutions were made for each component at the same concentration as found in the experiment. For example, 11.5 µL of hydrazine sulfate solution was added to 1587.5 µL of H_2O (total sample volume) and then examined by Raman spectroscopy. 100 µL of this solution was then added to 200 µL of silver

nanoparticles and SERS was performed. These normalised control spectra are shown in Figure 4.3.

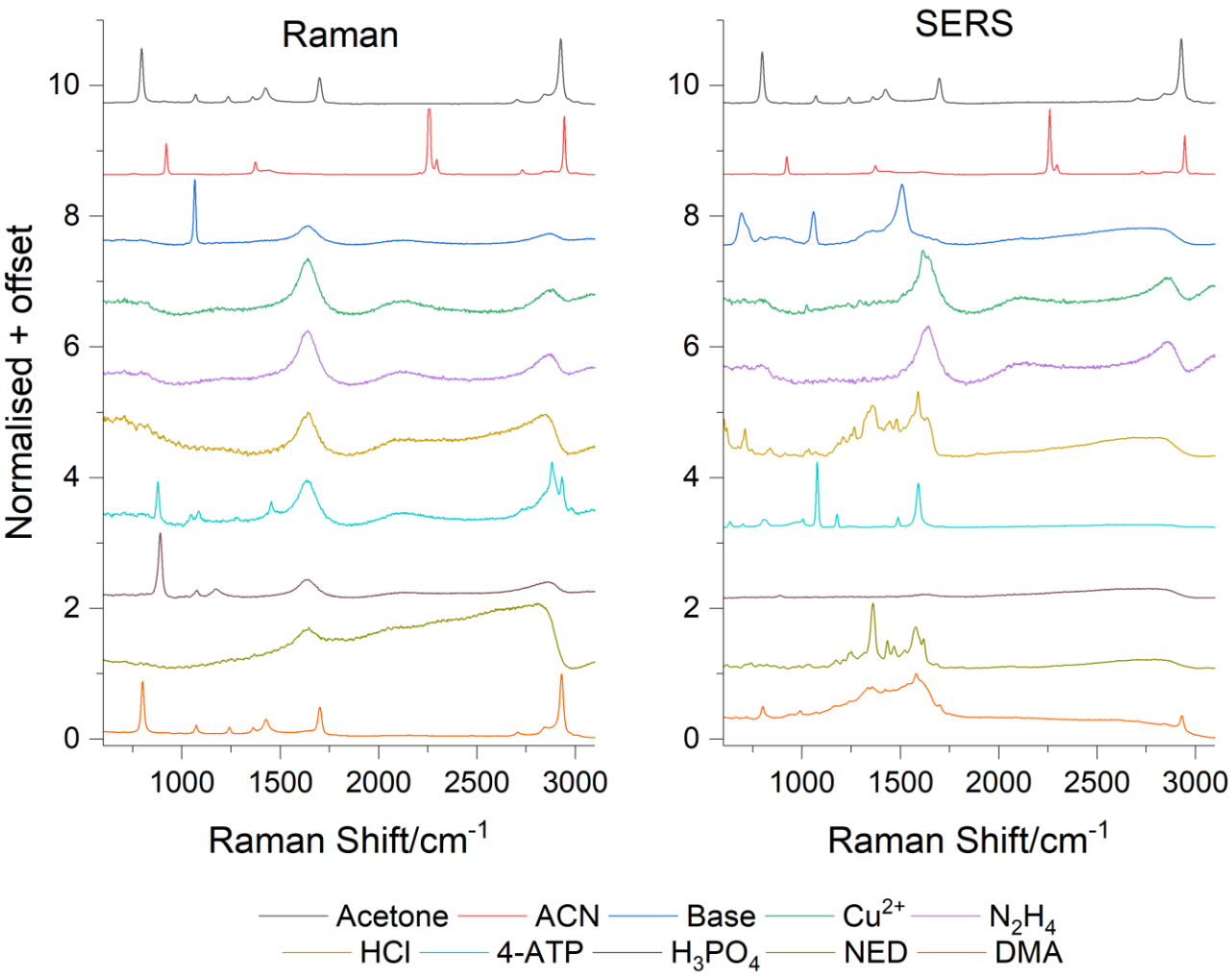

Figure 4.3: Raman (left) and SERS (right) spectra of controls for the assay. Each control was prepared at the same concentration as in the assay before Raman and SERS (100 µL sample added to 200 µL NP) were performed. Spectra were obtained using a Snowy benchtop instrument with an excitation wavelength of 532 nm (40 mW) and an acquisition time of 1s. the HCl and NED samples used 8 mW and 7 mW respectively, and have been normalised to the ethanol standard. All spectra were baselined, normalised between 0-1 and offset for clarity.

From the Raman spectra in Figure 4.3 it was observed that the strongest signals belong to the solvent used, acetone or acetonitrile (red and black), however, as all spectra have been normalised between the values of 0 and 1 the strength of the solvent peaks are less apparent. The base sample (dark blue) contains a vibrational band at 1068 cm^{-1} which is due to the CO_3^{2-}, whereas the Cu^{2+}, hydrazine, HCl and NED solutions had no strong peaks. The only bands observed in these spectra belong

to the glass background of the sample vial, which was amplified when normalising the data. No strong peaks were observed for these samples as they were used in small concentrations, and some of them were not Raman active. Only vibrational bands belonging to ethanol were observed in the 4-ATP sample as this was the solvent used to dissolve the molecule. The concentration of 4-ATP used would also be too small to be observed using Raman spectroscopy. For the phosphoric acid solution, one main band at 884 cm^{-1} was observed, which was likely due to the P-O stretching vibration[159]. This band was not very intense and appeared outside of the area of interest, and therefore can be disregarded. Lastly, several bands were observed in the DMA spectra, however, this solution was diluted in acetone: water, and therefore all the peaks observed can be assigned to acetone.

When silver nanoparticles were added to each solution some of the component's signals were enhanced. For example, the base solution, HCl acid, 4-ATP, NED, and DMA all gave unique SERS peaks. In the base solution, while the band at 1068 cm^{-1} is still apparent, two new bands at 691 cm^{-1} and 1505 cm^{-1} were observed. It can be assumed that these peaks are the result of Na_2CO_3 interacting with the hydroxylamine molecules leading to nanoparticle aggregation and therefore these hydroxylamine peaks. This was observed visually, as upon addition of the base solution, the nanoparticles aggregated, resulting in electromagnetic hotspots and increased SERS signal. A similar argument can be made for the SERS signal obtained for the HCl, as this also severely aggregated the nanoparticle solution. The strongest SERS signal in the control samples was obtained from the 4-ATP solution, where the two main bands are 1076 cm^{-1} (C-S stretch) and 1595 cm^{-1} (C-C ring stretch). An azo peak at 1370 cm^{-1} was also observed in the NED spectrum and bands at 1581 cm^{-1} (NED) and 1582 cm^{-1} (DMA) can be identified as C-C ring stretch vibrations, though it

should be noted that the peaks were difficult to interpret in the DMA sample as this spectrum contained a very high background.

As the DMA SERS spectrum was giving the most unique signal, the Raman and SERS of DMA were isolated and further examined (Figure 4.4) in an attempt to determine where the control signal was originating from in the DMA RR assay.

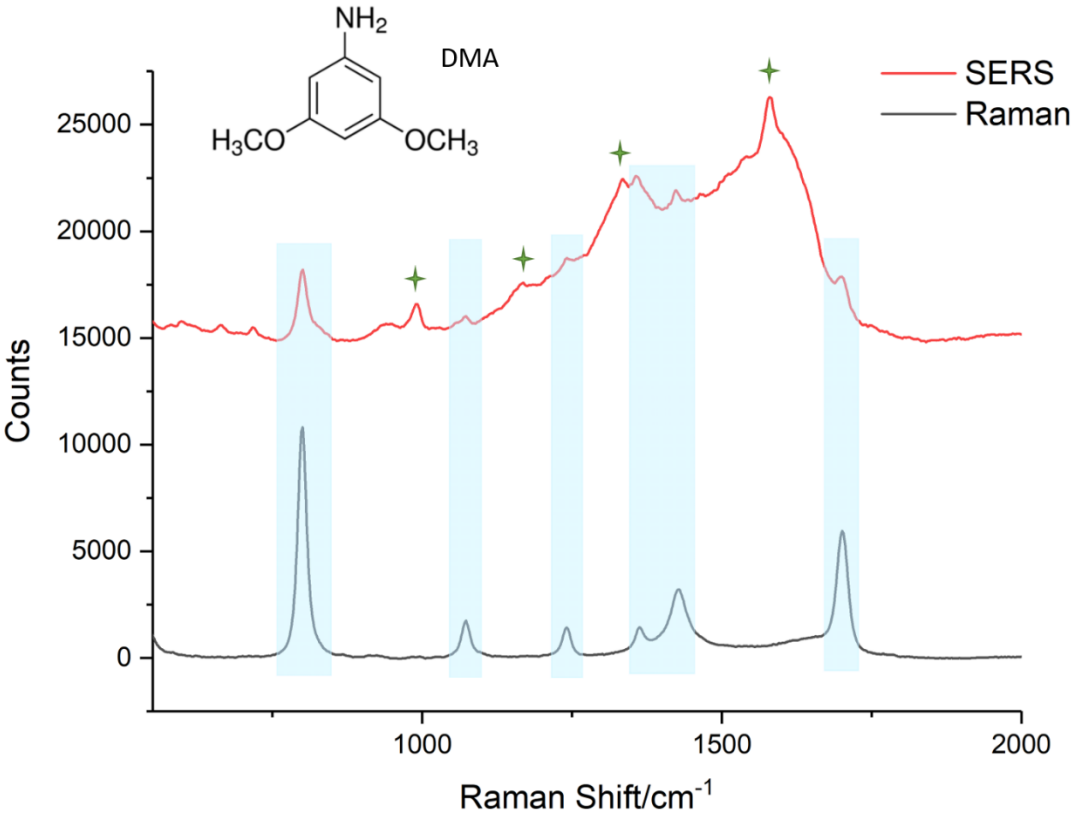

Figure 4.4: SERS and Raman spectra from the direct addition of DMA (20 mM) to either silver nanoparticles (red), or to water (black). Spectra were obtained using a Snowy benchtop instrument with an excitation wavelength of 532 nm (40 mW) and an acquisition time of 1s. Spectra have been baselined and offset for clarity. The acetone peaks are highlighted in a blue box and the DMA peaks by a green star.

The spectral peaks associated with acetone have been highlighted in blue boxes. The bands at 801 cm^{-1} and 1073 cm^{-1} are from the CH stretch, 1241 cm^{-1} is from the C-C stretching, 1357 cm^{-1} and 1424 cm^{-1} are from the CH_3 asymmetric stretch and lastly, the 1700 cm^{-1} is from the C=O stretch. The bands indicated with a green star are associated with the DMA molecule. The band at 992 cm^{-1} was due to the O-CH_3 stretch, 1168 cm^{-1} was due to CH_3 in-plane bending, 1335 cm^{-1} was from the C-OCH_3

stretching and lastly, the band at 1580 cm^{-1} was due to the C-C stretching in the aromatic ring.[151,153] As mentioned before, an unexpectedly large background was observed when obtaining the SERS spectrum of DMA. This background was not found in literature examples of DMA and made it difficult to identify some of the weaker peaks. When comparing the DMA peaks in Figure 4.4 to the peaks observed in Figure 4.2 (SERS of the DMA RR product), it was found that the bands at 992 cm^{-1} and 1335 cm^{-1} disappeared. These were the weakest peaks observed in the DMA SERS spectrum, and thus it is not surprising for these peaks to not be found in the SERS spectrum of the DMA RR azo product (Figure 4.2).

Given the large background obtained from the SERS of DMA, a theory was proposed that the addition of DMA in the reaction was causing problems in the resulting SERS spectrum of the azo product. It was decided to attempt the assay without adding the DMA molecule at the end, therefore attempting to detect the 4-ATP diazonium ion. Removing DMA was the assay would result in the absence of the vibrational bands associated with DMA, therefore creating a less complex SERS spectrum containing only 4-ATP diazonium ion bands.

Three samples were prepared for this experiment. The first was a control sample (black spectrum in Figure 4.5), which did not have any PETN, 4-ATP and DMA added. The second was another control sample (red), lacking in PETN and DMA. The third was a spiked sample (blue), lacking only in DMA. The resulting products (100 µL) were

added to hydroxylamine silver nanoparticles (200 µL) and subsequently interrogated with an excitation wavelength of 532 nm. The spectra are shown in Figure 4.5.

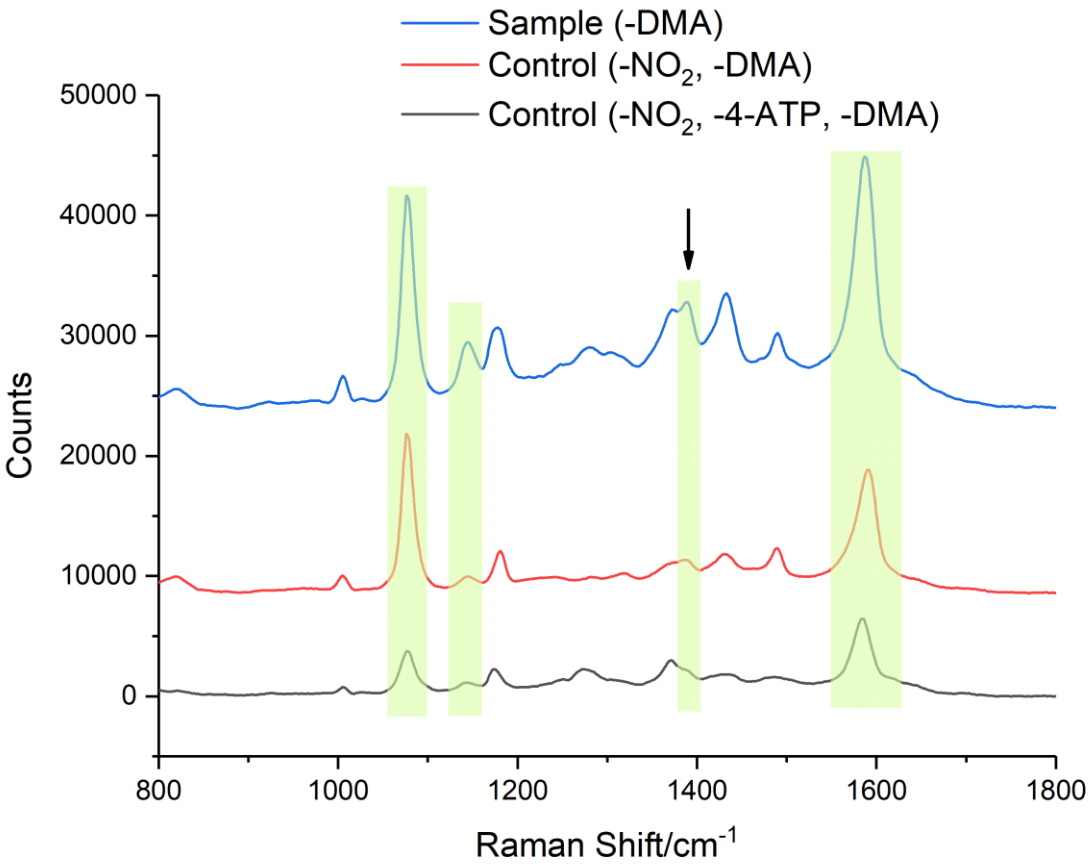

Figure 4.5: SERS spectra obtained from the PETN SERS assay without the last step of adding DMA. Two control samples, one missing an NO_2 source, 4-ATP and DMA (black) and the other missing NO_2 and DMA (red), and one spiked sample lacking only in NO_2 (blue) were interrogated with an excitation wavelength of 532 nm (40 mW for black, 7 mW for red and blue) and an acquisition time of 1s using a Snowy benchtop instrument. Spectra have been baseline corrected, offset for clarity and the 4-ATP peaks have been highlighted with a green box. An arrow points to the diazonium peak.

The data displayed in Figure 4.5 shows that a high laser power was used for the control sample which lacked the coupling components needed for the reaction (black) whereas a lower laser power was used for the other two samples. This control spectrum only contained peaks which were associated with acetone. A few differences can be observed between the control lacking any coupling components (black) and the other control and spiked sample (red and blue). It can be seen that the bands at ~1070 cm^{-1} and ~1595 cm^{-1} are apparent in all three spectra, however, the intensity has increased for the control and spiked sample containing 4-ATP. Both

of these bands result from acetone vibrations, hence why they are visible in the control spectrum (black), however, there are also corresponding 4-ATP bond vibrations in those bands regions. 4-ATP has a C-S stretching vibration at 1076 cm^{-1} and C-C ring stretching vibration at 1595 cm^{-1}. These vibrations increased in peak intensity when adding 4-ATP into the reaction, as found in Figure 4.5. Comparing the control (red) and spiked (blue) samples lacking in DMA an increase in the diazonium peak at 1390 cm^{-1},[156] and the C-H bending mode of benzene at 1144 cm^{-1} can be observed.

These peaks can be used to successfully differentiate between the control and spiked sample, however, the bands at 1370 cm^{-1} and 1390 cm^{-1} are of particular interest. By removing DMA from the assay, it was assumed that the peak at 1390 cm^{-1} (N≡N) would experience the greatest increase. However, the azo band at 1370 cm^{-1} also experienced a substantial increase. In Chapter 3 it was explained that a bonding vibration due to the CH_3 deformation in ACN would interfere with the azo band at 1370 cm^{-1} as the ACN band is found at a similar wavenumber, however, as this peak increased slightly in the spiked sample (red) it can be suggested that the 4-ATP diazonium ions are self-coupling, resulting in an increased azo signal.

This was a good result as it was the first time that PETN had been detected in a solution-based assay using SERS in this thesis. The chemistry of this assay has been summarised in Figure 4.6. By successfully developing a SERS assay, a lower PETN LOD

value should be able to be detected than that found in the resonance Raman assay in the previous chapter.

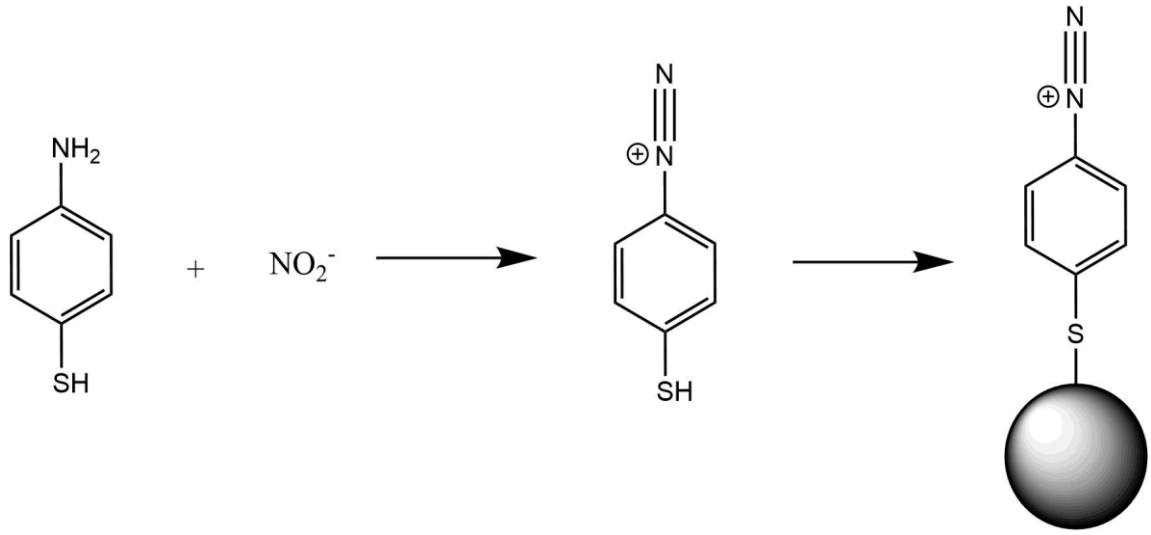

Figure 4.6: Reaction scheme of the SERS assay which forms a diazonium ion when reacting 4-ATP with nitrites. This ion can then be attached to nanoparticles (grey ball) via a thiol bond. Not drawn to scale.

4.3.3 Substituting 4-ATP

Due to the successful development of a SERS assay for the detection of PETN, various molecules, other than 4-ATP, that could conjugate to silver or gold nanoparticle and take part in the assay to form the azo product were investigated. The substitute compounds investigated were 2-amino pyridine, 3-amino pyridine and 2-amino-4,6-dimethoxypyrimidine. The structures of these compounds, and the original 4-ATP, are shown in Figure 4.7.

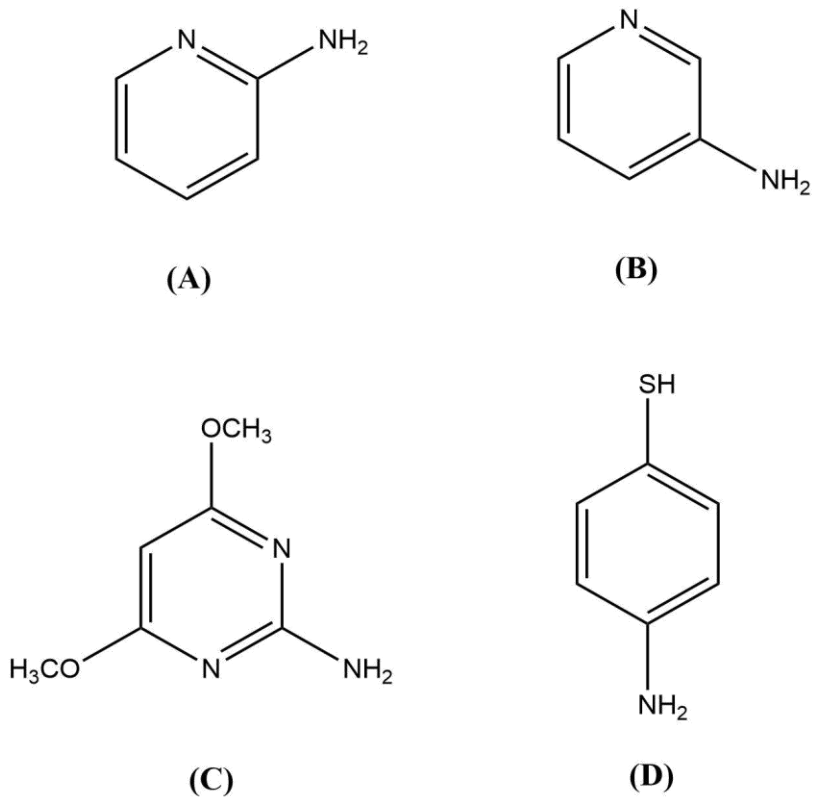

Figure 4.7: Structures of the compounds (A) 2-amino pyridine (B) 3-amino pyridine (C) 2-amino-4,6-dimethoxypyrimidine and (D) 4-aminothiophenol.

The substitute compounds were chosen as they were readily available, and they contained the required functional groups needed for this reaction. All three substitutes (A, B and C) contained a primary amine group which was needed for the azo reaction. The substitutes also consist of pyridine or pyrimidine rings, hence there are nitrogen atoms available in each of the compounds which would be used to attach to a gold or silver nanoparticle. All substitutes are also aromatic and should be reasonable Raman reporters.

10 mM solutions were made of each molecule in ethanol before diluting 9:1 in water to make 1.11 mM solutions. The SERS assay reaction was investigated using the highest concentration of PETN, 50 mg L^{-1} so that the results could be clearly interpreted. The assay was carried out as described in experimental section 6.5.4, substituting 4-ATP with the other molecules. The original reaction, with 4-ATP, was

carried out as a control. The resulting products were added to silver nanoparticles and analysed using 532 nm excitation, the resulting spectra are shown in Figure 4.8.

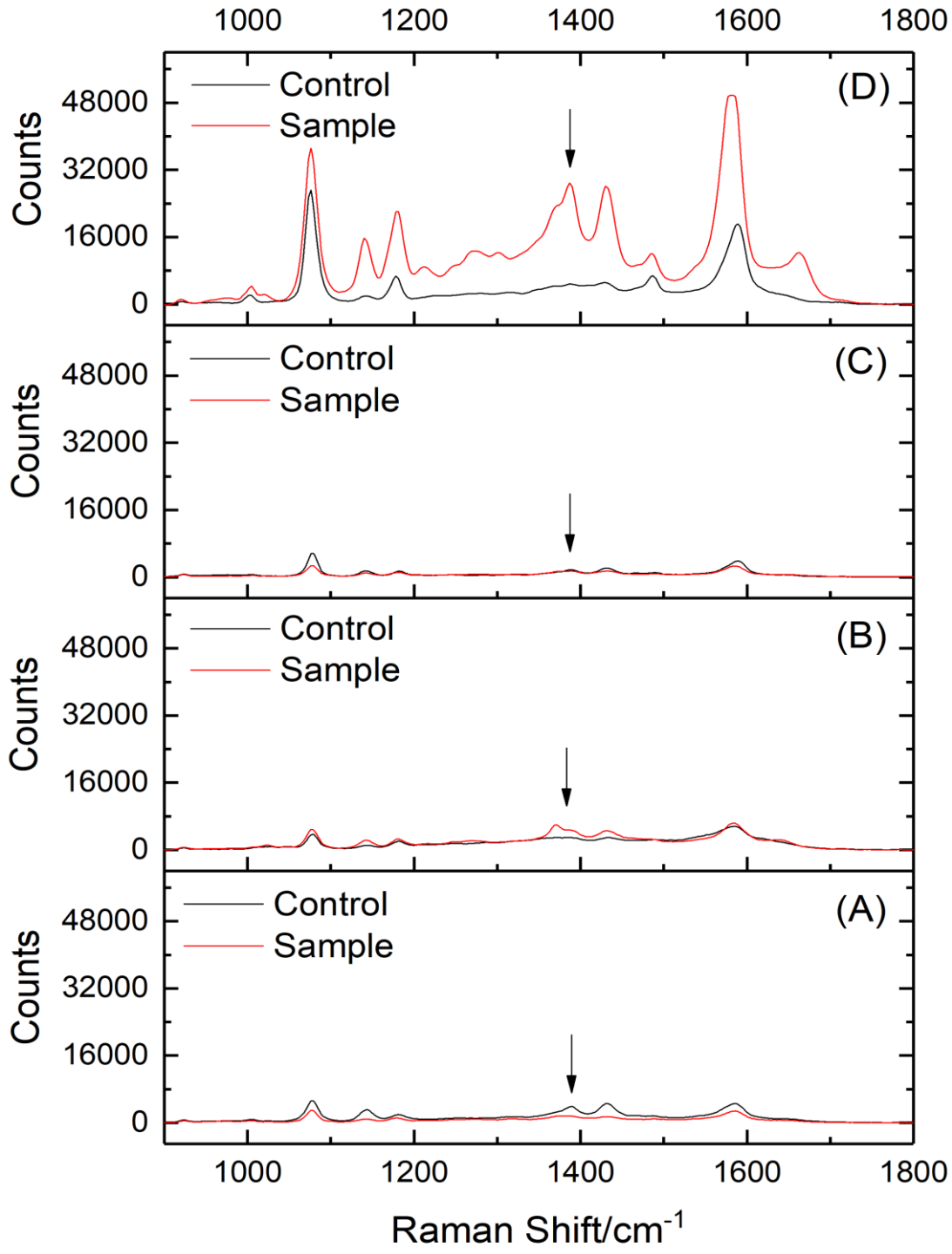

*Figure 4.8: SERS spectra obtained upon the addition of different azo complexes resulting from 4-ATP and it's substitutes, to hydroxylamine silver nanoparticles. Control samples (black) were performed without the presence of a NO_2^- donor and spiked samples (red) used 50 mg L^{-1} PETN. Spectrum **(A)** used 2-amino pyridine, **(B)** 3-amino pyridine, **(C)** 2-amino-4,6-dimethoxy pyrimidine and **(D)** used the original 4-aminothiophenol, all at the concentration of 1.11 mM. SERS spectra were obtained using a Snowy benchtop instrument with an excitation wavelength of 532 nm (15 mW) and an acquisition time of 1s. All spectra were baselined and plotted so the axes would be the same, for ease of comparison. The peak at 1390 cm^{-1} (N≡N) has been highlighted with an arrow.*

he data displayed in Figure 4.8 shows that the largest increase in SERS intensity observed for the 1390 cm^{-1} band was found in spectra (D), which was obtained from the original diazonium ion produced in the SERS assay using 4-ATP. The 4-ATP substitutes investigated (Spectra A, B and C) all gave poor SERS enhancement, especially in comparison to the original SERS intensity (spectra D)

The poor results can be explained by looking at the structure of 4-ATP and the substitutions investigated. While they all contained the necessary functional groups needed for the reaction and attachment to the nanoparticles, the structures are not ideal for the conjugation to nanoparticles. 2-Aminopyridine and 2-amino-4,6-dimethoxypyrimidine experience steric hindrance when attaching to the nanoparticle, as the nitrogen atom is close to the primary amine functional group, which takes part in the reaction. As these two compounds are both aromatic, their structures are rigid. This means that while the primary amine could experience rotational movement, there would be little to no ring bending resulting in the ring bound nitrogen being further away from the amine. This steric hindrance would mean that only a small number of compounds would manage to attach to the nanoparticle. This result is shown in the SERS spectra (A + C), where little difference was found between the controls sample (without NO_2^-) and the spiked sample (with PETN).

3-Aminopyridine should have experienced less steric hindrance than the other two substitute compounds, and this result is shown in the SERS spectra (B). Here the spiked sample SERS intensity (red) is greater than the control sample (black) for band 1390 cm^{-1} (N≡N), with the peak at 1370 cm^{-1} (N=N) being larger than the N≡N peak. This result was observed several times in the 4-ATP SERS samples during this project. It was proposed that the diazonium ion product had relaxes into a more stable alcohol with an azo therefore increasing the peak at 1370 cm^{-1}. However, the resulting SERS intensity from 3-aminopyridine pales in comparison to the original sample, which contains 4-ATP.

For 4-ATP, the primary amine and the thiol functional groups are the furthest apart from each other, therefore there was no steric hindrance. Furthermore, stronger binding was experienced as the thiol covalently bonded to the nanoparticle surface, rather than the electrostatic attraction of the ring bound nitrogen. Based on these results, it was decided that the 4-ATP molecule would not be replaced with any substitute.

4.3.4 Comparing acetone and acetonitrile for SERS assay

To increase the sensitivity of the SERS assay, the solvent was investigated. In the original paper, the solvent used was a mixture of acetone and water, as the solutions of PETN was made in HPLC-grade acetone. Pure solvents were previously investigated earlier in chapter 3, however, only the UV-Vis analysis was examined for the assays investigated. In this section, the solvent effect on the SERS assay was investigated.

The SERS assay was performed using the greatest concentration of PETN investigated in this chapter, 50 mg L^{-1}, with different solvents in the PETN solutions as described in experimental section 6.5.4. The solvent investigated were 1:1 ratio of water: acetone, and a 1:1 ratio of water: ACN. As the diazonium ions were almost colourless in the UV-Vis spectrum, only SERS analysis was performed with the excitation wavelength of 532 nm and an acquisition time of 1s. The resulting spectra are shown in Figure 4.9.

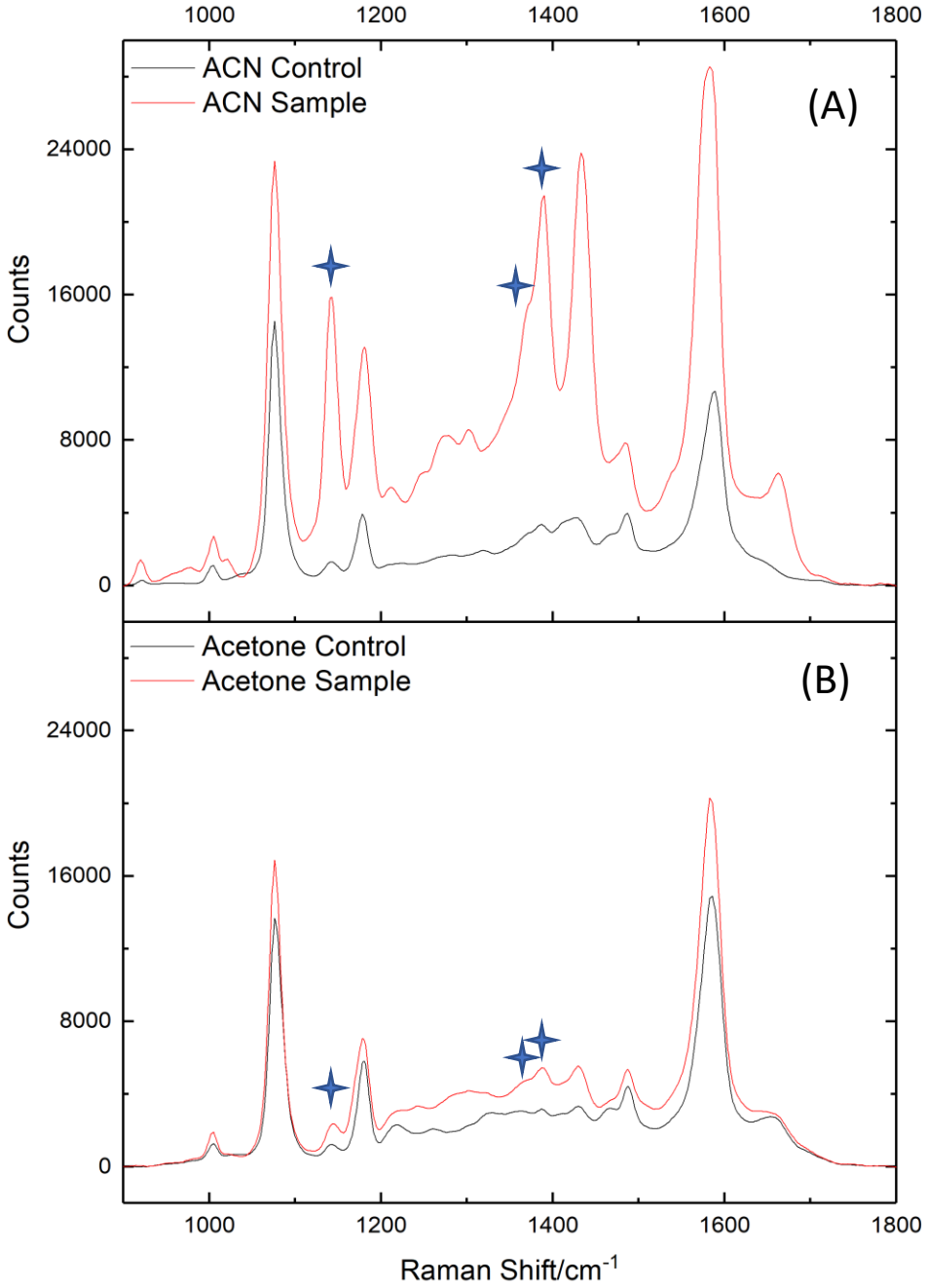

*Figure 4.9: SERS spectra obtained upon the addition of different azo complexes resulting from different solvent mediums, to hydroxylamine silver nanoparticles. Control samples (black) were performed without the presence of a NO_2^- donor and spiked samples (red) used 50 mg L^{-1} PETN. Spectrum **(A)** used a 9:1 ratio of water:ACN medium, whereas spectrum **(B)** used a 9:1 ratio of water:acetone medium. SERS spectra were obtained using a Snowy benchtop instrument with an excitation wavelength of 532 nm (15 mW) and an acquisition time of 1s. All samples were performed in 3 replicate samples with 5 measurements taken on each sample. The samples were normalised to the ethanol standards, averaged, baselined and then plotted so the axes would be the same, for ease of comparison. The peaks of interest have been identified with a blue marker.*

Figure 4.9 shows that the vibrational bands were located at similar wavenumbers in both samples (1:1 water-ACN and 1:1 water-acetone). Comparing spectra (A) and (B), there was a stark difference observed in SERS intensities between the control and the spiked sample. The spectra in Figure 4.9 were plotted from the average of 3 replicate samples and the SERS intensity of the bands 1143 cm^{-1}, 1370 cm^{-1} (N=N) and 1390 cm^{-1} (N≡N) and the calculated standard deviation are shown in Figure 4.10.

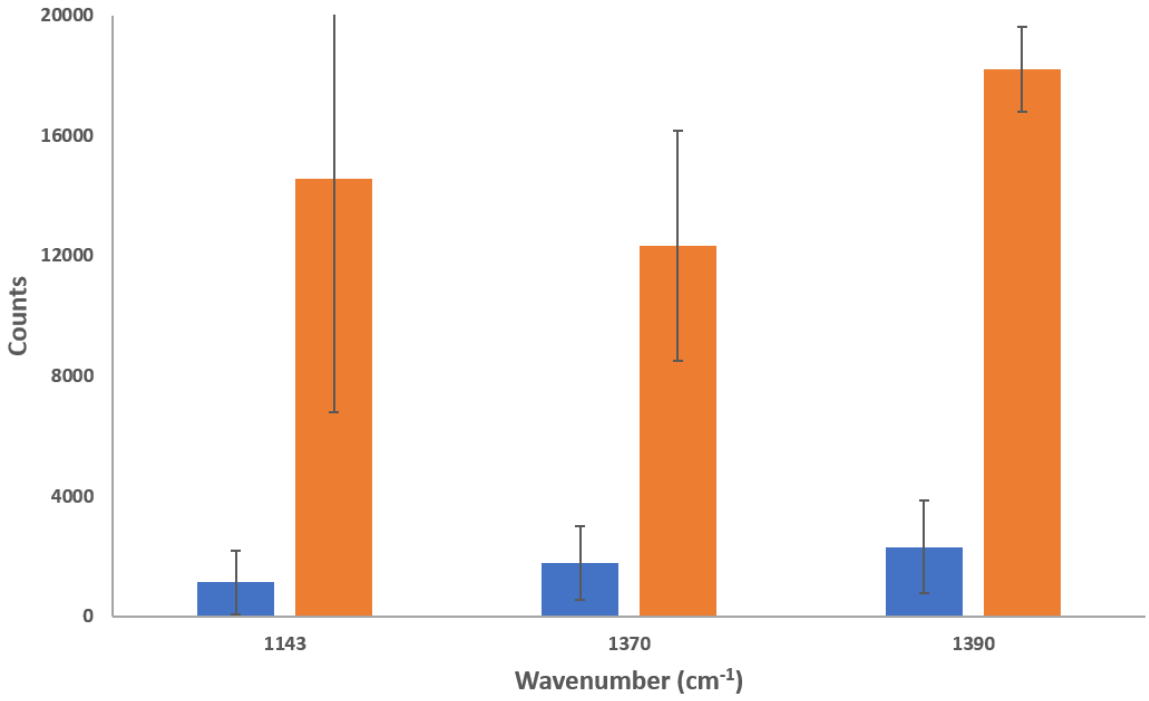

Figure 4.10: Average SERS intensities after subtracting the control for peaks 1143 cm^{-1}, 1370 cm^{-1} and 1390 cm^{-1} for the water: acetone and the water: ACN samples found in Figure 4.9. All samples were performed in triplicate with 5 measurements taken on each sample. The samples were normalised to the ethanol standards, averaged, baseline corrected. The error was calculated from the standard deviation of the 3 replicate samples. The acetone samples are blue, and the ACN samples are orange for ease of interpretation.

From Figure 4.10 it can be observed that the water: acetone solvent mixture samples (blue) experienced around a 1.6x enhancement in the monitored peaks when comparing the control to the spiked samples. The resulting band intensities from the various vibrations examined were relatively small, at around 1000-2000 counts and the standard deviation was almost as large. This enhancement, while it can be used to detect 50 mg L^{-1} of PETN, would struggle to differentiate between the control and spiked samples at lower concentrations of PETN.

The water: ACN solvent mixture samples (orange) experienced an increase in SERS of between 5-6.5x in the 1370 cm^{-1} and the 1390 cm^{-1} peaks when comparing the control to the spiked samples. There is one additional band found in Figure 4.9 which gave an interesting result from this solvent switch. The peak at 1143 cm^{-1} experienced a considerable enhancement of 12.3x in spectra (A), and a moderate 1.9x enhancement in spectra (B). This band is most likely due to the b_2 C-H bending mode of benzene in the product, which suggests an upright orientation, where the 4-ATP molecule is perpendicular to the surface of the nanoparticle[150]. This band, while it gave a greater enhancement factor than the two bands monitored at 1370 cm^{-1} and 1390 cm^{-1}, was not reliable as the standard deviation of this peak was around ± 7910 cm^{-1}. The enhancement experienced in the water: ACN samples is large enough that it can be assumed that the analyst would still be able to distinguish between the control and the spiked sample at lower concentrations of PETN.

The large enhancement experienced by using ACN instead of acetone suggests that the diazonium ion might be more soluble in ACN. More ions in solution allows for more efficient packing of the diazonium ion to the nanoparticle as it would force the ion to attach perpendicular to the surface, rather than parallel. This theory is supported by the 1143 cm^{-1} peak in Figure 4.9, which also suggests that the molecule is in an upright orientation. This upright position would also mean that the molecules would be ideally positioned for coupling to occur with other free diazonium ions, unreacted 4-ATP molecules, or potentially those bound to nanoparticles. This coupling would occur at the ortho position of the amine and would allow the nanoparticles or the molecules to come in close contact, resulting in a SERS signal enhancement for the molecular band vibrations.

While ACN can give a background signal to the 1370 cm^{-1} peak, the evidence is clear that the reaction is more efficient when performed in a water: ACN medium, rather than a water: acetone medium. It was therefore decided to deviate from the original paper and to perform the reactions in the preferred solvent medium.

4.4.4 LOD values for the SERS assay

To obtain an LOD value for the detection of PETN using the developed SERS assay the assay was performed in triplicate using PETN in the concentration range of 10-50 mg L^{-1}, following the experimental procedure listed in section 6.5.4. The solutions were analysed by absorption, Raman and then SERS spectroscopy. The reaction scheme and resulting absorbance spectra can be found in Figure 4.11.

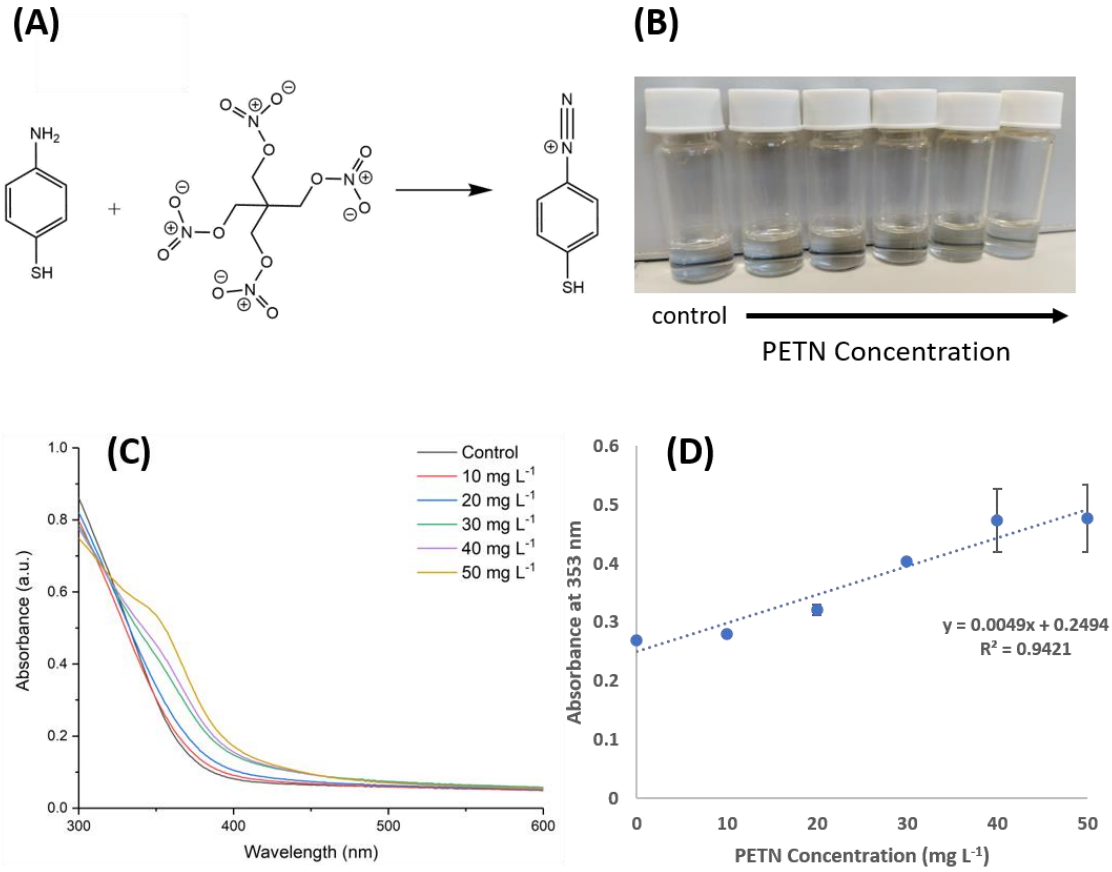

*Figure 4.11: **(A)** Reaction scheme of the SERS Assay with a visual picture **(B)** of the reaction of 10-50 mg L^{-1} PETN in the assay. Absorbance spectra **(C)** and the plot of absorbance of the 353 nm peak against PETN concentration (mg L^{-1}) **(D)** shows a linear relationship in the range of 10-50 mg L^{-1} (R^2 = 0.94). Error bars indicate standard deviation on 3 replicate samples.*

Unlike the other four assays in chapter 3, the product did not produce a change in colour. However, a slight peak at an absorbance maximum of around 353 nm was observed to increase with increasing PETN concentration. This peak is thought to belong to either the 4-ATP diazonium ion or from the coupling of the diazonium ions

with the free amine as they are very high in energy and therefore result in a low wavelength.[67] The R^2 value is lower than those found in the previous LOD studies in Chapter 3 (R^2 = 0.94) but it was still observed that a linear relationship between the absorbance and PETN concentration was found. The standard deviation found for the lower concentration samples was extremely low, and therefore the LOD calculated was 1.2 mg L^{-1}. This was the lowest LOD calculated from the UV-Vis results of all five assays studied in Chapter 3 and 4. Despite the low LOD found in these results, it is unlikely that absorption spectroscopy would be used to detect lower concentrations of PETN as the peak was only apparent at higher concentrations and only a small absorbance change was observed in the concentration range investigated, and no colour change could be visually tracked.

The main purpose of this assay was to analyse the samples by Raman and SERS spectroscopy. It is important to note that by performing SERS spectroscopy, the samples underwent a further 2/3 dilution as 100 µL sample was added to 200 µL silver nanoparticles. This would make the highest concentration examined 16.7 mg L^{-1} and the lowest 3.3 mg L^{-1}. These spectra can be found in Figure 4.12 and the experimental procedure is listed in section 6.5.4.

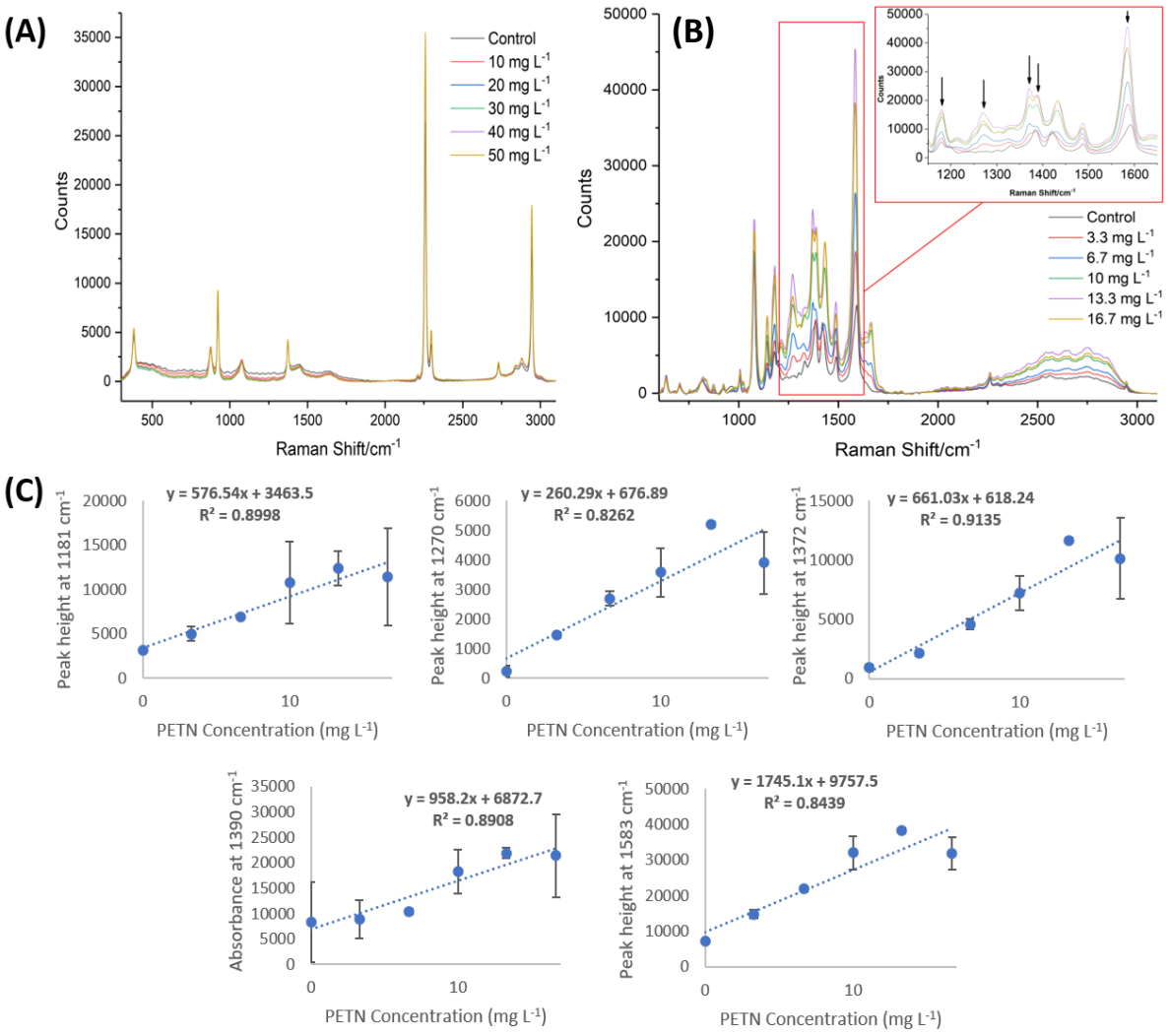

*Figure 4.12: Resonance Raman **(A)** and SERS spectra **(B)** obtained from the reaction of 10-50 mg L^{-1} PETN in the SERS assay. Spectra were collected using a Snowy benchtop instrument with an excitation wavelength of 532 nm (40 mW for Raman, 15 mW for SERS) and an acquisition time of 1s. **(C)** contains the plot of peak heights of five different peaks (1181 cm^{-1}, 1270 cm^{-1}, 1372 cm^{-1}, 1390 cm^{-1} and 1583 cm^{-1}) against PETN concentration (mg L^{-1}). Error bars indicate standard deviation on 3 replicate samples.*

While no unique Raman signal was observed for the assay product (Figure 4.12 (A)), an intense spectrum was observed in the SERS spectra (B) containing vibrational bands at 1181 cm^{-1} and 1270 cm^{-1} (C-H stretch)[150], 1372 cm^{-1} (azo), 1390 cm^{-1} (diazonium ion) and 1583 cm^{-1} (C-C stretch). The peak heights of the isolated SERS bands have been plotted against PETN concentration in Figure 4.12 (C) by subtracting the height of the trough from the height of its adjacent peak. This determines the relationship between peak height and PETN concentration, and can be used to calculate the LOD for PETN. None of the coefficient of determination values

calculated were between 0.95 – 0.99, however, a linear relationship between the peak intensity and PETN concentration was still observed. It also appears as if the assay reaches saturation by 13.3 mg L^{-1}. Saturation is where the silver nanoparticle surface is fully packed with product and can therefore enhance no more molecules. The LOD's were generally calculated to be between 1-2 mg L^{-1}, which was the lowest PETN LOD found in this thesis. However, the LOD for the 1390 cm^{-1} band was much larger at 10.2 mg L^{-1}, as it was observed that there was a background peak in the control sample. A peak shift of 10 cm^{-1} could also be found from the control sample (1592 cm^{-1}) to the spiked samples (1583 cm^{-1}). It was not possible to use the ~1585 cm^{-1} and 1390 cm^{-1} bands as they were observed in the control and were not very well resolved, however, the bands at 1270 cm^{-1} and 1372 cm^{-1} had no signal present in the control of 0 mg L^{-1} PETN, making them ideal for monitoring the reaction. The low LOD meant that the SERS assay had the potential to detect lower concentrations than those studied in this chapter using SERS spectroscopy.

Overall, the standard deviation observed in the peak height against concentration plots were larger than those found in the DMA RR assay in Chapter 3. First, the variation found in the sample would be amplified when using SERS. And secondly, nanoparticle aggregation, if not controlled properly, can lead to variation in the number of electromagnetic hotspots which also increases the error in the SERS spectra, especially at higher concentrations.

4.4.5 SERS assay performed on TNT and RDX

The optimised SERS assay was then used to detect other nitrite containing explosives. Three explosives (TNT, RDX and PETN) were investigated in this experiment at the same concentration of 50 mg L^{-1}. The experiment was performed as described in section 6.5.4 and the samples were then analysed via absorption spectroscopy and, after adding 100 µL to 200 µL of hydroxylamine silver nanoparticles, with SERS. The spectra can be found in Figure 4.13 and the average SERS intensity for the vibrational

bands 1370 cm^{-1} and 1390 cm^{-1} and their standard deviation can be found in Figure 4.14.

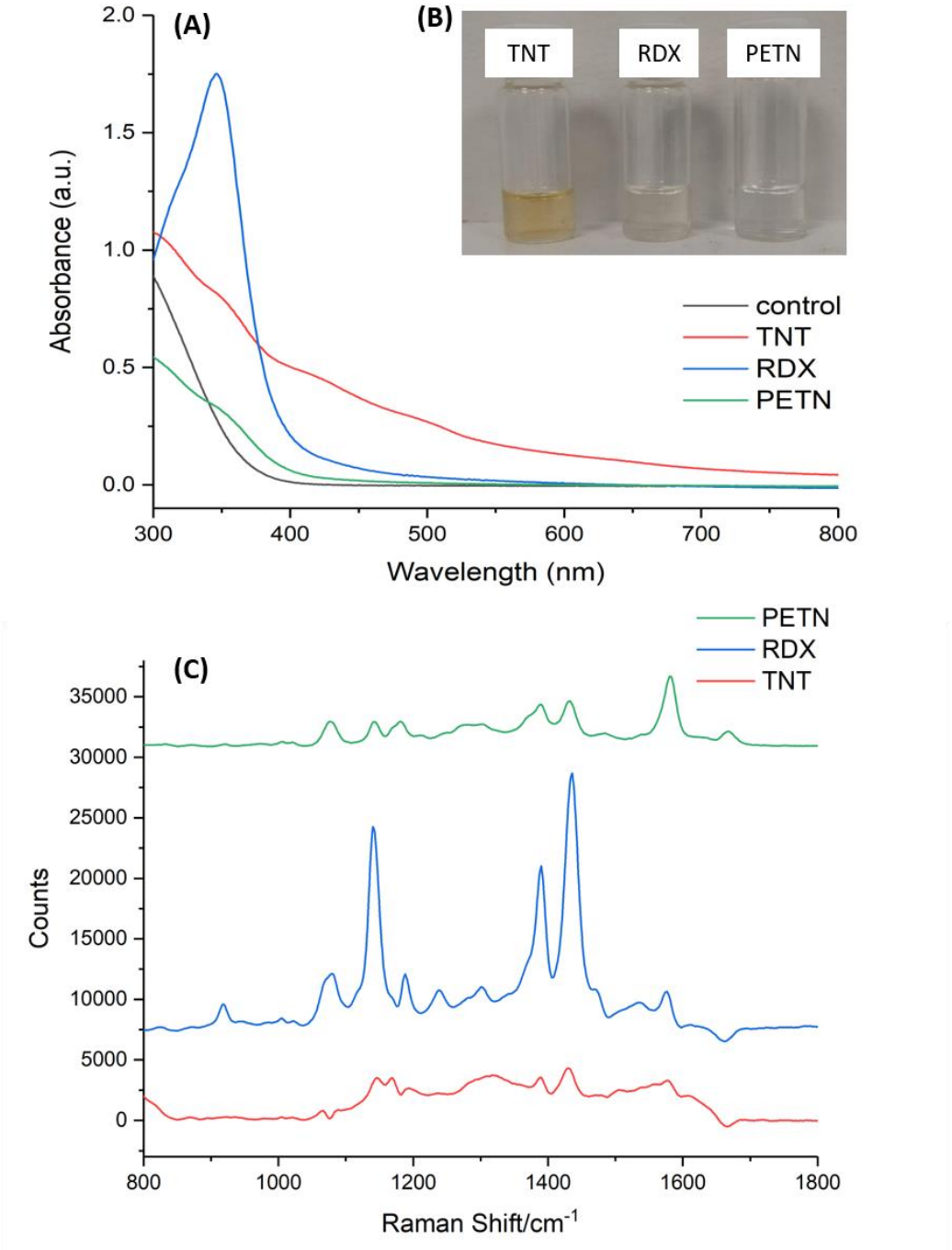

Figure 4.13: Data obtained from the detection of TNT (red), RDX (blue) and PETN (green) using the SERS assay. (A) absorbance spectra (B) visual picture of explosive samples (C) SERS spectra with the control subtracted. SERS spectra were obtained using a Snowy benchtop instrument with an excitation wavelength of 532 nm (3 mW) and an acquisition time of 1 s. All SERS spectra are the average of 3 replicate samples with 5 measurements taken on each sample. Each spectrum was baseline corrected before subtracting the control, and then were offset for clarity.

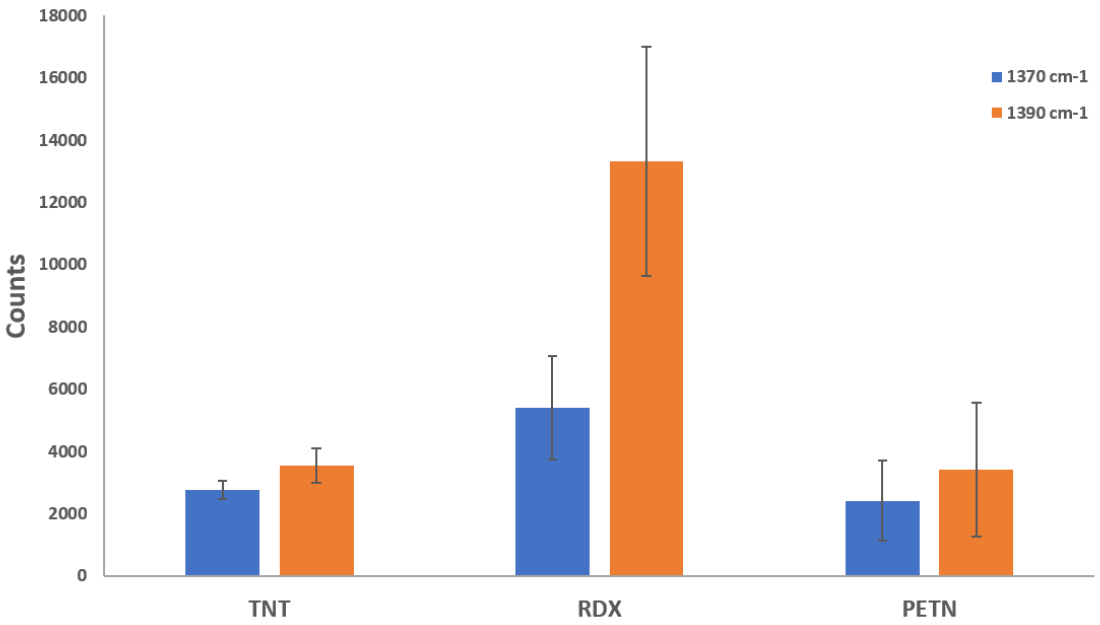

Figure 4.14: Average SERS intensities after subtraction of the control for the peaks 1370 cm^{-1} (blue) and 1390 cm^{-1} (orange) for the nitrate/nitrite containing explosives TNT, RDX and PETN, found in Figure 4.13. All samples were performed in triplicate with 5 measurements taken on each sample. The samples were averages, baseline corrected, and the error was calculated from the standard deviation of the 3 replicate samples.

It can be observed in Figure 4.13 (B) that the end product from TNT was the most coloured. However, it is uncertain that the colour produced is the resulting diazonium ion expected. When performing this experiment, it was visually observed that the TNT sample changed colour (clear to pink) after the addition of the base hydrolysing solution. This colour further changed (pink to peach) after 30 minutes of heating in a water bath, which was similar to the colour observed at the end of the experiment. From Figure 4.13 (A), it is observed that an unusual absorbance spectrum was found in the TNT sample, containing a relatively high background with potential absorbance bands at 360 nm, 420 nm and 500 nm. While the peak at 360 nm is similar to that observed in the RDX and PETN samples, the other two are unknown, thus suggesting that the coloured complex made upon the addition of the base to the sample affects the absorbance data. It is possible, as a side reaction, that TNT is forming a Meisenheimer complex upon addition of the base. The formation of a Meisenheimer or Janowsky complex creates a red coloured compound with an absorbance maximum of around 500 nm.[160,161] A very weak and unresolved SERS spectra (C) for

TNT was obtained, containing additional peaks not observed in the other two samples. Though difficult to identify peaks within the large background, there could potentially be a vibrational band at 1301 cm^{-1}, which would be due to the symmetrical nitro stretching within the TNT molecule.[116] While the SERS intensities of the two bands (1370 cm^{-1} and 1390 cm^{-1}) for TNT are comparable to those in PETN (Figure 4.14), the SERS spectrum was clearer for the PETN samples. The less resolved spectrum found in the TNT sample is also likely due to the TNT forming a side product upon reaction with the base solution.

A slight yellow colour of the RDX end product solution was observed (Figure 4.13 (B)) which was thought to be the forming of the diazonium ion. This was confirmed with UV-Vis analysis, where a strong peak at 346 nm was observed. RDX also gave the strongest SERS response and it required a lower laser power of 3 mW, rather than 7 mW which was optimum for the TNT and PETN sample. A likely reason for this is that RDX contains a potential of 3 x NO_2^- per molecule. While this is less than the potential of 4 x NO_2^- in PETN, the nitrite ions in RDX do not need to be reduced before being used in the reaction.

If full hydrolysis and reduction of the nitrate ions to nitrites occurred in the PETN molecule, then it would be expected that the PETN molecule would yield the strongest signal. This did not occur as it is known that nitrate reduction has a 50-85 % yield[139] and it was observed that the absorbance signal was reduced compared to the two explosives. The colour change for the diazonium ion cannot be visually observed, and the resulting SERS, while producing a clearer spectrum than TNT, was comparable in intensity to the TNT signal.

There are several issues here which could have caused the discrepancy between the samples, therefore causing large errors observed. When adding the reagents for the diazotisation reaction to the sample, a violent reaction was observed. As a basic pH is required for the hydrolysis of PETN, the pH of the sample in the nitrate reduction stage was also basic (~pH 10). The addition of 5M HCl and 5M H_3PO_4 in the

diazotisation step would cause the sample to rapidly change from a basic pH to an acidic one, a change which was needed as an acidic pH is required for the diazotisation reaction to occur. The volume of 5M HCl added was measured to neutralise the samples, whereas the volume of 5M H_3PO_4 was measured to acidify the sample to a pH of around ~4. The samples were thoroughly mixed after the addition of the acids and 4-ATP and care had to be taken when measuring 100 µL of a sample as it was very acidic and therefore bubbles of gas were often caught in the pipette tip. When 100 µL could be measured in the pipette tip without any bubbles of gas the measurement would then be added to 200 µL of silver nanoparticles. While the analyst aimed to measure 100 µL of a sample without gas bubbles, sometimes bubbles were not spotted. These bubbles would then decrease the volume of sample being added to the nanoparticles, therefore decreasing the overall signal intensity. Another issue which could cause unpredictable results was the addition of the sample to the nanoparticles, as this caused aggregation. This aggregation could not be controlled and therefore the number of electromagnetic hotspots and the resulting SERS intensity would vary.

These results show that the SERS assay can be used to successfully detect other nitro-based explosives. However, while it is apparent that the hydrolysis part of the assay works well (large RDX signal), the reduction using hydrazine sulfate and a copper catalyst might need additional investigation, to improve the conversion rate observed (Low PETN signal in comparison to the large RDX signal observed).

4.5.6 Optimising assay times for SERS assay

The final aim of this project was to reduce the timing required for the full SERS assay, as rapid assays are more useful to on-site analysis. Ideally, this would mean reducing the timing of the experiment to between 2-5 minutes. Currently it stands at 75 minutes.

In an attempt to reduce the timing of the overall assay, the SERS at different time points was evaluated. For each study, the time point of one step was altered, while keeping the time points constant for the other two steps. The steps were:

1. PETN hydrolysis
2. NO_3^- reduction
3. End reaction time

4.5.6.1 PETN hydrolysis step.

In the original protocol, the PETN hydrolysis step took 30 minutes in a heated water bath at 65 °C. The timed experiment was performed in the same conditions to accelerate the reaction. The concentration of PETN used for the samples was 50 mg L^{-1}, as this gave the greatest response in the concentration range previously investigated, and therefore was the easiest to monitor using SERS.

6 PETN spiked samples (containing 25 µL PETN) and 6 control samples (containing 25 µL of ACN) were prepared in 1:1 solutions of ACN-water. Each spiked sample and control were paired together, making a total of 6 pairs. Each pair represented a different time point investigated (t=5, 10, 15, 20, 25, 30 minutes), where the paired control and spiked sample would be removed from the heated water bath. After removing the samples from the water bath, step 2 (NO_3^- reduction) and step 3 (end reaction time) was performed the same way as in the original assay described in experimental section 6.5.4. For example, the t=5 minute samples were removed from the water bath after 5 minutes, the Cu^{2+} and hydrazine sulfate solutions were added and the samples returned to the water bath for an additional 15 minutes. The samples were then removed from the water bath, and the HCl, 4-ATP and H_3PO_4 solutions were added. The samples were then left to react for 30 minutes before adding to HA silver nanoparticles and performing SERS. The resulting spectra are the

average of each time point shown in Figure 4.15. The area of interest (1200-1500 cm^{-1}) has been isolated and enlarged. SERS intensity at 1370 cm^{-1} (N=N) and 1390 cm^{-1} (N≡N) has been plotted as a function of time for ease of interpreting the full SERS data.

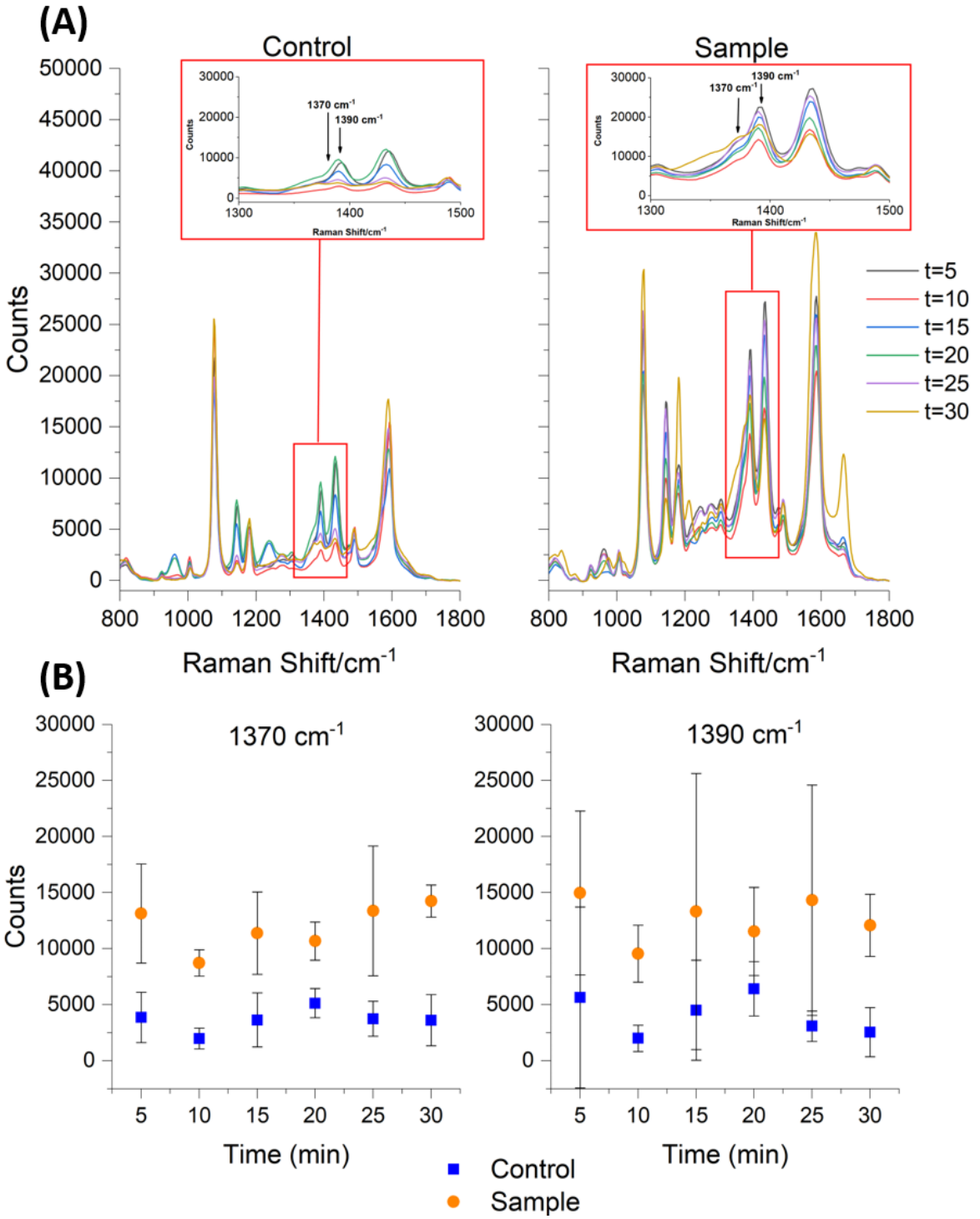

*Figure 4.15: SERS results for the control (left) and spiked sample (right) for all time points obtained from the PETN hydrolysis timed study **(A)**. The indicator peaks at 1370 cm^{-1} and 1390 cm^{-1} have been identified, and their intensities have been plotted against time **(B)**. Spectra were obtained using a Snowy benchtop instrument with an excitation wavelength of 532 nm (7 mW) and an acquisition time of 1s. All spectra are the average of 2 replicate samples with 5 measurements taken on each sample. Each spectrum was baseline corrected, normalised to the ethanol standard, and the error bars in (B) were calculated from the standard deviation for each data set.*

In this study, the SERS response of the 1370 cm^{-1} band (N=N) and the 1390 cm^{-1} band (N≡N) were monitored at each time point. Focusing on the diazonium ion peak, the results perplexingly showed that time points 5 minutes, 15 minutes and 25 minutes all showed more intense signals than 10 minutes, 20 minutes and 30 minutes, however, there was not a huge variation between all of the time points. Interestingly, a smaller error was found for the azo band at 1370 cm^{-1} in comparison to the diazonium peak at 1390 cm^{-1}, demonstrating how SERS results can be variable. As previously mentioned, the uncontrolled aggregation experienced by the nanoparticles after sample addition would also result in a large variation of SERS intensity. This error could also be attributed to human error/mechanical error in the pipettes when measuring the correct volumes of the reagents needed, and for preparing the sample for SERS analysis. Comparing the intensities for both bands at the beginning time point (5 minutes) and the end one (30 minutes), 5 minutes was found to have as intense a SERS signal and as large separation between the control and spiked sample as found in later time points, suggesting that the reaction had occurred by 5 minutes. This was a good result as it allowed the reaction time to be reduced by at least 25 minutes. It was therefore decided to proceed with 5 minutes at step 1 in the experiments after the timed studies.

However, it still needs to be remembered that while the first couple of time points have a reduced reaction time for the hydrolysis step, all samples then went on to react for a further 45 minutes before SERS was performed. 15 of these minutes were conducted in the heated water bath, and therefore the hydrolysis step could have proceeded during the time assigned to step 2 or 3. It is less likely the 30 minutes allotted to step 3 had as much of an effect, as this time was unheated and it has been previously proven that heated reactions proceed faster than the unheated versions.

4.5.6.2 NO_3^- reduction step

In the original protocol from the source paper, the NO_3^- reduction step was allotted 15 minutes in a water bath heated at 65 °C. This meant that the second timed study

performed altered the time in this reduction step. As with the first timed experiment, the conditions of each sample and the time points for step 1 and step 3 were kept the same, and the concentration of PETN used for the samples was 50 mg L^{-1}.

3 PETN spiked samples (containing 25 µL PETN) and 3 control samples (containing 25 µL of ACN) were prepared in 1:1 solutions of ACN-water. Each spiked sample and control were paired, making a total of 3 pairs. Each pair represented a different time point (t=5, 10, 15 minutes), where the paired samples would be removed from the heated water bath after the addition of the solutions in step 2. The samples were prepared and step 1 (PETN hydrolysis) proceeded for 30 minutes in the water bath at 65 °C. After removing all of the samples from the water bath and adding the Cu^{2+} and hydrazine sulfate solutions to each one, the samples were then returned to the water bath for further 5 minutes, 10 minutes or 15 minutes, depending on the sample time point. Step 3, the addition of HCl, 4-ATP and H_2PO_4 solutions, was done after the removal of the sample from the water bath, and the samples were then left to react at room temperature for 30 minutes before being added to silver nanoparticles and performing SERS. The resulting spectra are the average of each time point shown in Figure 4.16. The area of interest (1200-1500 cm^{-1}) has been isolated and enlarged. SERS intensity at 1370 cm^{-1} (N=N) and 1390 cm^{-1} (N≡N) has been plotted as a function of time for ease of interpreting the full SERS data.

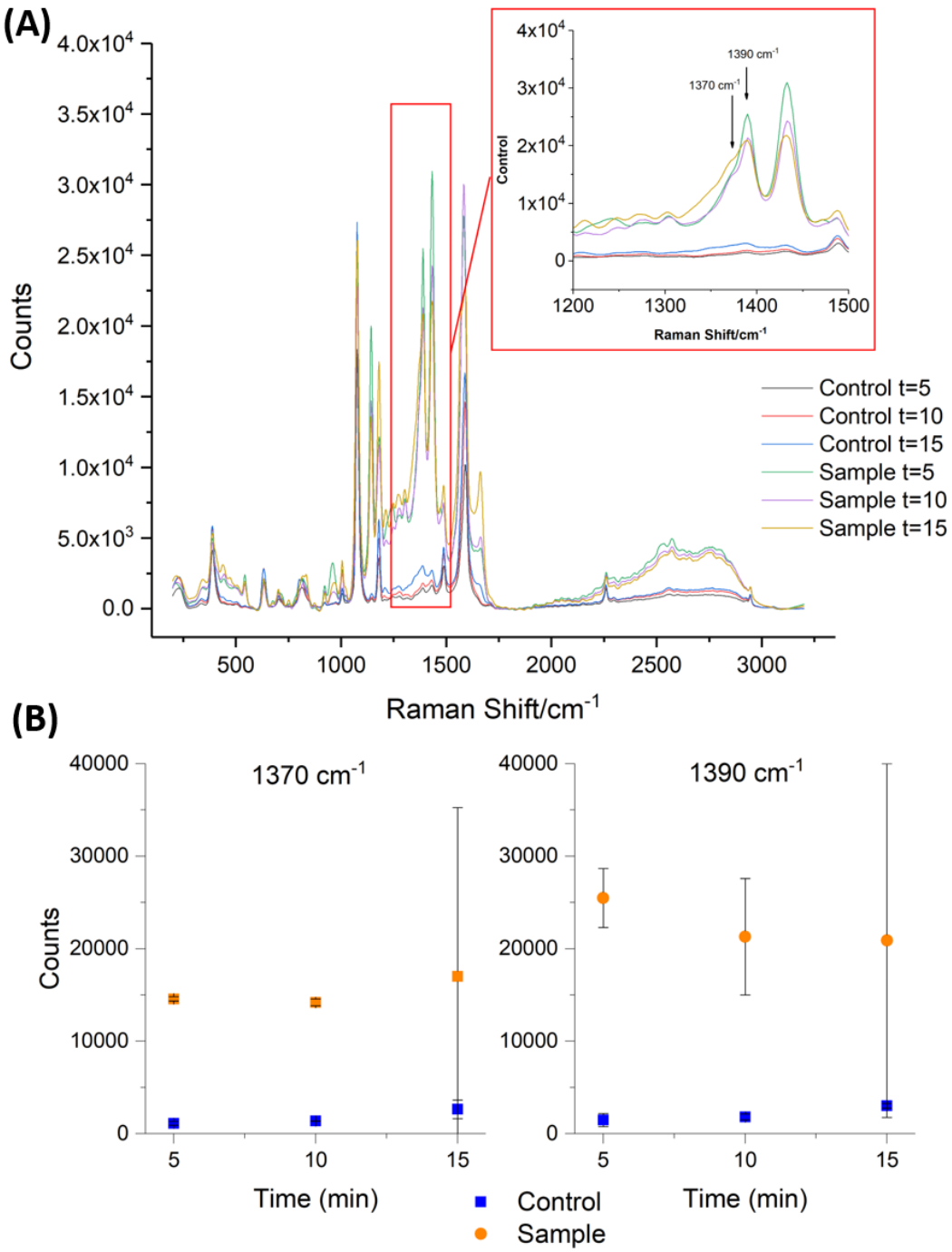

*Figure 4.16: SERS results for all time points obtained from the NO_3^- reduction timed study **(A)**. The indicator peaks at 1370 cm^{-1} and 1390 cm^{-1} have been identified, and their intensities have been plotted against time **(B)**. Spectra were obtained using a Snowy benchtop instrument with an excitation wavelength of 532 nm (15 mW) and an acquisition time of 1s. All spectra are the average of 2 replicate samples with 5 measurements taken on each sample. Each spectrum was baselined corrected, normalised to the ethanol standard, and the error bars in (B) were calculated from the standard deviation for each data set.*

It can be seen that the greatest intensity of the 1390 cm^{-1} peak (N≡N bond) was

observed for the t=5 minute spiked sample. In general, a substantial separation between the control samples (containing ACN rather than PETN) and the spiked samples can be seen in all three samples, however, there was significant error calculated for t=15 spiked sample. In the two replicas performed for this timed study, both t=15 minute spiked samples contradicted each other, the first resulting in a very low SERS intensity, and the second with a high one. This variation in the two samples created a very large standard deviation error and therefore created large error bars for the last time point samples. Again, this error could be attributed to human error/mechanical error in the pipettes or from the aggregation of the nanoparticles after sample addition.

Again, it should be remembered that the samples still had 30 minutes in step 3 to react, so it is possible that some of this time could have been spent in the reduction of NO_3^- to NO_2^- before the nitrite ion reacts with the 4-ATP molecule.

4.5.6.3 End reaction time

In the original protocol from the source paper, the end reaction time was allotted 30 minutes standing at room temperature and so the third timed study performed analysed the samples by SERS every 5 minutes of the 30 minutes allocated. This was the easiest timed study to monitor, as the reactions times altered were in the last step of the reaction, and therefore none of the times in the prior reaction steps needed to be altered. As with the first timed experiment, the conditions of each sample were the same, and the concentration of PETN used for the samples was 50 mg L^{-1}.

As this timed study focused on the SERS results after certain time points, multiple samples were not needed, as the sample could be tested and then left to react for further time points. A PETN spiked sample (containing 25 µL PETN) and a control sample (containing 25 µL ACN) were prepared in solutions of 1:1 ACN-water. After sample preparation, step 1 (PETN hydrolysis) and step 2 (NO_3^- reduction) was

performed the same way as in the original reaction, in a water bath at 65 °C. After the allotted 15 minutes for step 2, the samples were removed from the water bath and the reagents for step 3 were added. Immediately after the addition of the step 3 reagents, 100 µL of the sample was removed and added to 200 µL hydroxylamine silver nanoparticles and SERS was performed. This procedure was then repeated at every 5-minute time point, for 30 minutes. The resulting spectra are the average of each time point shown in Figure 4.17. The area of interest (1200-1500 cm^{-1}) has been isolated and enlarged. SERS intensity at 1370 cm^{-1} (N=N) and 1390 cm^{-1} (N≡N) has been plotted as a function of time for ease of interpreting the full SERS data.

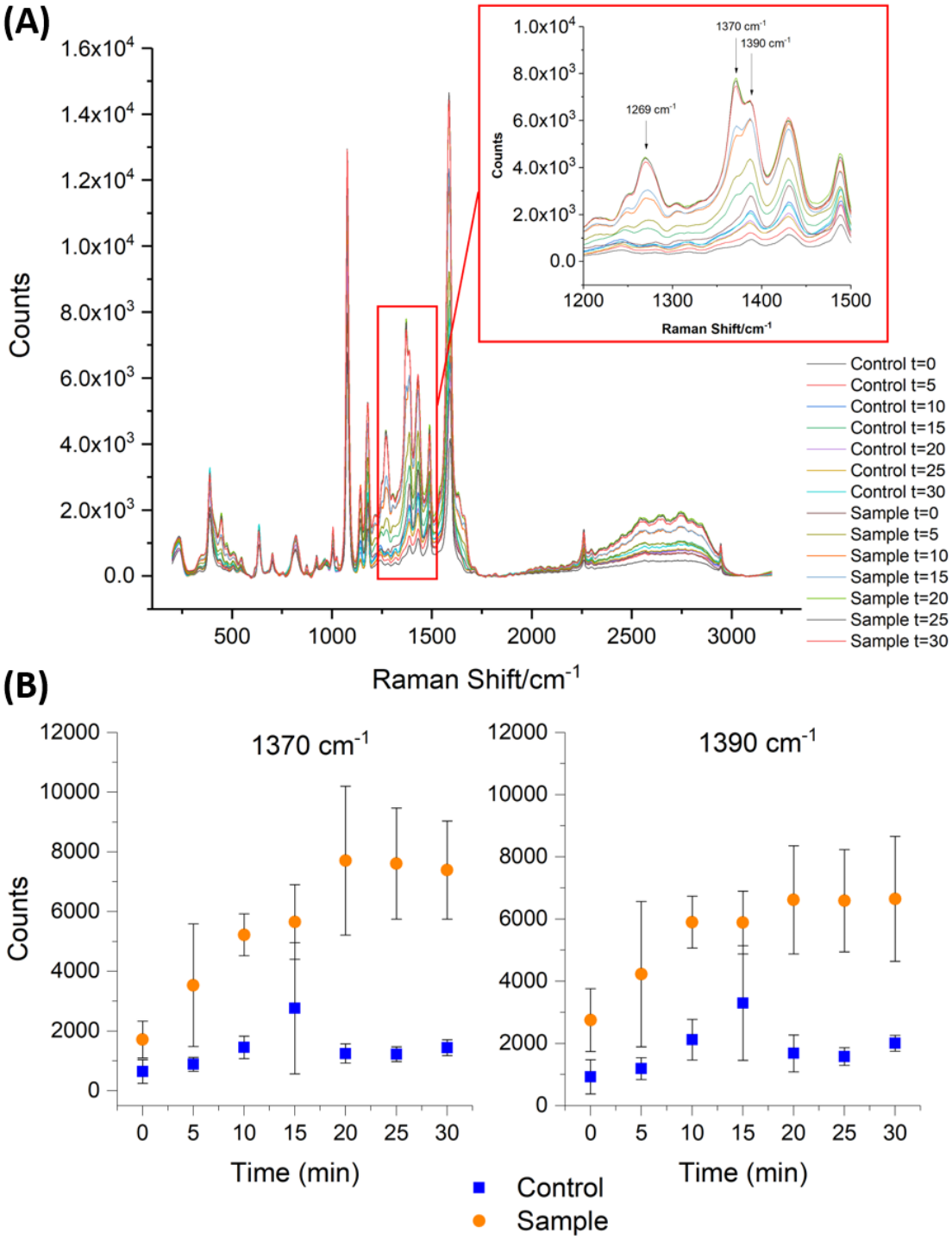

*Figure 4.17: SERS results for all time points obtained at the end reaction time **(A)**. The indicator peaks at 1370 cm^{-1} and 1390 cm^{-1} have been identified, and their intensities have been plotted against time **(B)**. Spectra were obtained using a Snowy benchtop instrument with an excitation wavelength of 532 nm (15 mW) and an acquisition time of 1s. All spectra are the average of 3 replicate samples with 5 measurements taken on each sample. Each spectrum was baselined corrected, normalised to the ethanol standard, and the error bars in (B) were calculated from the standard deviation for each data set.*

The SERS intensity plots against time can be seen to be quite different in this timed

study compared to the previous two as it monitored the last 30 minutes of the reaction, rather than the final value. It was observed that the peak intensity increased as the time of the reaction progressed from 0-20 minutes. The final three time points (t=20-30 minutes) showed a stabilising of the peak intensities, as the peak no longer grew in intensity. However, as one of the main aims of this chapter was to develop a test which could be used on-site, only the earlier time points were considered as the later ones, while of greater intensity, would take too long for the reaction to complete.

It was observed that the intensities of the control and spiked samples were similar at time point 0 minutes, which was expected as a SERS reading was taken directly after the addition of the reagents in step 3, only allowing enough time for proper mixing of the samples before analysing. While this would not have left a lot of time for the reaction to proceed, it can be noted that even immediately after the addition of the reagents, a separation between the control and the spiked sample was observed, as their error bars do not overlap. The results from this timed study suggested that the reaction time for this assay could be reduced to around 45 minutes, allowing 30 minutes for Step 1 and 15 minutes for step 2. However, as this timed study was investigated using the highest concentration of PETN looked at in this chapter, it might be suggested that this separation was not large enough, and therefore might not be observed when analysing a smaller concentration of PETN.

The sample results for the timed study in step 3 were found to be more consistent and contained less error than those the timed studies for step 1 or 2. This is likely because each time point was taken from the same sample, so there should not have been as much variation. The only source of variation should have occurred during the measuring of 100 µL sample, and 200 µL hydroxylamine silver nanoparticles, which could account for the high intensity found at time point 15 for the control sample. The error bars for this time point are also very large, and it can be observed that the

lower part of the error bar extends to an intensity which would have been in line with the intensities found at other time points for the control samples.

It was also observed that there was an additional band at 1269 cm^{-1} (C-H stretch in the benzene ring) which increased in intensity as time proceeded. As this peak did not appear in any other spectra performed, it was ignored.

4.5.6.4 Further timed studies

The most intense SERS signal for the time dependent SERS analysis for step 2 (NO_3^- reduction) was obtained at the 5-minute mark, and so it was decided to test what happened if the reaction proceeded directly to step 3 after step 2, with no additional heating or waiting time. It was proposed that the samples were already at a heated temperature after step 1, and therefore returning the samples for a further 5 minutes would not affect the sample as they should retain their heat for the addition of the reagents for step 2.

For this test, the spiked sample and control were prepared as usual, with 25 µL PETN or ACN, respectively. The spiked sample and control were then heated for 5 minutes in a water bath at 65 °C. They were removed and Cu^{2+} and hydrazine sulfate were added. Both the spiked sample and the control were then split in half, and the solutions were treated differently.

One of the control and spiked sample sets was placed back into the heated water bath for a further 5 minutes, before being removed for step 3 (addition of HCl, 4-ATP and H_3PO_4). The sample was then analysed by SERS every 5 minutes until 30 minutes had passed. The other sample set did not get heated again and proceeded immediately to step 3 with no waiting time. SERS intensity at 1390 cm^{-1} (N≡N) has been plotted as a function of time for ease of interpreting the full SERS data, and are shown in Figure 4.18.

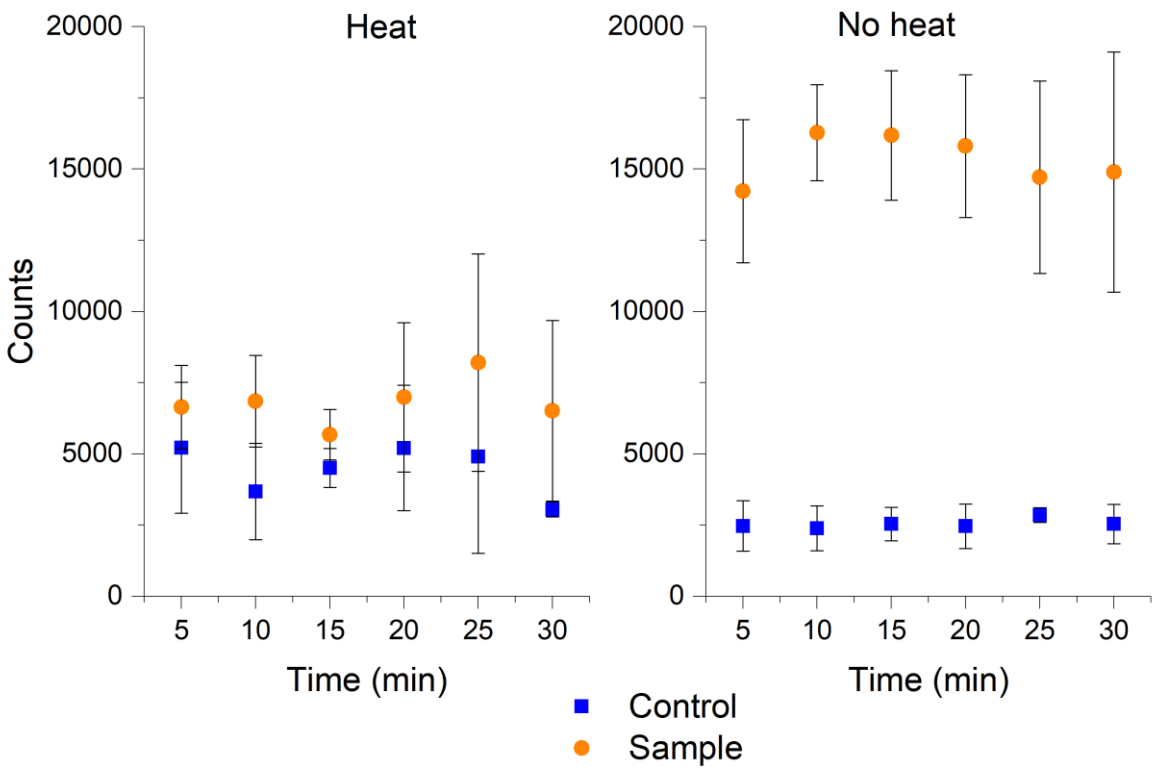

Figure 4.18: SERS intensity of 1390 cm^{-1} peak at all time points. Samples were heated for 5 minutes at step 2 ***(left)*** *or proceeded directly to step 3* ***(right)****. Spectra were obtained using a Snowy benchtop instrument with an excitation wavelength of 532 nm (15 mW) and an acquisition time of 1s. All spectra are the average of 3 replicate samples with 5 measurements taken on each sample. Each spectrum was baselined corrected, normalised to the ethanol standard and the error bars were calculated from the standard deviation for each data set.*

From the figure above, it can be observed that such a subtle change in procedure produced vastly different results. The samples which were kept in the heated water bath for 5 minutes at step 2 did not result in a clear separation between the control and sample when taking into account the standard deviation of the samples, which overlap with each other. On the other hand, the samples which proceeded immediately to the addition of the reagents in step 3 resulted in a clear separation between the sample and the control. The error bars observed for the method with no additional heating (right) were also much smaller than the other sample set. The major contribution to the larger error bars observed in time point 25 minutes and 30 minutes were from a single replicate, where the signal intensity of the band at 1390 cm^{-1} decreased with time. The spectra for the other two sample sets were observed at similar intensities to each other.

It was also observed that the spiked samples for the heated version did not react as successfully as the non-heated version, as a difference of around 10,000 counts was observed between the two experiments. As the samples were split in two after the addition of the reagents needed for step 2, error belonging to the measurements for both step 1 and 2 can be ignored. The only difference between the two sample sets is the heating and additional 5 minutes of reaction time, so whatever caused the reduction in SERS intensity experienced in the heated sample must have occurred during those 5 minutes of heating.

Comparing the control samples in each sample, it can also be noted that the controls for the heated sample were more intense than the non-heated version. The intensities at each time point for the heated control ranged from 3000 – 5200 counts, whereas the non-heated controls were at a consistent 2500 counts. As the same samples were examined in subsequent time points this difference cannot be blamed on the sample preparation before the deviation in step 2. This variation could be the result of a number of things, including the error associated with the pipettes for the addition of the HCl, 4-ATP and H_3PO_4, and for the analysis by SERS, where 100 µL of the sample was removed and added to 200 µL of hydroxylamine silver nanoparticles. The error would also be influenced by the uncontrolled aggregation of the nanoparticles after sample addition, likely caused by the abundance of salts and ions in the solution competing for the nanoparticle surface.

To summarise the results from the timed experiments, despite the variation of results obtained for step 1, it was observed that a large SERS intensity was found for all time points. It was decided to use 5 minutes heating during the PETN hydrolysis step as the SERS intensity observed for this time point was comparable to the final one. From the timed study for step 2, it was decided that no time or further heating was needed after the addition of the nitrate reduction agents and the samples would proceed immediately to step 3. This resulted in less variation to the resulting SERS and the separation of the control and spiked sample was much larger for the non-heated

version than found in the heated counterpart. Finally, in the timed experiment for step 3, it was observed that the SERS intensity increased as time went by, however, there was a visible difference between the control and spiked sample at t=0.

4.5.7 Original time vs Optimum time

The optimum time points were then compared to the original protocol. As with all the timed experiments in the previous section, the concentration of PETN used for the samples was 50 mg L^{-1}. Two sets of PETN spiked samples (containing 25 µL PETN) and control samples (containing 25 µL ACN) was prepared in solutions of 1:1 ACN-water. After sample preparation, one sample set was performed as the original protocol, with 30 minutes heating in a water bath at 65 °C for step 1 and a further 15 minutes heating after the addition of step 2 reagents. For the other sample set, step 1 (PETN hydrolysis) was performed for 5 minutes in a heated water bath at 65 °C, the reagents for step 2 (NO_3^- reduction) were added and the reaction proceeded immediately to the addition of the reagents used in step 3. After the addition of the step 3 reagents, the samples were vigorously mixed and 100 µL sample was immediately removed to be added to 200 µL of hydroxylamine silver nanoparticles. 100 µL sample was removed after every subsequent 5 minutes to perform SERS. The resulting spectra shown in Figure 4.19 are the average of each time point and Figure 4.20 shows the SERS intensity at 1390 cm^{-1} (N≡N) plotted as a function of time.

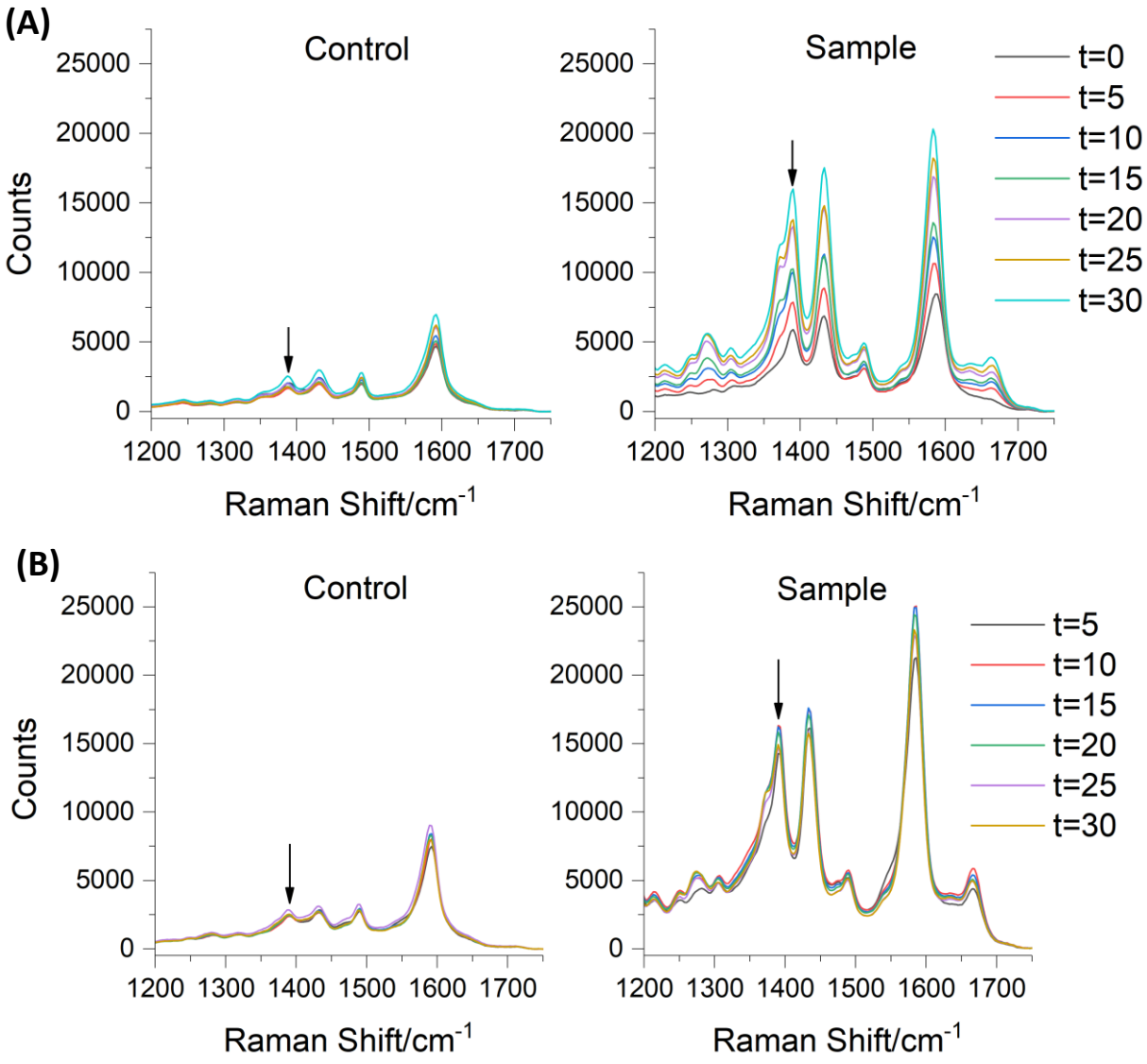

*Figure 4.19: SERS results for all time points obtained at the end reaction time for the original reaction **(A)** and the optimum timing reaction **(B)**. The indicator peak 1390 cm^{-1} has been identified with a black arrow. Spectra were obtained using a Snowy benchtop instrument with an excitation wavelength of 532 nm (15 mW) and an acquisition time of 1s. All spectra are the average of 3 replicate samples with 5 measurements taken on each sample. Each spectrum was baselined corrected and normalised to the ethanol standard.*

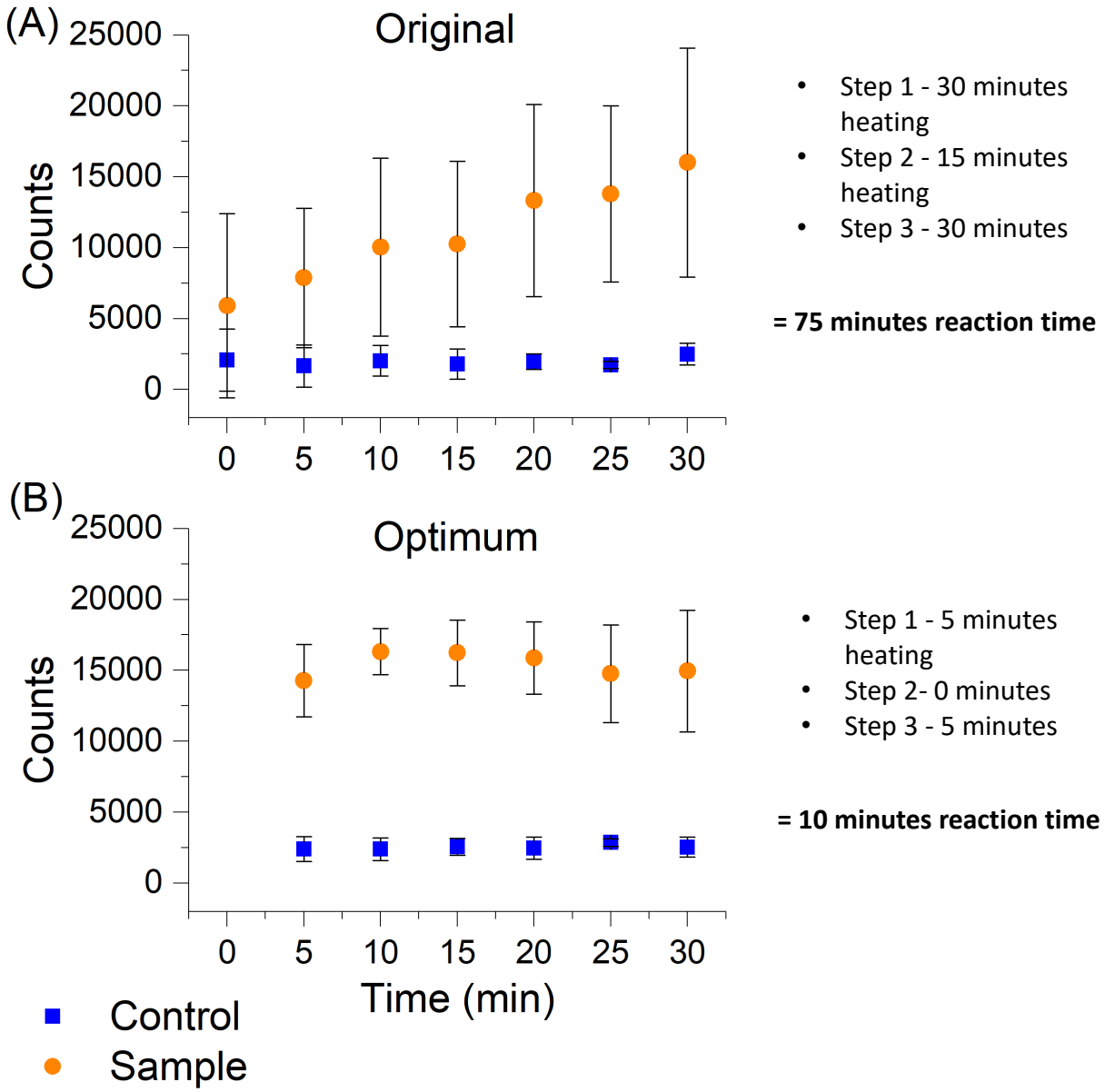

*Figure 4.20: SERS intensity of 1390 cm^{-1} peak for the original reaction **(A)** and the optimum timing reaction **(B)**, spectra taken for 0-30 minutes after addition of 4-ATP. Summaries of the timings in each step, and the total reaction time can be found to the right of the spectra. Spectra were obtained using a Snowy benchtop instrument with an excitation wavelength of 532 nm (15 mW) and an acquisition time of 1s. All spectra are the average of 3 replicate samples with 5 measurements taken on each sample. Each spectrum was baselined corrected, normalised to the ethanol standard and the error bars were calculated from the standard deviation for each data set.*

As previously found in the time study for step 3 (Figure 4.17), the original time course (Figure 4.19 (A) and Figure 4.20 (A)) shows that the average SERS intensity for the 1390 cm^{-1} band increases with time over the 30 minute period at the end of the experiment. However, while the SERS intensity for the time study in step 3 plateaus at around the 20-30 minute point of the reaction, in Figure 4.19 and Figure 4.20 it

was observed that the reaction continued to increase. A clear separation between the control and the spiked sample was only observed at around 10 minutes and after, explaining why the original paper required 30 minutes of reaction time before performing any analysis. However, 75 minutes is a very long time for a reaction which can only be used for presumptive testing of nitrate and nitrite ions.

For the optimum timing's spectra (B), a distinct separation between the control and the PETN spiked sample was observed after just 5 minutes. This intensity shows minimal increases as the reaction proceeds with time, therefore suggesting that the reaction reaches completion after 5-10 minutes as indicated by the highest intensity for the band monitored. It can also be observed that the standard deviation was much smaller for the optimum timing compared to the original timing, suggesting that the reaction results in a more reliable and consistent SERS output for this concentration of PETN.

From these findings, the reaction for the detection of PETN using SERS was successfully reduced from the original 75 minutes to 10 minutes, with the optimum timing producing less variation in the results. This would allow the reaction to be used as a presumptive test for on-site analysis using portable Raman instrumentation, thus significantly improving the reaction from the original 75 minute concept reaction (Griess reaction). The next step in the development of the SERS assay would be to perform PETN concentration studies using the optimised timings to calculate the LOD.

4.4 Chapter Conclusions

In conclusion, it has been demonstrated that the resonance Raman assays developed in Chapter 3 were easily altered to detect PETN using SERS spectroscopy by removing NED/DMA. Removing the nucleophile halted the reaction at the formation of the diazonium ion which, although couldn't be detected by the naked eye, could be functionalised to silver nanoparticles and detected with SERS. The electrophile and

the solvent used in the assay was investigated and it was found that 4-ATP and acetone resulted in the strongest SERS signal. These modifications resulted in a SERS assay able to detect 1 mg L^{-1} (3.2 µM) of PETN, which is the lowest concentration of PETN detected in this thesis.

It was demonstrated that this reaction could be used to detect other nitro-based explosives, such as TNT and RDX. However, when working with TNT, a coloured Meisenheimer by-product was formed which affected the UV results and created a larger background in the SERS result, causing difficulties in interpreting the results.

Finally, the timings of each step of the assay were investigated and the assay was successfully reduced from 75 minutes to 10 minutes, resulting in no signal loss. While this SERS assay still did not have as low an LOD as reported in Üzer et al's work, this SERS assay could be considered superior as the modifications allow for a portable presumptive test with a reduced reaction time to be developed, which could be used for on-site analysis of nitro-based explosives.

4.5 Further work

In this chapter it was demonstrated that the reaction time could be reduced from the original 75 minutes to 10 minutes. As this was a preliminary proof of concept study, further work should be done to fully investigate this reaction, including concentration studies to obtain the LOD.

Similar to Chapter 3, further work should also be done to improve the nitrate ion reduction step to obtain the best signal from samples. This was evidenced by the poor PETN signal in comparison to the RDX signal in Figure 4.13 and Figure 4.14. By improving the efficiency of the nitrate reduction step, an increase in PETN signal should be observed, thus allowing for a lower detection limit to be obtained. Further work should also be done on testing dirty samples, as the aim of this chapter was to develop a portable assay to be used for on-site analysis and real-life samples rarely

consist of pure explosives. This would involve the swabbing of samples using a material which provides little background in the SERS spectrum and developing a method of removing contaminants which would provide SERS background. One particular concern would be removing Meisenheimer complexes formed from nitro-aromatic explosives, as these would interfere with the SERS signal.

Chapter 5 : Conclusions and Further work

It has been demonstrated that resonance Raman and surface enhanced Raman spectroscopy had a number of advantages which result in more sensitive assays that can use portable instrumentation. The enhancement experienced by PETN on the previously commercially available substrate, Klarite^{TM}, was investigated to better understand the cause of enhancement for this molecule. From investigating the signal difference between the pit and the area around the pit on the substrate chip, it was found that while there was a signal intensity difference observed, the area around the pit also resulted in PETN signal. PETN SERS signal was only obtained on Klarite^{TM} and was not observed on substrates with similar materials and structure. These findings suggested that the enhancement was a result of both the molecule concentrating in the pit and a SERS effect experienced from the roughened gold surface. PETN was detected to a concentration of 50 mg L^{-1}, or 1.7 ag in the examined area, when using SERS mapping instrumentation. However, these substrates were expensive to make and the low mass detected in this work would not be observed with handheld instrumentation as they would have a larger interrogation area than the mapping instrument.

It is difficult to detect PETN in solution-based Raman experimentation as PETN contains a poor Raman cross-section. It was decided to hydrolyse the PETN molecule, reduce the resulting nitrate ions to nitrite, and use them to produce an azo reaction. Four assays able to detect PETN in the concentration range of 2-50 mg L^{-1} using absorption and/or resonance Raman spectroscopy were developed. By modifying the resonance Raman assays to react in ACN: water instead of acetone: water, the assay was optimised to give a more intense signal. However, using this solvent meant that the azo band was unreliable as an indicator peak as ACN had a similar band visible in the control. Nevertheless, there were still several bands in the DMA and 4-ATP molecule which could be monitored, which resulted in limits of detection of 1.7-6.5 mg L^{-1}. While these assays could be used to detect relatively low

concentrations of PETN, the reaction was not specific and was found to react with other samples containing nitrite ions.

The Griess and resonance Raman assays were easily developed into a SERS assay by removing the nucleophile. The incorporation of a thiol functionality on the diazonium ion allowed for strong attachment to the silver nanoparticles, after product formation, resulting in a strong SERS signal where several of the 4-ATP bands and the diazonium peak could be monitored. The electrophile was investigated and it was found 4-ATP resulted in the best signal. The solvent the reaction was performed in was also examined, and it was found that using ACN not only resulted in a large signal increase, but the position of the 4-ATP molecule on the nanoparticle surface could be confirmed as perpendicular by the changing peak ratio of an indicator band. These modifications resulted in a SERS assay which was able to detect 1 mg L^{-1} (3.2 μM) of PETN. The main advantages of this SERS assay in comparison to the Griess and resonance Raman assays was that the SERS assay had been optimised for a short time taken until analysis (10 minutes), whereas the previous assays required 75 minutes before analysis could occur. The removal of the nucleophile would also result in a reduction to the overall cost of the assay, thus making it more desirable. Further work should be done to obtain the PETN LOD value for the optimised timing reaction, and to improve the nitrate ion reduction step, so that the optimum signal could be obtained from the sample. Further development on this assay should also be to incorporate the analysis of real life samples.

PETN is a challenging explosive to detect using current methods because of its low water solubility, low vapour pressure and small size, with a lot of research being performed on explosive molecules which are considered easier to detect, for example TNT. Commercially available colourimetric testing kits boast LODs down to 0.02 mg L^{-1}, but this value is for the detection of nitrate/nitrite ions rather than explosives. While the SERS assay developed in Chapter 4 did not achieve as low a detection limit as the commercial kits, the cost for our SERS assay is much reduced compared to commercial ones, and would not need to be performed within a time limit or a limited number of uses. Commercial colourimetric testing kits typically cost around £300 for 64 assays,

usually only a fraction of which can be used for nitrate detection as this requires an additional reduction step. However, the assay developed only requires 4-ATP, copper sulfate, hydrazine sulfate and a few other chemicals often found in a laboratory, reducing the cost to under £50 for a much larger number of assays. The assay developed also uses SERS, which allows for analysis with portable instrumentation, rather than relying on naked-eye detection, or absorption spectroscopy for lower concentrations of analyte, where the colour change will be less noticeable. While the LOD for the developed SERS assay was larger than those in commercial colourimetric testing kits, it was found that the LOD was lower than some PETN assays developed in literature, including the research by Andrew et al[103] where an LOD of 1.3×10^{-4} M was detected using fluorescence spectroscopy.

Chapter 6 : Experimental

6.1 Materials

TNT (1mg/mL), RDX (1 mg/mL) and PETN (1mg/mL) dissolved in acetone/acetonitrile (ACN) was supplied by Defence Science and Technology Laboratory (Porton Down, Salisbury, UK). Klarite^{TM} was supplied by DSTL (Porton Down, Salisbury, UK). Uncoated Klarite (gold free Klarite) and in house Klarite substrates were supplied by Dr Stacey Laing. All other chemicals were purchased from Sigma-Aldrich unless stated otherwise.

6.2 Instrumentation

6.2.1 UV-Vis Spectroscopy

All absorption spectroscopy was carried out on an Agilent Cary60 UV-Vis spectrophotometer with Win UV Scan Application version 2.0 software. All samples were scanned using a wavelength range of 300-800 nm and were diluted accordingly before addition to a 1 cm^2 cuvettes.

6.2.2 DLS and zeta potential

A Malvern Zetasizer Nano ZS was used to carry out all zeta potential and zeta sizing measurements along with Zetasizer μV and APS version 6.20 software. Approximately 1 mL of sample was run in a 1 mL disposable plastic cuvette, with a standard Malvern Zeta Dip Cell.

6.2.3 Resonance Raman measurements

Raman solution spectra were collected using a Snowy Range Sierra series reader with a 532 nm excitation wavelength (40 mW) laser power and a 1 second acquisition time,

depending on the sample. Each spectrum was normalised against a standard solution of ethanol, and baseline corrected using the asymmetrical least squared smoothing method in Matlab 2016 software.

6.2.4 SERS measurements

Substrates

SERS maps from commercial substrates were performed on 633 nm and 785 nm laser using a Renishaw InVia Confocal Raman microscopy with a helium-neon ion laser (633 nm) and a diode laser (785 nm) fitted with a Leica DMLM attachment. The laser was focused on the sample using a 50x long working distance objective lens (unless stated otherwise), and a grating of 1200 l/mm (785 nm) and 1800 l/mm (633 nm). Detection was achieved using a charge coupled device and the spectra maps were recorded in the range of 500 - 1650 cm^{-1}. Each point on the map was interrogated at 10 % laser power (4.9 mW for 633 nm, 20.0 mW for 785 nm), with single 1 s acquisitions. A silica standard was used to calibrate the instruments used for the SERS substrates. All SERS maps were noise deducted, baseline corrected and analysed using Renishaw's WiRE 4.4 software, unless stated otherwise. The SERS intensity maps were generated by plotting the intensity of the peak at 1290 cm^{-1} for each map point. All map averages were processed and baselined corrected using the asymmetrical least squared smoothing method on Matlab 2016 software.

Solution

SERS solution spectra were obtained by adding 100 µL sample to 200 µL of silver nanoparticles. The nanoparticle solutions were interrogated using a 532 nm excitation wavelength (0.2 - 40 mW) laser power and a 1 second acquisition time, depending on the sample. The instrumentation used was a Snowy Range Sierra series reader. Each spectrum was normalised against a standard solution of ethanol, and

baseline corrected using the asymmetrical least squared smoothing method in Matlab 2016 software.

6.2.5 SEM measurements

Samples were analysed using a FEI Quanta 250 environmental (low vacuum) field emission gun scanning electron microscope operating at an accelerating voltage of 30 kV.

6.3 SERS Substrates

Diluted solutions of PETN were prepared in lab, making concentrations ranging between 1000 mg L^{-1} and 10 mg L^{-1}. The Renishaw Klarite™ substrates were sonicated in first isopropyl alcohol, and then methanol for 10 minutes to remove any surface contaminants before being air dried. The other substrates were left untreated before sampling. The substrates were fixed to glass microscopy slides using a double-sided adhesive dot to prevent movement, and a known volume of the analyte (0.5 µL, unless stated otherwise) was then deposited onto the substrate and the solvent left to evaporate for 5 minutes. SERS maps were performed in 5 random positions in the sample area, using a Renishaw InVia Raman microscopy with an excitation wavelength of 633 nm and 785 nm. The spectra were averaged and then baseline corrected using Matlab 2016 software.

This process was performed on flat silica substrates, flat gold substrates, Klarite with no gold coating, and with Klarite™.

6.4 Colourimetric and Resonance Raman Detection of PETN

6.4.1 Preparation of Griess Reagents

The original Griess reagent was prepared by combining a sulfanilamide solution (4 %, w/v) prepared in 10 % phosphoric acid with an NED solution (0.2 %, w/v) prepared in distilled water. These solutions were mixed at equal volumes to form the reagent.

The modified Griess reagent was prepared in a similar way, substituting the same concentration of DMA for NED.

6.4.2 Nanoparticle colloid synthesis

Synthesis of 4-ATP Gold Nanoparticles

Prior to nanoparticle colloid synthesis, all glassware was cleaning using aqua regia (1 HNO_3: 3 HCL), and rinsed using distilled water.

4-ATP functionalised nanoparticles were prepared by adding a solution of trisodium citrate (1 %) to a boiling solution of hydrogen tetrachloroaurate (0.002 %). The heat was kept constant until a red-wine colour was obtained. This nanoparticle solution was allowed to cool to room temperature before the pH was adjusted to pH 3. The nanoparticle solution was then mixed with a solution of 4-ATP in ethanol (10 mM) at an 8:1 ratio. The nanoparticles were continuously stirred for 3 hours at 60 °C, making sure to keep the temperature constant.

6.4.3 Characterisation of colloids

After cooling to room temperature, the nanoparticle colloid was analysed by UV-Vis absorption spectroscopy using an Agilent Cary60 UV-Vis spectrometer. Appropriate dilutions were made so 1 mL of colloid added to 1 cm^3 quartz cuvette gave an extinction spectrum between the absorbance values of 0.6 - 1.

DLS and zeta potential measurements were carried out using a Malvern Zetasizer Nano ZS. 1 mL of colloid was added to a 1 cm^3 disposable plastic cuvette and a standard Malvern Zeta Dip cell. Measurements were carried out using Zetasizer μV and APS version 6.20 software.

To further characterise the 4-ATP functionalised gold nanoparticles, Raman and SERS spectra were obtained from a 1.11 mM solution of 4-ATP, and the functionalised nanoparticles using a Snowy Range Sierra series reader with a 532 nm excitation wavelength (40 mW) and 1s acquisition time.

6.4.4 Original Griess and NP Assay from the source paper

The original Griess assay

To a solution of PETN (5 mL, 10 mg L^{-1}) in 4:1 acetone-water medium, H_2O_2 (1 mL, 20 %) was added and left to react for 20 minutes. After, solutions of $CuSO_4.5H_2O$ (0.1 mL, 0.25 %), NaOH (0.1 mL, 0.1 M) and hydrazine sulfate (0.1 mL, 0.208 %) were added and left to react for a further 15 minutes in a water bath at 65 °C. This was followed by the addition of 2.7 mL Griess reagent, and the analysis of the samples by absorption spectroscopy as described in section 6.2.1.

Nanoparticle based assay

To a solution of PETN (5 mL, 10 mg L^{-1}) in 1:1 acetone-water medium, H_2O_2 (1 mL, 6 %) was added and left to react for 20 minutes. After, solutions of $CuSO_4.5H_2O$ (0.1 mL, 0.25 %), NaOH (0.1 mL, 0.1 M) and hydrazine sulfate (0.1 mL, 0.208 %) were added and left to react for a further 15 minutes in a water bath at 65 °C. This was followed by the addition of 4-ATP nanoparticles (1 mL), HCl (1 mL, 0.1 M) and NED (0.5 mL, 20 mM). Samples were analysed by absorption spectroscopy 30 minutes after NED addition as described in section 6.2.1.

6.4.5 Alterations of original Griess assay

Hydrolysing solution

The H_2O_2 hydrolysing solution was replaced with a base hydrolysing solution comprised of Na_2CO_3 (1 M) and NaOH (0.04 M).

Replacing Nucleophile

NED was replaced with 0.2 % DMA in a modified Griess reagent as seen in Section 6.4.1, and 20 mM DMA in the nanoparticle based assay.

Changing solvents

The solvent acetone was switched to acetonitrile, keeping the solvent-water ratio the same in each assay (4:1).

6.4.6 Griess and nanoparticle assays

Original Griess Assay

To a solution of PETN (1 mL, 10 mg L^{-1}) in 4:1 ACN-water medium, base hydrolysing solution (0.2 mL, Na_2CO_3 (1 M) and NaOH (0.04 M)) was added and left to react for 30 minutes in a water bath at 65 °C. After, solutions of $CuSO_4.5H_2O$ (20 µL, 0.25 %) and hydrazine sulfate (20 µL, 0.208 %) were added and left to react for a further 15 minutes in the water bath at 65 °C. This was followed by the addition of 0.6 mL of the original Griess reagent, and the analysis of the samples by UV-Vis absorbance spectroscopy as described in section 6.2.1.

Modified Griess Assay

To a solution of PETN (1 mL, 10 mg L^{-1}) in 4:1 ACN-water medium, base hydrolysing solution (0.2 mL, Na_2CO_3 (1 M) and NaOH (0.04 M)) was added and left to react for

30 minutes in a water bath at 65 °C. After, solutions of $CuSO_4.5H_2O$ (20 µL, 0.25 %) and hydrazine sulfate (20 µL, 0.208 %) were added and left to react for a further 15 minutes in the water bath at 65 °C. This was followed by the addition of 0.6 mL of the modified Griess reagent, and the analysis of the samples by UV-Vis absorbance spectroscopy as described in section 6.2.1.

NED Resonance Raman Assay

To a solution of PETN (500 µL, 50 mg L^{-1}) in 1:1 ACN-water medium, base hydrolysing solution (500 µL, Na_2CO_3 (1 M) and NaOH (0.04 M)) was added and left to react for 30 minutes in a water bath at 65 °C. After, solutions of $CuSO_4.5H_2O$ (20 µL, 0.25 %) and hydrazine sulfate (20 µL, 0.208 %) were added and left to react for a further 15 minutes in the water bath at 65 °C. The sample was neutralised with HCl (100 µL, 5M) before adding 4-ATP (250 µL, 1.11 mM), and then acidified to pH 3 with H_3PO_4 (100 µL, 5M). Finally, NED (125 µL, 20 mM) was added and after 30 minutes the samples were analysed by absorption, Raman and SERS spectroscopy as described in sections 6.2.1, 6.2.3 and 6.2.4.

NED Resonance Raman Assay

To a solution of PETN (500 µL, 50 mg L^{-1}) in 1:1 ACN-water medium, base hydrolysing solution (500 µL, Na_2CO_3 (1 M) and NaOH (0.04 M)) was added and left to react for 30 minutes in a water bath at 65 °C. After, solutions of $CuSO_4.5H_2O$ (20 µL, 0.25 %) and hydrazine sulfate (20 µL, 0.208 %) were added and left to react for a further 15 minutes in the water bath at 65 °C. The sample was neutralised with HCl (100 µL, 5M) before adding 4-ATP (250 µL, 1.11 mM), and then acidified to pH 3 with H_3PO_4 (100 µL, 5M). Finally, DMA (125 µL, 20 mM) was added and after 30 minutes the samples were analysed by absorption, Raman and SERS spectroscopy as described in sections 6.2.1, 6.2.3 and 6.2.4.

6.4.6 Concentration Studies

PETN concentrations ranges were analysed on all four assays using the procedures described in sections 6.4.6. The original Griess and modified Griess assays investigated 2-10 mg L^{-1}, whereas the resonance Raman assays investigated 10-50 mg L^{-1}. These concentration ranges were analysed by absorption, Raman and SERS spectroscopy.

6.5 Indirect SERS Detection of PETN

6.5.1 Silver Hydroxylamine nanoparticle synthesis

Prior to nanoparticle colloid synthesis, all glassware was cleaning using aqua regia (1 HNO_3: 3 HCL), and rinsed using distilled water.

Hydroxylamine silver nanoparticles were prepared using a method first reported by Leopold and Lendl.[19] Sodium hydroxide (47 mg) was dissolved in distilled water (360 mL) and then added to an aqueous solution of hydroxylamine hydrochloride (41.6 mg dissolved in 4 mL dH_2O). Silver nitrate (67 mg dissolved in 40 mL dH_2O) was then rapidly added, and the solution was stirred for a further 10 minutes at room temperature. The resulting nanoparticles were characterised by UV-Vis, DSL and zeta potential as described in 6.2.1 and 6.2.2.

6.5.2 Attempts for SERS analysis of the nanoparticle product

Adding azo directly to NP

100 µL of each sample was added to 200 µL of silver nanoparticles. Spectra were collected using a Snowy Range Sierra series reader with a 532 nm excitation wavelength (40 mW for Raman, 15 mW for SERS) laser power and a 1 second acquisition time, depending on the sample. Each spectrum was normalised against a

standard solution of ethanol, and baseline corrected using the asymmetrical least squared smoothing method in Matlab 2016 software.

Controls

Each control was made at the same concentration as would be present in the final product. Raman spectra were obtained from each control, then 100 µL of each sample was added to 200 µL of silver nanoparticles to take the SERS spectra. Spectra were collected using a Snowy Range Sierra series reader with a 532 nm excitation wavelength (7-40 mW) laser power and a 1 second acquisition time, depending on the sample. Each spectrum was normalised against a standard solution of ethanol, baseline corrected using the asymmetrical least squared smoothing method in Matlab 2016 software, normalised between 0-1 and offset.

6.5.3 SERS and Raman of DMA

A solution of DMA (1.5 mM) was prepared in 1:1 ACN-water medium.

The sample was characterised by Raman and SERS as described in sections 6.2.3 and 6.2.4.

6.5.4 SERS assay

To a solution of PETN (500 µL, 50 mg L^{-1}) in 1:1 ACN-water medium, base hydrolysing solution (500 µL, Na_2CO_3 (1 M) and NaOH (0.04 M)) was added and left to react for 30 minutes in a water bath at 65 °C. After, solutions of $CuSO_4.5H_2O$ (20 µL, 0.25 %) and hydrazine sulfate (20 µL, 0.208 %) were added and left to react for a further 15 minutes in the water bath at 65 °C. The sample was neutralised with HCl (100 µL, 5M) before adding 4-ATP (250 µL, 1.11 mM), and then acidified to pH 3 with H_3PO_4 (100 µL, 5M). After 30 minutes the samples were analysed by absorption, Raman and SERS spectroscopy as described in sections 6.2.1, 6.2.3 and 6.2.4.

6.5.5 Substituting 4-ATP

10 mM solutions of 2-amino pyridine, 3-amino pyridine, 2-amino-4,6-dimethoxypyrimidine and 4-ATP were prepared in ethanol and were diluted to 1.11 mM in a 9:1 ratio of water. The SERS assay procedure was performed as described in section 6.4.4, substituting 4-ATP for the other three compounds. The resulting products were analysed by SERS as described in section 6.2.4.

6.5.6 Concentration Study

The PETN concentrations range of 10-50 mg L^{-1} was analysed by absorption spectroscopy. The PETN concentrations were subsequently diluted by 2/3 and the range of 3.3-16.7 mg L-1 was analysed by SERS spectroscopy.

6.5.7 SERS Assay for TNT, RDX and PETN

The SERS assay described in section 6.5.4 was performed separately for TNT, RDX and PETN, all at 10 mg L^{-1}.

Sample characterisation by UV-Vis absorbance spectroscopy and SERS was performed as described in sections 6.2.1 and 6.2.4.

6.5.8 Time Optimisation Studies

Timed studies were performed on the PETN hydrolysis, nitrate reduction and the end reaction time, altering the timing (by 5 minute intervals) for one step while keeping the timing of the other two constant. The reaction proceeded as described in section 6.5.4, but with altered times for each step. The samples were analysed by SERS spectroscopy as described in sections 6.2.4.

6.5.9 Optimum timing for SERS assay

To a solution of PETN (500 µL, 50 mg L^{-1}) in 1:1 ACN-water medium, base hydrolysing solution (500 µL, Na_2CO_3 (1 M) and NaOH (0.04 M)) was added and left to react for 5 minutes in a water bath at 65 °C. Solutions of $CuSO_4.5H_2O$ (20 µL, 0.25 %) and hydrazine sulfate (20 µL, 0.208 %) were added before the sample was neutralised with HCl (100 µL, 5M). 4-ATP (250 µL, 1.11 mM) was added before the solution acidified to pH 3 with H_3PO_4 (100 µL, 5M). After 5 minutes the samples were analysed by SERS spectroscopy as described in sections 6.2.4.

Chapter 7 References

1 M. Laura Soriano, M. Zougagh, M. Valcárcel and Á. Ríos, *Talanta*, 2017, **177**, 104–121.

2 J. Ramsden, *Nanotechnology: An Introduction*, Elsevier Inc., 2011.

3 L. M. Katz, K. Dewan and R. L. Bronaugh, *Nanotechnology in Cosmetics*, 2015, vol. 85.

4 A. F. Hamad, J. H. Han, B. C. Kim and I. A. Rather, *Saudi J. Biol. Sci.*, 2017, 0–3.

5 I. R. Hardin and Y. Kim, *Nanotechnology for antimicrobial textiles*, Elsevier Ltd, 2016.

6 S. Mishra, *Indian Heart J.*, 2016, **68**, 437–439.

7 R. P. Feynman, *Calif. Inst. Technol. J. Eng. Sci.*, 1960, 4, 22–36.

8 V. V. Mody, R. Siwale, A. Singh and H. R. Mody, *J. Pharm. Bioallied Sci.*, 2010, **2**, 282–289.

9 The Lycurgus Cup, https://www.britishmuseum.org/, (accessed 25 September 2017).

10 I. Freestone, N. Meeks, M. Sax and C. Higgitt, *Gold Bull.*, 2007, **40**, 270–277.

11 M. Faraday, *Philos. Trans. R. Soc. London*, 1857, **147**, 145–181.

12 Q. Huang, S. Wen and X. Zhu, *RSC Adv.*, 2014, **4**, 37187.

13 L. Shang, K. Nienhaus and G. U. Nienhaus, *J. Nanobiotechnology*, 2014, **12**, 1–11.

14 R. X. He, R. Liang, P. Peng and Y. Norman Zhou, *J. Nanoparticle Res.*, 2017, **19**, 267.

15 R. J. Stokes, A. Macaskill, P. Johan Lundahl, W. Ewen Smith, K. Faulds and D. Graham, *Small*, 2007, **3**, 1593–1601.

16 N. Grillet, D. Manchon, E. Cottancin, F. Bertorelle, C. Bonnet, M. Broyer, J. Lermé and M. Pellarin, *J. Phys. Chem. C*, 2013, **117**, 2274–2282.

17 J. Turkevich, P. C. Stevenson and J. Hillier, *Discuss. a Faraday Soc.*, 1951, **11**, 55.

18 P. C. Lee and D. Meisel, *J.Phys.Chem.*, 1982, **86**, 3391–3395.

19 N. Leopold and B. Lendl, *J. Phys. Chem.*, 2003, **107**, 5723–5727.

20 M. Grzelczak, J. Perez-Juste, P. Mulvaney and L. M. Liz-Marzán, *Chem. Soc. Rev.*, 2008, **37**, 1783–1791.

21 S. J. Oldenburg, Silver Nanoparticle: Properties and Applications, http://www.sigmaaldrich.com/materials-science/nanomaterials/silver-nanoparticles.html#sur, (accessed 24 March 2016).

22 J. Stetefeld, S. A. McKenna and T. R. Patel, *Biophys. Rev.*, 2016, **8**, 409–427.

23 B. J. Inkson, in *Materials Characterization Using Nondestructive Evaluation (NDE) Methods*, eds. G. Hubschen, I. Altpeter, R. Tschuncky and H.-G. Herrmann, Elsevier Ltd, 2016, pp. 17–43.

24 T. Wriedt, in *The Mie Theory: Basics and Applications*, eds. W. Hergert and T. Wriedt, Springer, 2012, pp. 53–71.

25 L. Saa, M. Coronado-Puchau, V. Pavlov and L. M. Liz-Marzán, *Nanoscale*, 2014, **6**, 7405–7409.

26 D. Gardiner, *Practical Raman Spectroscopy*, 1989.

27 N. John and S. George, in *Spectroscopic Methods for Nanomaterials Characterization*, eds. S. Thomas, R. Thomas, A. K. Zachariah and R. K. Mishra, Elsevier Inc., Cambridge, 2017, pp. 95–127.

28 C. E. Housecroft and A. G. Sharpe, in *Inorganic Chemistry*, Pearson Education Limited, 4th editio., 2001, pp. 72–73.

29 D. W. Ball, *Spectroscopy*, 2001, **16**, 28–30.

30 H. Fujimori, M. Kakihana, K. Ioku, S. Goto and M. Yoshimura, *Appl. Phys. Lett.*, 2001, **79**, 937–939.

31 Raman spectroscopy in more detail, http://www.renishaw.com/en/raman-spectroscopy-in-more-detail--25806, (accessed 5 June 2020).

32 L. E. Jamieson, J. Greaves, J. A. McLellan, K. R. Munro, N. C. O. Tomkinson, L. H. Chamberlain, K. Faulds and D. Graham, *Spectrochim. Acta - Part A Mol. Biomol. Spectrosc.*, 2018, **197**, 30–36.

33 M. Schmitt and J. Popp, *J. Raman Spectrosc.*, 2006, **37**, 20–28.

34 S. Laing, A. Hernandez-santana, D. L. Asquith, I. B. Mcinnes, K. Faulds and D. Graham, *Anal. Chem.*, 2011, **83**, 297–302.

35 P. Matousek, M. Towrie and A. W. Parker, *J. Raman Spectrosc.*, 2002, **33**, 238–242.

36 E. C. Le Ru, E. Blackie, M. Meyer and P. G. Etchegoint, *J. Phys. Chem. C*, 2007, **111**, 13794–13803.

37 E. Smith and G. Dent, in *Modern Raman Spectroscopy - A Practical Approach*, John Wiley & Sons, Ltd, 2005, pp. 113–133.

38 G. C. Schatz, M. A. Young and R. P. Van Duyne, in *Surface-EnhancedRaman*

Scattering: Physics and Applications, eds. K. Kneipp, M. Mosovits and H. Kneipp, Springer, 2006, vol. 103, pp. 19–46.

39 K. L. Wustholz, A. I. Henry, J. M. McMahon, R. G. Freeman, N. Valley, M. E. Piotti, M. J. Natan, G. C. Schatz and R. P. V. Duyne, *J. Am. Chem. Soc.*, 2010, **132**, 10903–10910.

40 S. L. Kleinman, R. R. Frontiera, A. Henry, J. A. Dieringer and R. P. Van Duyne, *Phys. Chem. Chem. Phys.*, 2013, **15**, 21–36.

41 G. B. Braun, M. Moskovits, S. J. Lee, T. Laurence, N. Fera, L. Fabris, G. C. Bazan and N. O. Reich, *J. Phys. Chem. C*, 2009, **113**, 13622–13629.

42 A. Kamińska, I. Dzięcielewski, J. L. Weyher, J. Waluk, S. Gawinkowski, V. Sashuk, M. Fiałkowski, M. Sawicka, T. Suski, S. Porowski and R. Hołyst, *J. Mater. Chem.*, 2011, **21**, 8662.

43 K. Wu, T. Rindzevicius, M. S. Schmidt, K. B. Mogensen, S. Xiao and A. Boisen, *Opt. Express*, 2015, **23**, 12965.

44 G. McNay, D. Eustace, W. E. Smith, K. Faulds and D. Graham, *Appl. Spectrosc.*, 2011, **65**, 825–837.

45 R. Keir, E. Igata, M. Arundell, W. E. Smith, D. Graham, C. McHugh and J. M. Cooper, *Anal. Chem.*, 2002, **74**, 1503–1508.

46 Terrorism, https://en.oxforddictionaries.com/definition/terrorism, (accessed 5 September 2017).

47 J. Tukel, 2010, 1–8.

48 H. Mizrahi, *YNet News*, 2009.

49 Manchester attack latest: U.S. lawmaker says U.K. bomb showed 'sophistication', http://www.ctvnews.ca/world/manchester-attack-latest-u-s-lawmaker-says-u-k-bomb-showed-sophistication-1.3426624, (accessed 10 February 2020).

50 H. Pidd, Manchester Arena bomb was designed to kill largest number of innocents, https://www.theguardian.com/uk-news/2017/jun/09/manchester-arena-bomb-designed-kill-largest-number-innocents, (accessed 10 February 2020).

51 Manchester attack: Extradition bid for Salman Abedi's brother, http://www.bbc.co.uk/news/uk-england-manchester-41839277, (accessed 10 February 2020).

52 J. Akhavan, in *The Chemistry of Explosives*, Royal Society of Chemistry, Cambridge, Edition 2., 2004, pp. 1–20.

53 W. Ling, *Hist. Sci. Soc.*, 1947, **37**, 160–178.

54 T. Andrade, in *The Gunpowder Age: China, Military Innovation, and the Rise of the West in World History*, Princeton University Press, 2016, pp. 29–43.

55 T. Andrade, in *The Gunpowder Age: China, Military Innovation, and the Rise of the West in World History*, 2016, pp. 44–54.

56 J. L. Humar, in *Dynamics of Structures*, Taylor & Francis Group, LLC, Third Edit., 2012, pp. 5–7.

57 J. Akhavan, *Classification of Explosive Materials*, Royal Society of Chemistry, Cambridge, 3rd Editio., 2004.

58 D. S. Moore, *Rev. Sci. Instrum.*, 2004, **75**, 2499–2512.

59 L. L. Altgilbers, J. Baird, C. S. Lynch and S. I. Shkuratov, in *Explosive Pulsed Power*, Imperial College Press, London, 2011, pp. 59–60.

60 P.-A. Persson, R. Holmberg and J. Lee, in *Rock Blasting and Explosive Engineering*, CRC Press LLC, Boca Raton, Florida, 1994, pp. 55–59.

61 J. G. St. Perrott and D. B. Gawthrop, *J. Franklin Inst.*, 1926, **203**, 870–876.

62 J. P. Agrawal, *High Energy Materials: Propellants, Explosives and Pyrotechnics*, Wiley-VCH, 1st editio., 2010.

63 N. Mehta, K. Oyler, G. Cheng, A. Shah, J. Marin and K. Yee, *Zeitschrift für Anorg. und Allg. Chemie*, 2014, **640**, 1309–1313.

64 M. A. Fox, in *Glossary for the Worldwide Transportation of Dangerous Goods and Hazardous Materials*, CRC Press LLC, 2000, pp. 119–127.

65 P. Das Sharma, 2000, 1–15.

66 P. Cooper, *Explosives Engineering*, Wiley-VCH, the University of Michigan, 1996.

67 T. M. Klapotke, *Chemistry of High-Energy Materials*, De Gruyter, Berlin, 4th Editio., 2017.

68 F. Zapata and C. García-ruiz, *Crit. Rev. Anal. Chem.*, 2020, 1–18.

69 X. Song, *Propellants, Explos. Pyrotech.*, 2006, **31**, 306–310.

70 J. Herbst, *Major Inventions through History: The History of Weapons*, Lerner Books, 2nd editio., 2008.

71 J. Yinon and S. Zitrin, *Modern Methods and Applications in Analysis of Explosives*, John Wiley & Sons, Ltd, 1993.

72 W. Cao, Z. He and W. Chen, *Shock Waves*, 2014, **24**, 619–624.

73 B. Thieme, 1895.

74 D. Chambers, C. Brackett and O. Sparkman, *Lawrence Livermore Natl. Lab.*

75 E. F. Loftus, *Memory*, 2013, **21**, 584–590.

76 L. Z. Mcdonald, *Relig. State Soc.*, 2011, **39**, 177–189.

77 K. Cabell, *Law Psychol. Rev.*

78 I. Sample, *Guard.*, 2009.

79 A. Homburg, *Propellants, Explos. Pyrotech.*, 2017, **42**, 851–853.

80 E. V. Herz, 1920.

81 S. M. Beebe and R. H. Pherson, *Cases in Intelligence Analysis: Structure analytic techniques in action*, SAGE publishing, 2012.

82 B. Karkaria, *BBC NEWS*, 2015.

83 T. B. Hansen, *Wages of Violence: Naming and Identity in Postcolonial Bombal*, Princeton University Press, 2001.

84 *Dly. News Anal. India*, 2019.

85 K. Ju and R. E. Parales, *Microbiol. Mol. Biol. Rev.*, 2010, **74**, 250–272.

86 D. E. Rickert, *Toxicity of Nitroaromatic Compounds*, Hemisphere Publishing Corporation, 1985.

87 G. Harding, *Radiat. Phys. Chem.*, 2004, **71**, 869–881.

88 G. Harding and A. Harding, in *Counterterrorist Detection Techniques of Explosives*, ed. J. Yinon, Elsevier Science, 1st edn., 2007, pp. 199–235.

89 R. G. Ewing, D. A. Atkinson, G. A. Eiceman and G. J. Ewing, *Talanta*, 2001, **54**, 515–529.

90 J. E. Hayes, P. D. Mcgreevy, S. L. Forbes, G. Laing and R. M. Stuetz, *Talanta*, 2018, **185**, 499–512.

91 W. Acree Jr and J. S. Chickos, *Jorunal Phys. Chem. Ref. Data*.

92 B. Pinsker, Confessions of a Baggage Screener, https://www.wired.com/2003/09/bagscan/, (accessed 30 June 2020).

93 A. V Kuznetsov, A. V Evsenin, I. Y. Gorshkov, O. I. Osetrov and D. N. Vakhtin, *Appl. Radiat. Isot.*, 2004, **61**, 51–57.

94 P. Griess, J. Chem. Soc., 1864, 18, 268-271.

95 H. Barnes and A. R. Folkard, *Analyst*, 1951, **76**, 599–603.

96 R. J. Pollitt and E. C. Saunders, *J. Chem. Soc.*, 1965, 4615–4628.

97 J. Almog and S. Zitrin, in *Aspects of Explosives Detection*, eds. M. Marchall

and J. C. Oxley, Elsevier B.V., 2009, pp. 41–58.

98 J. Almog, S. Kraus and B. Glattstein, *J. Energ. Mater.*, 1986, **4**, 159–167.

99 Nitrite/Nitrate, Colorimetric test, https://www.sigmaaldrich.com/catalog/product/roche/11746081001?lang=en&region=GB&cm_sp=Insite-_-caContent_prodMerch_cooccuranceModel-_-prodMerch10-1, (accessed 1 July 2020).

100 G. A. Eiceman, Z. Karpas and H. H. Hill, *Ion Mobility Spectroscopy*, CRC Press, 3rd Editio., 2014.

101 K. G. Furton and L. J. Myers, *Talanta*, 2001, **54**, 487–500.

102 J. C. Oxley and L. P. Waggoner, in *Aspects of Explosives Detection*, eds. M. Marchall and J. C. Oxley, Elsevier B.V., 2009, pp. 27–40.

103 T. L. Andrew and T. M. Swager, *J. Am. Chem. Soc.*, 2007, **129**, 7254–7255.

104 C. Wang, H. Huang, B. R. Bunes, N. Wu, M. Xu, X. Yang, L. Yu and L. Zang, *Sci. Rep.*, 2016, **6**, 1–9.

105 M. Arruebo, M. Valladares and Á. González-Fernández, *J. Nanomater.*, 2009, 1–24.

106 G. P. Anderson, M. Moore, P. T. Charles and E. R. Goldman, *Anal. Lett.*, 2010, **43**, 2913–2922.

107 S. Chaudhary, P. Sonkusre, A. Chopra, K. K. Bhasin and C. R. Suri, *Anal. Chim. Acta*, 2019, **1077**, 266–272.

108 K. L. McNesby, J. E. Wolfe, J. B. Morris and R. A. Pesce-rodriguez, *J. Raman Spectrosc.*, 1994, **25**, 75–87.

109 L. Nagli, M. Gaft, L. D. Spectrometry and M. Rosenbluh, *Opt. Mater. (Amst).*, 2008, **30**, 1747–1754.

110 D. D. Tuschel, A. V. Mikhonin, B. E. Lemoff and S. A. Asher, *Appl. Spectrosc.*, 2010, **64**, 425–432.

111 A. N. K. Bourne, S. P. Mathematical and E. Sciences, *Proc. Math. Phys. Eng. Sci.*, 2000, **457**, 1401–1426.

112 K. Eberhardt, C. Stiebing, C. Matthaus, M. Schmitt and J. Popp, *Expert Rev. Mol. Diagn.*, 2015, **15**, 773–787.

113 J. I. Jerez-Rozo, O. M. Primera-Pedrozo, M. A. Barreto-Caban and S. P. Hernandez-Rivera, *IEEE Sens. J.*, 2008, **8**, 974–982.

114 J. Y. Xu, J. Wang, L. T. Kong, G. C. Zheng, Z. Guo and J. H. Liu, *J. Raman Spectrosc.*, 2011, **42**, 1728–1735.

115 S. S. R. Dasary, D. Senapati, A. K. Singh, Y. Anjaneyulu, H. Yu and P. C. Ray, *ACS Appl. Mater. Interfaces*, 2010, **2**, 3455–3460.

116 K. Milligan, N. C. Shand, D. Graham and K. Faulds, *Anal. Chem.*, 2020, **92**, 3253–3261.

117 M. J. Q. Jr, L. C. . B. Crouse, C. A. Mcfarland, E. M. Lafiandra and M. S. Johnson, *Birth Defects Res. Part B*, 2009, **86**, 65–71.

118 N. M. B. Perney, J. J. Baumberg, A. Tang, M. C. Netti, M. D. B. Charlton and M. E. Zoorob, *Phys. Rev. B*, , DOI:10.1103/PhysRevB.76.035426.

119 S. Botti, S. Almaviva, L. Cantarini, A. Palucci, A. Puiu and A. Rufoloni, *J. Raman Spectrosc.*, 2012, **44**, 463–468.

120 S. Botti, L. Cantarini, S. Almaviva, A. Puiu and A. Rufoloni, *Chem. Phys. Lett.*, 2014, **592**, 277–281.

121 A. Dowgiallo, A. Branham and D. Guenther, *Spectroscopy*, 2017, **32**, 8, 10, 12, 14–17.

122 T. Liyanage, A. Rael, S. Shaffer, S. Zaidi, J. V. Goodpaster and R. Sardar, *Analyst*, 2018, **143**, 2012–2022.

123 P. M. Fierro-mercado and S. P. Hern, *Int. J. Spectrosc.*, 2012, 1–7.

124 G. E. Walrafen and L. A. Blatz, *J. Chem. Phys.*, 1973, **59**, 2646–2650.

125 Y. Han, X. Lan and T. Wei, *Appl. Phys. A*, 2009, **97**, 721–724.

126 C. Lin, L. Jiang, Y. Chai, H. Xiao, S. Chen and H. Tsai, *Opt. Express*, 2009, **17**, 2386–2391.

127 M. Elsayed, A. Gouda, Y. Ismail and M. A. Swillam, *J. Light. Technol.*, 2017, **35**, 3075–3081.

128 O. Péron, E. Rinnert, M. Lehaitre, P. Crassous and C. Compère, *Talanta*, 2009, **79**, 199–204.

129 M. P. Cecchini, V. A. Turek, J. Paget, A. A. Kornyshev and J. B. Edel, *Nat. Mater.*, 2012, **12**, 165–171.

130 A. Chou, E. Jaatinen, R. Buividas, G. Seniutinas, S. Juodkazis, E. L. Izake and P. M. Fredericks, *Nanoscale*, 2012, **4**, 7419–7424.

131 H. Wackerbarth, C. Salb, L. Gundrum, M. Niederkrüger, K. Christou, V. Beushausen and W. Viöl, *Appl. Opt.*, 2010, **49**, 4362–4366.

132 *Raman Data and Analysis, https://static.horiba.com/fileadmin/Horiba/Technology/Measurement_Techniques/Molecular_Spectroscopy/Raman_Spectroscopy/Raman_Academy/Raman_Tutorial/Raman_bands.pdf, (accessed 20 July 2020).*

133 D. Lin-Vien, N. Colthup, W. Fateley and J. Grasselli, *The Handbook of Infrared and Raman Characteristic Frequencies of Organic Molecules*, Academic Press, San Diego, 1st edn., 1991.

134 D. Mampallil and H. B. Eral, *Adv. Colloid Interface Sci.*, 2018, **252**, 38–54.

135 S. Yang, X. Dai, B. B. Stogin and T. Wong, *Proceesings Natl. Acad. Sci. United States Am.*, 2016, **113**, 268–273.

136 A. Üzer, U. Yalçın, Z. Can, E. Erçağ and R. Apak, *Talanta*, 2017, **175**, 243–249.

137 K. L. Peters, I. Corbin, L. M. Kaufman, K. Zreibe, L. Blanes and B. R. McCord, *Anal. Methods*, 2015, **7**, 63–70.

138 A. Üzer, Z. Can, Ii. Akin, E. Erçağ and R. Apak, *Anal. Chem.*, 2014, **86**, 351–356.

139 L. J. Kamphake, S. A. Hannah and J. M. Cohen, *Water Res.*, 1967, **1**, 205–216.

140 D. V. J. Dalal, in *Chemistry*, 2010, pp. 163–232.

141 J. G. M. M. Smeenk, *Anal. Chem.*, 1974, **46**, 302–304.

142 M. Clugston and R. Flemming, in *Advanced Chemistry*, Oxford University Press, 2000, pp. 556–568.

143 A. Tacic, V. Nikolic, L. Nikolic and I. Savic, *Adv. Technol.*, 2017, **6**, 58–71.

144 N-(1-naphthyl)ethylenediamine, https://www.chemicalbook.com/ChemicalProductProperty_EN_CB3921106.htm, (accessed 14 September 2020).

145 E. Rossini, A. D. Bochevarov and E. W. Knapp, *ACS Omega*, 2018, **3**, 1653–1662.

146 3,5-Dimethoxyaniline, https://www.chemicalbook.com/ProductMSDSDetailCB2218117_EN.htm, (accessed 14 September 2020).

147 M. G. Haag and L. C. Haag, in *Shooting Incident Reconstruction*, Elsevier Inc., 2011, pp. 87–103.

148 D. Graham, C. McLaughlin, G. McAnally, J. C. Jones, P. C. White and W. E. Smith, *Chem. Commun.*, 1998, 1187–1188.

149 F. Li, H. Zhang, B. Dever, X. F. Li and X. C. Le, *Bioconjug. Chem.*, 2013, **24**, 1790–1797.

150 M. Osawa, N. Matsuda, K. Yoshii and I. Uchida, *J. Phys. Chem.*, 1994, **98**, 12702–12707.

151 A. Enright, L. Fruk, A. Grondin, C. J. McHugh, W. E. Smith and D. Graham, *Analyst*, 2004, **129**, 975–978.

152 G. McAnally, C. McLaughlin, R. Brown, D. C. Robson, K. Faulds, D. R. Tackley, W. E. Smith and D. Graham, *Analyst*, 2002, **127**, 838–841.

153 Y. Luo, Y. Xiao, D. Onidas, L. Iannazzo, M. Ethève-Quelquejeu, A. Lamouri, N. Félidj, S. Mahouche-Chergui, T. Brulé, N. Gagey-Eilstein, F. Gazeau and C. Mangeney, *Chem. Commun.*, 2020, **56**, 6822–6825.

154 P. R. West, S. Ishii, G. V. Naik, N. K. Emani, V. M. Shalaev and A. Boltasseva, *Laser Photonics Rev.*, 2010, **4**, 795–808.

155 Acetonitrile, https://webbook.nist.gov/cgi/inchi?ID=C75058&Mask=800, (accessed 3 October 2020).

156 N. Xiao and C. Yu, *Anal. Chem.*, 2010, **82**, 3659–3663.

157 E. Tomaszewska, K. Soliwoda, K. Kadziola, B. Tkacz-Szczesna, G. Celichowski, M. Cichomski, W. Szmaja and J. Grobelny, *J. Nanomater.*, , DOI:10.1155/2013/313081.

158 D. Sun, S. Kang, C. Liu, Q. Lu, L. Cui and B. Hu, *Int. J. Electrochem. Sci.*, 2016, **11**, 8520–8529.

159 L. Popović, D. De Waal and J. C. A. Boeyens, *J. Raman Spectrosc.*, 2005, **36**, 2–11.

160 S. Samanman, N. Masoh, Y. Salah, R. Wattanayon, P. Wangsirikul and K. Phumivanichakit, *OIP Conf. Ser. Mater. Sci. Eng.*, 2017, **172**, 1–7.

161 S. Hughes, S. S. R. Dasary, S. Begum, N. Williams and H. Yu, *Sens. Bio-Sensing Res. 5*, 2015, 37–41.